

Effect of surface and interface on the carrier dynamics of quantum wells

By

Salahuddin Khan

PHYS 03201004001

Raja Ramanna Centre for Advanced Technology,
Indore

*A thesis submitted to the
Board of Studies in Physical Sciences*

*In partial fulfillment of requirements
For the Degree of*

DOCTOR OF PHILOSOPHY

of

HOMI BHABHA NATIONAL INSTITUTE



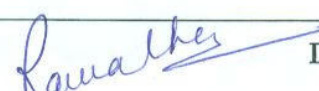
August, 2016

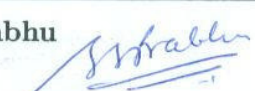
Homi Bhabha National Institute

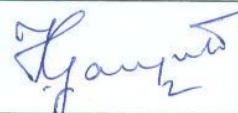
Recommendations of the Viva Voce Committee

As members of the Viva Voce Committee, we certify that we have read the dissertation prepared by **Salahuddin Khan** entitled "**Effect of surface and interface on the carrier dynamics of quantum wells**" and recommend that it may be accepted as fulfilling the thesis requirement for the Degree of Doctor of Philosophy.

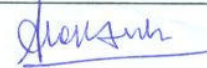
Chairman: **Dr. P. K. Gupta**  Date: 23.2.17

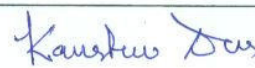
Guide: **Dr. Rama Chari**  Date: 23.2.17

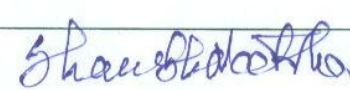
External Examiner: **Dr. S. S. Prabhu**  Date: 23/02/2017

Member 1: **Dr. D. K. Palit**  Date: 23/02/2017

Member 2: **Dr. K. I. Priyadarshini**  Date: 23/02/2017

Member 3: **Dr. Alok Dubey**  Date: 23/2/17

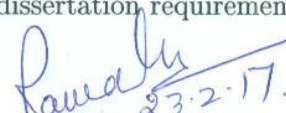
Member 4: **Dr. Kastuv Das**  Date: 23/2/17

External Member : **Dr. S. N. Jha**  Date: 23.2.17

Final approval and acceptance of this dissertation is contingent upon the candidate's submission of the final copies of the dissertation to HBNI.

I hereby certify that I have read this dissertation prepared under my direction and recommend that it may be accepted as fulfilling the dissertation requirement.

Date: 23.2.17
Place: RR CAT, Indore

Guide:  23.2.17.
Dr. Rama Chari

STATEMENT BY AUTHOR

This dissertation has been submitted in partial fulfillment of requirements for an advanced degree at Homi Bhabha National Institute (HBNI) and is deposited in the Library to be made available to borrowers under rules of the HBNI.

Brief quotations from this dissertation are allowable without special permission, provided that accurate acknowledgement of source is made. Requests for permission for extended quotation from or reproduction of this manuscript in whole or in part may be granted by the Competent Authority of HBNI when in his or her judgment the proposed use of the material is in the interests of scholarship. In all other instances, however, permission must be obtained from the author.

Salahuddin Khan

DECLARATION

I, hereby declare that the investigation presented in the thesis has been carried out by me. The work is original and has not been submitted earlier as a whole or in part for a degree / diploma at this or any other Institution / University.

Salahuddin Khan

List of Publications arising from the thesis

Journals

1. “Probing Carrier Dynamics of Individual Layers in a Heterostructure using Transient Reflectivity”, **Salahuddin Khan**, J. Jayabalan, Asha Singh, Rachana Yogi, Rama Chari, *App. Phys. Lett.*, **2015**, *107*, 121905(1-5).
2. “Studies on non-radiative recombination in a two-dimensional electron gas formed in AlGaAs-GaAs heterostructure”, **Salahuddin Khan**, Asha Singh, Rachana Yogi, J. Jayabalan and Rama Chari, *Int. J. Appl. Eng. Res.*, **2015**, *10*, 27646-27649.
3. “Quantum beats from the coherent interaction of hole states with surface state in near-surface quantum well”, **Salahuddin Khan**, J. Jayabalan, Rama Chari, Suparna Pal, Sanjay Porwal, Tarun Kumar Sharma and S. M. Oak, *App. Phys. Lett.*, **2014**, *105*, 073106(1-4).
4. “Modulations in low-temperature transient reflectivity measurements”, **Salahuddin Khan**, Rama Chari, J. Jayabalan, Suparna Pal, T. K. Sharma, A. K. Sagar, M. S. Ansari and P. K. Kush, *Surf. Rev. Lett.*, **2014**, *21*, 1450005(1-7).
5. “Coherent oscillations of holes in GaAs_{0.86}P_{0.14}/Al_{0.7}Ga_{0.3}As surface quantum well”, **Salahuddin Khan**, J. Jayabalan, Rama Chari, Asha Singh, S. Porwal, Suparna Pal, T. K. Sharma and S. M. Oak, *Pramana*, **2014**, *82*, 359-364.
6. “Effect of light-hole tunnelling on the excitonic properties of GaAsP/AlGaAs near-surface quantum wells”, Suparna Pal, S. D. Singh, S. Porwal, T. K.

Sharma, **Salahuddin Khan**, J. Jayabalan, Rama Chari, and S. M. Oak, *Semicond. Sci. Technol.*, **2013**, *28*, 035016(1-8).

7. “Effect of excitation wavelength in the two-dimensional electron gas formation and dynamics at the interface of a AlGaAs-GaAs heterostructure at low temperature”, Salahuddin Khan, J. Jayabalan, Asha Singh and Rama Chari (*Manuscript under Preparation*).

Conferences

1. “Ultrafast dynamics of two-dimensional hole gas formed in an AlGaAs(p-doped)-GaAs heterostructure at room temperature”, **Salahuddin Khan**, J. Jayabalan, Asha Singh, Rama Chari, *Proceedings of DAE-BRNS National Laser Symposium-25*, KIIT University, Bhubaneswar, **2016**, Dec., 20-23.
2. “Optimization of Ultrafast Pump-Probe Experiment and Detection Parameters to Obtain High Signal to Noise Ratio”, Mrigya Shrivastava, Asha Singh, B. K. Ahirwar, **Salahuddin Khan**, J. Jayabalan, and Rama Chari, *Proceedings of DAE-BRNS National Laser Symposium-24*, RRCAT, Indore, **2015**, Dec., 2-5.
3. “Free carrier and excitonic recombination in a Al_{0.7}Ga_{0.3}As-GaAs heterostructure at low temperature and its effect on ultrafast dynamics of two-dimensional electron gas”, **Salahuddin Khan**, J. Jayabalan, Asha Singh, Rama Chari, *Proceedings of DAE-BRNS National Laser Symposium-24*, RRCAT, Indore, **2015**, Dec., 2-5.
4. “Studies on non-radiative recombination in a two-dimensional electron gas formed in AlGaAs-GaAs heterostructure”, **Salahuddin Khan**, Asha Singh, Rachana Yogi, J. Jayabalan, Rama Chari, *National Conference on Science*,

Engineering and Technology (REDSET-2014), Gurgaon, India, **2014**, Oct., 17-18.

5. "Carrier dynamics and photoluminescence studies of triangular quantum well in an $\text{Al}_{0.7}\text{Ga}_{0.3}\text{As}$ -GaAs heterostructure", **Salahuddin Khan**, J. Jayabalan, Asha Singh, Suparna Pal and Rama Chari, *Proceedings of DAE-BRNS National Laser Symposium-23*, S.V. University, Tirupati, **2014**, Dec., 3-6.
6. "Carrier relaxation dynamics of a two-dimensional electron gas in an $\text{Al}_{0.7}\text{Ga}_{0.3}\text{As}$ -GaAs heterostructure", **Salahuddin Khan**, J Jayabalan, Asha Singh and Rama Chari, *Proceedings of DAE-BRNS National Laser Symposium-22*, Manipal University, Manipal, **2014**, Jan., 8-11.
7. "Coherent oscillations of holes in $\text{GaAs}_{0.86}\text{P}_{0.14}/\text{Al}_{0.7}\text{Ga}_{0.3}\text{As}$ surface quantum well", **Salahuddin Khan**, J. Jayabalan, A. Singh, Rama Chari, S. Pal, S. Porwal, T. K. Sharma, and S. M. Oak, *Proceedings of DAE-BRNS National Laser Symposium-21*, BARC, Mumbai, **2013**, Feb., 6-9.
8. "Ultrafast photo-excited carrier dynamics in $\text{GaAs}_{0.86}\text{P}_{0.14}/\text{Al}_{0.7}\text{Ga}_{0.3}\text{As}$ single quantum well: tunneling of carriers from substrates", **Salahuddin Khan**, J. Jayabalan, Rama Chari, Suparna Pal, S. Porwal, T K Sharma, S. M. Oak, *Proceedings of DAE-BRNS National Laser Symposium-20*, Anna University, **2012** Jan., 9-12.

To my beloved parents

Acknowledgement

This thesis is by far the most significant scientific accomplishment in my life. This could not have been realized without the support extended by many people. It is a pleasant opportunity for me to express my gratitude to all of them.

I express my sincere gratitude and deep sense of indebtedness to my research guide Dr. Rama Chari for her valuable guidance, enthusiastic encouragement and constant support in carrying out the research work.

I am extremely grateful to Dr. J. Jayabalan for his invaluable guidance and deep insight have helped me grow scientifically. He has taught lot of experimental and analytical skills throughout my doctoral work. I take this opportunity to express my sincere thanks to Mrs. Asha Singh for her everlasting support and cooperation. I thank my colleague Mr. Vijay Shukla for his support.

I thank Dr. Suparna Pal for introducing me to the semiconductor field, fruitful discussions and constant help during my doctoral work. I thank Dr. Vijay Dixit, Dr. T. K. Sharma and Mr. Sanjay Porwal for the sample along with its characterisation measurements and fruitful discussions.

It is my pleasure to thank Dr. P. K. Gupta, former Director, RRCAT for his guidance and support during my Ph.D. work. I take this opportunity to express my sincere thanks to the Doctoral Committee members Dr. D. K. Palit, Dr. D. K. Aswal, Dr. K. I. Priyadarshini, Dr. Alok Dubey, Dr. Kastav Das and Dr. S. N. Jha for guidance and support during my Ph.D. work.

It is my pleasure to thank Dr. P. D. Gupta, Vice-Chancellor, Homi Bhabha National Institute, Mumbai and former Director, RRCAT for his constant support and encouragement. I thank Dr. S. M. Oak and Dr. S. C Mehendele for their support.

I am happy to acknowledge support of Shri Pradeep Kumar Kush, Shri A. K. Sagar and Mr. M. S. Ansari, Cryo-engineering and Cryo-module Development Di-

vision, RRCAT for providing support for low temperature measurements. I thank Shri V.P. Bhanage, Shri P.P. Deshpande, Shri Mandar J. Joshi and Smt. Shradha Tiwari, Laser Electronics Support Division, RRCAT for data acquisition support.

I would like to thank all my friends and colleagues Mr. Vijay Shukla, Mr. Ravindra Jangir, Dr. C. Kamal, Mrs. Sapana Rege for their support and help when ever needed.

I would like to convey my deepest regards to my parents whose enormous encouragement and support have motivated me in my academic growth. I want to thank my daughters, Sheza and Shazfa, for their love. Finally, I want to express my greatest appreciation for my wife, Saba, for her support and sacrifice to finish this work in time.

Salahuddin Khan,

August 2016.

CONTENTS

Synopsis	iii
List of Figures	x
List of Tables	xxiv

CHAPTERS

1. Introduction	1
1.1 Motivation	2
1.2 Background	5
1.3 Organisation of the thesis	11
1.4 Summary	13
2. Experimental Techniques	15
2.1 Introduction	15
2.2 Samples	16
2.3 Characterization	18
2.3.1 Photoluminescence	18
2.3.2 Photoreflectance	19
2.4 Time Resolved Degenerate Pump-Probe Reflectivity	20
2.5 Establishment of low temperature transient reflectivity measurements	23
2.6 Summary	33
3. Transient reflectivity in GaAs	35
3.1 Introduction	35
3.2 Calculation of photoinduced refractive index change in GaAs	36
3.2.1 Band filling	36
3.2.2 Band gap renormalization	40
3.2.3 Free carrier absorption	42
3.2.4 Combined effect of band filling, band gap renormalization and free carrier absorption	44

3.3	Transient reflectivity measurements on GaAs	46
3.4	Summary	48
4.	Carrier Dynamics in Near-Surface Quantum Well	49
4.1	Introduction	49
4.2	Experimental details	51
4.3	Transient Reflectivity	54
4.4	Coherent Coupling	59
4.5	Conclusion	64
5.	Carrier Dynamics in an AlGaAs-GaAs Heterostructure at low temperature	65
5.1	Introduction	65
5.2	Experimental details	67
5.3	Results	68
5.3.1	Photoluminescence	69
5.3.2	Transient Reflectivity	75
5.4	Conclusion	80
6.	Room Temperature Carrier Dynamics in AlGaAs-GaAs Heterostructures	81
6.1	Introduction	81
6.2	Experimental details	82
6.3	Transient reflectivity results	83
6.3.1	n-doped Al _{0.7} Ga _{0.3} As-GaAs heterostructure	83
6.3.2	p-doped Al _{0.7} Ga _{0.3} As-GaAs heterostructure	93
6.4	Dynamics of 2DEG with carrier density	94
6.5	Conclusion	101
7.	Conclusion and Future Scope	103
	References	107

SYNOPSIS

The optical properties of semiconductors change significantly when the size in any dimension is reduced below the Bohr radius (typically 15 nm in GaAs). The resonance (energy) shifts towards the blue due to quantum confinement and photoluminescence emission become narrower and stronger. Confinement in one dimension leads to structures like quantum wells and superlattices which have sharp, intense and tunable resonances. The now widely used diode lasers utilize a quantum well as the active medium. The reduction in dimension has another advantage. It is seen that the time response of a device based on a nanostructure can be very fast as the carrier relaxation times of these nanostructures range from few tens of femtoseconds (thermalisation, scattering, coherent processes), to picoseconds (intra-band relaxation, scattering, recombination) and nanoseconds (inter-band recombination). This has led to development of electronic, optoelectronic and optical devices like fast photodetectors, all-optical switches, fast transistors etc. An understanding of the different factors affecting the ultrafast carrier relaxation mechanism is essential for development of such devices. In semiconductor quantum wells, interface states and, in some cases, surface states strongly affect the carrier relaxation process. In this doctoral work we have studied the effect of surface and interface states on the carrier dynamics of III-V quantum wells. Carrier relaxation mechanism studies in quantum wells have been mostly carried out using the technique of time-resolved photoluminescence at low temperatures. At room temperature the photoluminescence intensity reduces markedly due to increased non radiative relaxation and therefore time resolved measurements with sub-ps resolution become almost impossible. On the other hand, transient reflectivity has no such constraints. However, extracting the carrier dynamics from transient

reflectivity data has been a challenge. In this work we have opted for femtosecond laser based pump probe reflectivity measurements because of its advantages. For this we have developed new methodologies for extracting carrier dynamics information from transient reflectivity measurements. In quantum wells, once the carriers are excited, the dominant recombination process is radiative recombination which occurs on time scales ranging from hundreds of picoseconds to a few nanoseconds. One way to obtain a much faster carrier relaxation is to introduce recombination centers in the vicinity of the quantum wells where photo-generated carriers can recombine non-radiatively. In a single quantum well, this can be achieved by reducing the top barrier layer down to a few nm such that an interaction between surface and quantum well states becomes possible. This can provide an alternate path for carrier relaxation. Indeed, it has been shown that, in such near-surface quantum wells, excited carriers can tunnel towards the surface and relax in few tens of picoseconds. Recently, ultrafast all-optical switching up to 10 Gbit/s has been demonstrated using a surface quantum well. In this work we have explored carrier dynamics in near surface $\text{GaAs}_{0.86}\text{P}_{0.14}/\text{Al}_{0.7}\text{Ga}_{0.3}\text{As}$ single quantum wells using pump-probe transient reflectivity performed at room temperature. $\text{GaAsP}/\text{AlGaAs}$ is one of the successful materials used to build high-power emitters in the 800 nm wavelength range and mode-locked vertical cavity surface emitting lasers. Tunneling towards surface can lead to interesting coherent phenomena also. There have been several studies on tunneling of carriers in asymmetric double quantum wells. The observation of beating in such systems shows that the tunneling process involves coherent carriers. Although the mechanism of carrier tunneling in near-surface single quantum wells has been shown to be similar to that in asymmetric double quantum wells at low temperature, so far coherent interactions have not been reported in near-surface quantum wells. We have demonstrated tunneling assisted quantum beats in a $\text{GaAsP}/\text{AlGaAs}$ near-surface single quantum well and interestingly the

phenomenon is observable at room temperature. These transient reflectivity studies on single quantum well showed that the carrier dynamics was strongly affected by the presence of interfaces. In a quantum well multiple interfaces are present. Therefore, to study the effect of the interface we have used an AlGaAs-GaAs heterostructure where only one interface exists at the GaAs-AlGaAs junction. In a heterostructure, the built-in field between two layers can result in the formation of a triangular well at the interface. Photoexcited carriers generated in the GaAs layer drift towards the triangular well under the influence of the built-in electric field and relax there. Ultrafast carrier relaxation studies on AlGaAs-GaAs heterostructures have been reported at low temperatures again using time-resolved photoluminescence. At room temperature, some measurements using transient reflectivity have been reported, but the isolation of carrier dynamics of the two-dimensional electron gas has been a challenge since the transient reflectivity signal contains contributions from various layers in the multilayer structure. We have developed a technique which allows unambiguous extraction of individual layer contributions to the transient reflectivity signal. To summarize the main results from the above studies we have shown that in a near-surface GaAsP/AlGaAs single quantum well, the room temperature relaxation time of the photoexcited carriers in the quantum well reduces to 1ps due to the proximity of the surface to the quantum well. We have proved that this fast relaxation time is caused by tunneling of holes from the quantum well towards the surface which also leads to the observed quenching of photoluminescence. We have also shown that if two particular hole states are excited simultaneously, a tunneling assisted quantum beating can be observed at room temperature. This result is of interest in obtaining coherent control of carriers at room temperature. We have also shown that the formation of a two dimensional electron or hole gas at an AlGaAs/GaAs interface not only leads to a faster relaxation of carriers excited in the GaAs layer but also makes the excitonic recombination dominate over the

donor-to-acceptor pair recombination as compared to bulk GaAs. These results have provided a greater understanding of the ultrafast carrier relaxation in III-V quantum wells. Moreover, the new techniques developed in this thesis are expected to be very useful for ultrafast carrier dynamics studies in multilayer nanostructures.

Thesis Outline:

The outline of thesis is as follows.

Chapter 1: Introduction

In chapter the optical properties of semiconductor nanostructures are discussed briefly. This chapter also includes a brief description of fast optical and optoelectronic devices based on these structures. The role of ultrafast spectroscopic studies in developing an understanding of the carrier relaxation mechanisms in these materials is discussed. The various ultrafast processes and their time scales have been described. The motivation for choosing the specific problems addressed in this doctoral work are discussed with reference to the information already available in literature. At the end a chapter wise summary of thesis is given.

Chapter 2: Experimental Techniques

Chapter 2 describes the samples and the experimental techniques used for the work presented in this thesis. The time-resolved pump probe reflectivity setup with a 100 femtosecond (fs) laser is described in detail. Low temperature measurements were found to be not repeatable at first. This problem was investigated and it was found that a condensate film growing on the sample surface was causing modulations on the true transient reflectivity signal. This was solved by introducing a metal shield around the sample. A brief description of the standard photoluminescence and photorefectance techniques is also included in this chapter.

Chapter 3: Effect of Excited Carriers on Transient Reflectivity in GaAs

In chapter 3, various processes which cause a reflectivity change in GaAs occurring due to excited charge carriers have been described. These include band filling, band gap renormalization and free carrier absorption. The relative contribution of these processes to the change in the refractive index at different carrier densities has been evaluated. It is shown that at low intensities the only significant mechanism is band filling. Therefore all measurements have been done in this regime, as the analysis become complicated when multiple processes are present.

Chapter 4: Carrier Dynamics in a Near-Surface Quantum Well

Near-surface quantum wells have a thin top barrier. Consequently, photoexcited carriers generated in the quantum well can easily tunnel to the top surface. We have used time-resolved reflectivity to investigate room temperature carrier dynamics in a near-surface single GaAsP/AlGaAs quantum well and the results are described in chapter 4. We have been able to measure and analyze very low magnitude sub-ps oscillations superimposed on the slower bi-exponential transient reflectivity decay. These oscillations are attributed to tunneling assisted coherent beating of quantum well hole states with the surface states. The observed beating signal has a period of 120 ± 6 fs. We have also studied the dependence of decay of coherence on the excited carrier density and have found that the dephasing rate increases nearly linearly with the increase in the excitation fluence. This demonstration that a coherent interaction between surface state and quantum well states can exist even at room temperature could open up the possibility of coherent manipulation of tunneling carriers in quantum well.

Chapter 5: Carrier Dynamics in an AlGaAs-GaAs Heterostructure at Low Temperature

In chapter 5 studies on the role of interface states on the photoexcited carrier dynamics of a heterostructure at low temperature are described. In the studies done on quantum wells, described in chapter 4, it was realized that the AlGaAs/GaAs interface also plays a strong role in the carrier dynamics. Hence, we have selected an $\text{Al}_{0.7}\text{Ga}_{0.3}\text{As}$ -GaAs heterostructure which is similar to the structure on which the single-quantum well was grown. In this heterostructure, a triangular well is formed near the interface due to the built-in electric field and a two-dimensional electron gas (2DEG) forms. By exciting at wavelengths that correspond to different resonances in GaAs, we have been able to track the carrier drifts and their decay. We have shown that the drift of carriers towards the interface can be recognized by modulations in the early part (sub-ps) of the degenerate transient reflectivity decay. Exciton formation is observed in this heterostructure despite the presence of a built-in field. This is possibly due to the stronger confinement of electrons in the triangular quantum well.

Chapter 6: Dynamics of Carriers in AlGaAs-GaAs Heterostructure

Chapter 6 describes the room temperature degenerate transient reflectivity measurements on AlGaAs/GaAs heterostructures. For an n-doped AlGaAs grown on undoped GaAs, a 2DEG forms at the GaAs side of the interface. However, since the lowest energy transitions in GaAs and 2DEG are very close, the measured transient reflectivity has contributions from excited carriers in both the 2DEG layer as well as the GaAs layer. So far there was no method available to allow unambiguous separation of the contributions from the 2DEG and bulk GaAs layers of the heterostructure. In this work we have developed a new technique which allows isolation of individual layer contributions to the transient reflectivity by suitably

choosing the excitation wavelength. This utilizes the fact that there are certain wavelengths at which the contributions to the total change in the reflectivity from all layers except one cancels out. The applicability of this technique is demonstrated in two heterostructure samples, one having a two-dimensional electron gas and the other one with a two-dimensional hole gas (2DHG). It is also shown that the carrier lifetime in the 2DEG reduces as the triangular quantum well becomes more shallow.

Chapter 7: Conclusion and Future Scope

The concluding chapter, summarizes the main results of this doctoral work. A coherent interaction has been demonstrated between surface states and hole states of a near-surface single GaAs_{0.86}P_{0.14}/Al_{0.7}Ga_{0.3}As quantum well. This opens up an area to explore coherent manipulation of tunneling carriers. Further, a new method has been developed to extract the carrier dynamics of two-dimensional electron and hole gases in AlGaAs/GaAs heterostructures by degenerate transient reflectivity measurements at appropriate wavelengths. This technique enables determination of the sign as well as the relative magnitude of individual contributions from various layers to the total transient reflectivity signal, which is essential for understanding carrier dynamics in any multilayer sample.

LIST OF FIGURES

Figure

1.1	Density of states for bulk (3D) and quantum well (2D) as a function of energy.	6
1.2	Tunneling of electron and hole wave-function in case of a finite and infinite quantum well.	7
1.3	Band bending near interface in an AlGaAs-GaAs heterostructure. AlGaAs is n-doped.	7
1.4	Band bending when the AlGaAs is p-doped in the AlGaAs-GaAs heterostructure.	8
1.5	Band bending diagram near surface states in case of n-type doped semiconductor. The band bending becomes flat away from the surface.	8
1.6	Carrier excitation mechanism (a) band to band absorption by a single photon (b) band to band absorption of two photons (c) free carrier absorption within band.	9

1.7	Carrier scattering (a) carrier-carrier scattering to thermalize to fermi-dirac distribution (b) carrier-phonon scattering	10
1.8	Carrier recombination (a) band to band radiative recombination (b) defect and surface recombination.	11
2.1	Layer structure of samples (a) near-surface quantum well (NSQW) (b) buried quantum well (BQW) (c) AlGaAs(n-doped)-GaAs heterostructure (d) AlGaAs(p-doped)-GaAs heterostructure.	17
2.2	Schematic showing photoluminescence(PL) measurement setup. . .	19
2.3	Room temperature photoreflectance (PR) experiment schematic (L-Lens, MCH-Monochromator, M-Mirror, PD-Photodiode and LIA-Lockin-amplifier). The wavelength of pump laser used here is generally less than 400 nm.	20
2.4	Time-resolved degenerate pump-probe reflectivity setup. The laser used is femtosecond laser. (BS-Beam splitter, C-Chopper, L-Lens, WP-Waveplate, M-Mirror, PD-Photodiode, P-Polarizer, A-Aperture and LIA-Lockin-amplifier).	22

2.5	(a) Two representative scans of transient reflectivity signal from GaAsP/AlGaAs quantum well at room temperature (300 K) under identical conditions. The data was always repeatable within the experimental errors. (b) Two representative scans of transient reflectivity signal ($\Delta R/R$) of GaAsP/AlGaAs quantum well at 50 K. The time evolution of the signal was different on each scans.	24
2.6	The variations in the linear reflectivity from various materials at 50 K in the cryostat. The incident He-Ne laser power was 0.8 mW. For ease of viewing, the reflected signals have been scaled by suitable multiplier.	25
2.7	Schematic of multiple reflection from a thin film-substrate system. l is the thickness of thin film. n' and n are the refractive index of the thin film material and the sample respectively.	26
2.8	The calculated variation of linear reflectivity from a sample and a thin film on its top surface with time using Eq.2.1: thick line - constant g and no absorption in the film ($\alpha = 0$), thin line - constant g with finite absorption in the film and dashed line - linearly decreasing g and $\alpha = 0$	27

2.9	The variation of the measured linear reflectivity of bulk GaAs sample. The calculated curve is the best fit with Eqn. 2.1 neglecting any absorption in the film. For ease of viewing, the reflected signal has been normalized by dividing it with its maximum value. The refractive index of the GaAs used in fitting as well as the best fit parameters are given in Table 1.	28
2.10	Measured time dependence of the linear reflectivity of a glass plate in a optical cryostat at temperature 50 K in much longer time of observations. For ease of viewing, the reflected signal has been normalized by dividing it with its maximum value.	29
2.11	The temperature dependence of period of linear reflectivity oscillations measured from bulk GaAs.	31
2.12	Reflectivity signal for glass at 50 K under different nitrogen purging times as well as with an additional metal shielding around the sample. All signals have been scaled by suitable multiplier for ease of viewing.	32
2.13	Two representative scans of transient reflectivity of GaAsP/AlGaAs quantum well at 50 K after conditioning the cryostat and with the metal shield a around the sample.	32
3.1	The band structure of GaAs at room temperature. <i>lh</i> stands for light hole and <i>hh</i> stands for heavy hole. <i>SO</i> is spit-off band.	37

3.2	Calculated change in refractive index as function of photon energy due to band filling effect in GaAs. The results are shown at four different carrier densities.	39
3.3	The change in refractive index due band filling effect in GaAs as a function of carrier density at three different wavelengths.	39
3.4	Calculated change in refractive index as function of photon energy due to band gap renormalization in GaAs. The results are shown at different carrier densities. The band gap renormalization starts to contribute above critical density which is $5 \times 10^{16} \text{ cm}^{-3}$ for GaAs.	41
3.5	The band gap renormalisation induced change in refractive index in GaAs as a function of carrier density at three different wavelengths.	41
3.6	The refractive index change as function of photon energy due to free carrier absorption effect in GaAs. The results are shown at different carrier densities.	42
3.7	Change in refractive index due to free carrier absorption in GaAs as a function of carrier density at three different wavelengths.	43
3.8	Calculated change in refractive index due to all three effects at carrier density $2 \times 10^{17} \text{ cm}^{-3}$ as function of energy due to combinations of effect in GaAs. All effects are shown individually and combined is also plotted.	44

3.9	Calculated change in refractive index in GaAs as function of energy due to combinations of effect. The results are shown at different carrier densities.	45
3.10	The change in refractive index (a) with carrier density at three different wavelengths in GaAs due to sum of all effects (b) the same refractive index change at zoomed scale which shows linear variation.	45
3.11	Transient reflectivity signal from GaAs at 768 nm at different pump intensity.	46
3.12	The initial peak (ΔR_{max}) of transient reflectivity signal from GaAs at 768 nm as function of pump intensity.	47
3.13	(a)Transient reflectivity signal from GaAs at 800 nm at different pump intensity. (b)The initial peak (ΔR_{max}) of transient reflectivity signal from GaAs at 800 nm as a function of pump intensity.	47
4.1	Layer structure of the single quantum wells. $d= 5\text{nm}$ for near-surface quantum well (NSQW) and $d= 50 \text{ nm}$ for buried quantum well (BQW).	52
4.2	Photoluminescence (PL) spectrum of BQW at room temperature. The observed spectrum is resolved into three peaks shown by dashed and dotted lines. The transition corresponding to each peak is also indicated.	52

4.3	Photoreflectance spectrum of the NSQW and BQW. The energy levels of the GaAs substrate and barrier AlGaAs are also shown. FKO: Franz-Keldysh oscillations.	53
4.4	Energy levels: A schematic diagram showing the lowest energy levels and the transition energies in eV for the NSQW. The error in the energy of transitions is ± 2 meV estimated by the fitting of photoreflectance spectrum. <i>e1</i> : first electron level, <i>lh1</i> : first light hole, <i>hh1</i> : first heavy hole level, <i>hh2</i> : second heavy hole level, SS: surface state (approximate position). The energy levels of BQW are same except that the surface is too far away and the SS-hole transitions would be much less prominent.	53
4.5	Transient reflectivity signal from (a) NSQW and (b) BQW. The laser photon energy is 1.577 eV and the pump fluence incident at sample was $26 \mu\text{Jcm}^{-2}$ (intensity was kept 2.1 kWcm^{-2}).	55
4.6	The wave functions corresponding to different hole states in the NSQW showing the higher tunneling of <i>lh1</i> and <i>hh2</i> as compared to <i>hh1</i>	56
4.7	The transient reflectivity signal of NSQW. (a) The dots are the as measured $ \Delta R/R $ and the line is the best fit to the data after 0.15 ps with a single exponential decay function. (b) The time dependence of \Re obtained from the experimental data. The solid line is the best fit to the data with <i>F</i>	57

4.8	The FFT of the data after subtraction of the exponential decay function from experimental data (\mathfrak{R}).	58
4.9	Same as Fig. 4.7 but for photon energy 1.6 eV. Inset shows the data after subtracting best fitted single exponential decay function.	60
4.10	Transient reflectivity for sample NSQW at photon energy 1.55 eV. Inset shows the data after subtracting best fitted single exponential decay function.	60
4.11	Same as Fig. 4.7 but for sample BQW at photon energy 1.577 eV. Inset shows the data after subtracting best fitted single exponential decay function.	61
4.12	The dependence of the observed beating on the excitation fluence. Solid lines are best fit to the experimental data with the Eq.4.1.	63
4.13	The dependence of beating oscillations on the pump fluence. Solid circles is the amplitude (A) and open circles are the $1/\tau$. The lines are the linear best fit to the data.	63
5.1	Sample structure of the $\text{Al}_{0.7}\text{Ga}_{0.3}\text{As}$ -GaAs heterostructure.	68
5.2	Band bending diagram of the $\text{Al}_{0.7}\text{Ga}_{0.3}\text{As}$ -GaAs heterostructure. CB and VB are the conduction and valence bands respectively.	68

5.3	Photoluminescence spectrum of $\text{Al}_{0.7}\text{Ga}_{0.3}\text{As}$ -GaAs heterostructure at 11 K. Excitation wavelength is 632.8 nm.	69
5.4	Photoluminescence signal measured from bulk GaAs at 11K. Excitation laser wavelength was kept at 632.8 nm.	70
5.5	Photoluminescence signal from $\text{Al}_{0.7}\text{Ga}_{0.3}\text{As}$ -GaAs heterostructure showing PL from GaAs features at 11K. The photoluminescence from bulk GaAs is also shown at the same temperature. The excitonic and Donor to Acceptor (DAP) peaks are shown.	71
5.6	Photoluminescence signal from $\text{Al}_{0.7}\text{Ga}_{0.3}\text{As}$ -GaAs heterostructure showing PL from GaAs features at 40 K. The photoluminescence from bulk GaAs is also shown at the same temperature. The excitonic and Donor to Acceptor (DAP) peaks are shown.	71
5.7	Area under curve plotted against input pump power for excitonic as well as DAP peak at 11 K. Solid line is fit to the curve using Eqn. 5.1. Excitonic recombination showed linear variation whereas DAP showed nonlinear variation with input pump power.	72

5.8	Contribution of 2DEG and defect state to the low temperature photoluminescence spectrum of the $\text{Al}_{0.7}\text{Ga}_{0.3}\text{As}$ -GaAs heterostructure at 11 K. The two peaks above ~ 840 nm are due to free carriers and DAP recombination as shown in Fig. 5.6. The broad peak below 870 nm can be resolved in two peaks. The peak at nearly 890 nm is attributed to 2DEG recombination and that at ~ 905 nm to the recombination from defect states.	74
5.9	The variation of peak wavelength of two-dimensional electron gas and defect state peaks with excitation power at 11 K; circles - 2DEG peak and squares - defect state peak.	74
5.10	Transient reflectivity signal at 40 K measured on $\text{Al}_{0.7}\text{Ga}_{0.3}\text{As}$ -GaAs heterostructure at three different wavelengths.	75
5.11	Photoluminescence spectrum of $\text{Al}_{0.7}\text{Ga}_{0.3}\text{As}$ -GaAs heterostructure measured at different temperatures. DAP peak becomes weaker with increasing temperature. It completely disappears at 100 K.	76
5.12	Transient reflectivity signal from $\text{Al}_{0.7}\text{Ga}_{0.3}\text{As}$ -GaAs heterostructure at room temperature at 890 nm. No transient signal is observed. . .	77
5.13	Transient reflectivity signal measured at 100 K from $\text{Al}_{0.7}\text{Ga}_{0.3}\text{As}$ -GaAs heterostructure at wavelength 830 nm.	78

5.14	Transient reflectivity signal measured from $\text{Al}_{0.7}\text{Ga}_{0.3}\text{As}$ -GaAs heterostructure and GaAs at room temperature at 800 nm. The signal from heterostructure showed modulation.	79
5.15	The figure shows the that when femtosecond laser falls on the sample, electron hole pairs are generated in GaAs. Some of the excited electrons in conduction which are near the interface will move towards the triangular well and accumulate there. The holes will be moving away from the interface.	79
6.1	Transient reflectivity signal measured at different wavelengths for the n-type heterostructure. Note that the signal at 836 nm has been multiplied by three for clarity.	84
6.2	Transient reflectivity signal from bulk GaAs at three different wavelengths. Note that the signal at 836 nm has been multiplied by three for clarity.	85
6.3	(a) Schematic of the n-type heterostructure. (b) The band bending diagram. n_1 , n_2 and n_3 are the refractive indices for AlGaAs, 2DEG region and GaAs respectively. d_1 and d_2 are the thickness of the top AlGaAs layer and the 2DEG layer respectively.	85
6.4	The linear reflectivity spectrum of the $\text{Al}_{0.7}\text{Ga}_{0.3}\text{As}$ (n-doped)-GaAs heterostructure. Black line: measured linear reflectivity, pink thin line: best fit to data using Eqn. 6.2.	87

6.5	The calculated variation of \mathfrak{R}_2 (blue dotted line) and \mathfrak{R}_3 (red dashed line) with the wavelength of light. Vertical lines show the wavelengths at which the TR results are reported.	87
6.6	TR signal from $\text{Al}_{0.7}\text{Ga}_{0.3}\text{As}$ (n-doped)-GaAs heterostructure at three different wavelengths. Note that the signal at 836 nm has been multiplied by three for clarity.	89
6.7	Transient reflectivity signal at 786 nm from bulk GaAs and $\text{Al}_{0.7}\text{Ga}_{0.3}\text{As}$ (n-doped)-GaAs heterostructure sample. Inset shows the same TR signal zoomed near zero delay.	90
6.8	Transient reflectivity from bulk GaAs and $\text{Al}_{0.7}\text{Ga}_{0.3}\text{As}$ (n-doped)-GaAs measured at 800 nm. Note that the $\Delta R/R$ for the heterostructure sample recovers much faster. Inset shows the same TR signal zoomed near zero delay.	91
6.9	(a) Schematic of the p-type heterostructure. (b) The band bending diagram. The refractive indices for AlGaAs, 2DHG region and GaAs n_1 , n_2 and n_3 respectively. The thickness of the 2DHG layer is obtained by the same technique as used for 2DEG in case of n-type heterostructure.	92
6.10	Transient reflectivity from $\text{Al}_{0.62}\text{Ga}_{0.38}\text{As}$ (p-doped)-GaAs heterostructure at different wavelengths. Note that the $\Delta R/R$ recovers to zero for 774 nm.	92

6.11	The wavelength dependence of \mathfrak{R}_2 and \mathfrak{R}_3 for the $\text{Al}_{0.62}\text{Ga}_{0.38}\text{As}$ (p-doped)-GaAs heterostructure (similar to Fig. 6.5 for the n-doped heterostructure).	93
6.12	Time resolved reflectivity change within 1 ps for the $\text{Al}_{0.7}\text{Ga}_{0.3}\text{As}$ -GaAs n-type heterostructure at different pump intensities. Excitation wavelength is 800 nm.	94
6.13	Full time resolved reflectivity curves from $\text{Al}_{0.7}\text{Ga}_{0.3}\text{As}$ -GaAs n-doped heterostructure at 800 nm at different pump intensities. The signal recovers almost completely in 150 ps.	95
6.14	(a) Single exponential fit to transient reflectivity curve at pump intensity of 2.1kWcm^{-2} which gives a recover time constant of 59.8 ps. The wavelength kept is 800 nm. Similar fit are done at other pump intensities. (b) Dependence of transient reflectivity recovery time on pump intensity for the n-doped heterostructure. Error bars are estimated from the fitting error.	95
6.15	(a) Shorter decay time obtained from double exponential decay fit to the transient reflectivity curve from GaAs at different pump intensity. (b) The second decay time which is obtained from double exponential decay fit to the transient reflectivity curve from GaAs at different pump intensity. The inset in both (a) and (b) shows one of the fit at pump intensity of 2.1kWcm^{-2} . The wavelength kept is 786 nm.	97

6.16	Change in band bending with photoexcited carriers in the $\text{Al}_{0.7}\text{Ga}_{0.3}\text{As}(\text{n-doped})\text{-GaAs}$ heterostructure. The triangular well formed near the interface become shallow with photoexcitation. CB and VB are the conduction and valence bands respectively.	97
6.17	Time resolved reflectivity from $\text{Al}_{0.7}\text{Ga}_{0.3}\text{As}(\text{n-doped})\text{-GaAs}$ heterostructure at 786 nm at different pump intensity. The data is fit to a two exponential decay with opposite sign.	98
6.18	(a) Recombination time vs pump intensity for GaAs contribution obtained from double fit of transient reflectivity from $\text{Al}_{0.7}\text{Ga}_{0.3}\text{As}(\text{n-doped})\text{-GaAs}$ heterostructure at 786 nm as shown in Fig. 6.17. (b) Recombination time vs pump intensity for the two-dimensional electron gas contribution.	98
6.19	Transient reflectivity signal from 2DHG and 2DEG. The measurements has been performed at 774 nm on $\text{AlGaAs}(\text{p-doped})\text{-GaAs}$ heterostructure to measure the decay of 2DHG and at 800 nm on $\text{AlGaAs}(\text{n-doped})\text{-GaAs}$ heterostructure sample for measuring the decay of 2DEG. The inset shows the same data at zoomed scale. . .	99
6.20	Photoluminescence spectrum of $\text{AlGaAs}(\text{p-doped})\text{-GaAs}$ heterostructure and $\text{AlGaAs}(\text{n-doped})\text{-GaAs}$ heterostructure sample. The photoluminescence peak from exciton, DAP and defect state comes nearly at same position for both samples. The 2DHG peak is blue shifted by nearly 14 nm compared with 2DEG peak.	100

LIST OF TABLES

Table

- 2.1 The estimated values of refractive index n' and growth rate g in nm/min of the film condensing on different materials. Approximate values of real and imaginary part of refractive index n and k used in the calculation is also listed in the table along with average reflectivity R . The wavelength is 632.8 nm. 29

Chapter 1

Introduction

Semiconductors start showing a strong change in their optical properties when their sizes are reduced below tens of nm (\sim Bohr radius) [1–4]. The resonance (energy) shifts towards the blue due to quantum confinement. Photoluminescence emission become narrower and stronger. These properties have led to widespread use of semiconductor nanostructures in optoelectronic devices [2–5]. For example, confinement in one dimension leads to structures like quantum wells and superlattices. The now widely used diode lasers have quantum wells as the active medium [6, 7]. Confinement in two dimensions gives quantum wires which are beginning to be used in transistors and sensing applications [8, 9]. Confinement in three dimensions leads to formation of quantum dots. Quantum dots are currently being investigated for very interesting applications in cryptography and as quantum bits for quantum computing [10, 11]. The reduction in dimension has another advantage of making the time response of the material much faster [12–17]. This has led to a number of electronic, optoelectronic and optical devices [15–19]. Ultrafast optical spectroscopy of nanostructures provides an insight into the physical processes and carrier dynamics which is essential for designing structures for fast devices [20, 20–22].

Nanostructures of excellent epitaxial quality can be grown with III-V semiconductor, using techniques like metal-organic chemical vapour deposition(MOCVD) and molecular beam epitaxy (MBE) [23–25]. Some of the most popular material combinations are AlGaAs/GaAs, InGaAs/GaAs, GaAsP/AlGaAs and InAs/InP [26]. In this class of materials lattice mismatch is very small which results in a low interface state density [23, 24, 26, 27]. Due to this, devices based on these materials have higher electron mobility and better current carrying capacity as compared to Si and Ge based device [28]. Moreover, many of these materials have a direct band gap and are therefore used as efficient emitters in the near infrared and short-wavelength infrared range [29–31].

Photoexcited carriers in III-V materials relax through various processes with time scales ranging from few tens of femtoseconds (thermalization, scattering, coherent process) to picoseconds (intra-band relaxation, scattering, recombination) and nanoseconds (inter-band recombination) [21, 22, 32, 33]. This relaxation dynamics is strongly affected by material parameters (e.g doping, crystalline quality, temperature) as well as the structural properties (e.g. thickness of a quantum well, diameter of a quantum dot) [22].

In this work we have studied how the surface and interface affect the dynamics of excited carriers generated by ultrafast laser pulses in III-V semiconductor quantum wells. Two types of quantum wells have been studied, a near surface GaAsP/AlGaAs single quantum well and a triangular well formed at the interface of an AlGaAs-GaAs heterostructure.

1.1 Motivation

Quantum wells are created by sandwiching a thin low band gap material layer between two large band gap layers resulting in two dimensional confinement of carriers. The quantum well width has to be less than the Bohr radius of the material (\sim

15 nm for GaAs) for quantum confinement to be effective. Due to the confinement, photogenerated carriers live longer and emission due to recombination has a narrower spectrum. This is useful for devices like diode laser [6, 29]. However, the long lifetime limits its use for applications like fast detectors and switches. One way to make the carrier recombination faster is to reduce the confinement by making the barrier on one side very thin resulting in a near-surface or surface (no barrier) quantum well [34, 35]. If the barrier is thin enough, photogenerated carriers can tunnel out from the quantum well and recombine through the mid-gap surface states [34, 36]. This process can be much faster than the radiative recombination. Fast switches based on surface quantum wells has been demonstrated in laboratory [37]. Therefore it is of interest to have a better understanding of the effect of the proximity of surface states on the carrier relaxation in a quantum well. For this work, we have used a $\text{GaAs}_{0.86}\text{P}_{0.14}/\text{Al}_{0.7}\text{Ga}_{0.3}\text{As}$ near-surface single quantum well. GaAsP/AlGaAs quantum wells are widely used for making diode lasers at 800 nm and our motivation was to investigate the possibility of obtaining ultrafast carrier relaxation in this material. The $\text{GaAs}_{0.86}\text{P}_{0.14}/\text{Al}_{0.7}\text{Ga}_{0.3}\text{As}$ quantum well selected for our work had a 5 nm thick top AlGaAs barrier and its photoluminescence was almost fully quenched.

Our interest was also to look into the possibility of observing coherent effects in this system. Simultaneous excitation of two transitions with a common level can lead to a coherent interaction like population beating [22, 38]. Ultrashort pulses have a wide enough spectrum to excite several close-lying transitions in a quantum well and coherent oscillations have been reported [38–40]. In superlattices, which are multiple quantum wells with very thin inter-well barrier, coherent interaction between carriers in neighbouring quantum wells have been reported [22]. To the best of our knowledge no coherent phenomenon has been observed in surface quantum wells. Our motive was to investigate what effect, if any, the nearness of the surface can have on any possible coherent process.

The second type of quantum well studied in this work was a triangular quantum well formed in an $\text{Al}_{0.7}\text{Ga}_{0.3}\text{As}(\text{n-doped})\text{-GaAs}$ heterostructure. AlGaAs-GaAs heterostructures are used in devices like metal-oxide semiconductor field effect transistor and high mobility transistors [41, 42]. In the heterostructure, an electric field is developed at the interface due to the difference between the band gaps of GaAs and AlGaAs and the difference in doping. This field causes a band-bending resulting in a triangular well at the interface [2, 43, 44]. Photo-excited carriers generated in GaAs near the interface of AlGaAs-GaAs will move towards the interface under the influence of this built-in electric field and get trapped in the triangular well. Such systems are called two-dimensional electron gas or two-dimensional hole gas depending on which type of carriers have been confined.

Carrier dynamics study of these two-dimensional system in a heterostructure is challenging because the two-dimensional electron gas has transition energies in the same spectral region as the underlying substrate. For example, at low temperatures, photoluminescence from an AlGaAs-GaAs heterostructure will have contribution from exciton, donor-to-acceptor pair recombination, other defect states in GaAs as well as recombination from the two-dimensional electron gas (2DEG) [45]. However, the photoluminescence from the two-dimensional electron gas is much weaker compared to other peaks. Time-resolved photoluminescence measurements are limited because of this [45–47]. At room temperature the 2DEG photoluminescence is practically absent. For any practical application, information on room temperature dynamics would be very useful, and hence this study on $\text{Al}_{0.7}\text{Ga}_{0.3}\text{As}(\text{n-doped})\text{-GaAs}$ heterostructure was taken up.

As already mentioned, in both the quantum well and 2DEG samples, the photoluminescence gets quenched at room temperature. Moreover the GaAs substrate in these samples is highly absorbing at the wavelengths of interest. Therefore, the transient reflectivity technique was selected for ultrafast carrier dynamics measure-

ments. This technique has the advantage of giving sufficiently large signals at room temperature as well as at low temperature. The time resolution is limited only by the laser pulse width. However, there are some constraints in using this technique for our samples. At the wavelengths of interest, there is always a large photo-carrier population generated in the GaAs substrate which can interfere in the identification of dynamics of the carriers in the quantum well or 2DEG. Most of the carrier dynamics studies on similar quantum wells and heterostructures have used photoluminescence measurement at low temperature with time resolution limited to ~ 10 ps [27]. Although, some transient reflectivity measurements have been reported [46, 48] the results are not full understood. Therefore, part of this work involved evolving new methodologies for extracting the required carrier dynamics information for transient reflectivity measurements.

1.2 Background

In this section, a brief discussion on optical properties of semiconductor nanostructure and ultrafast processes relevant to the work of the thesis is presented.

GaAs is a direct band gap semiconductor with zinc blende crystal structure [26]. In the quantum well, the energy levels get quantized due to confinement. The general density of states vs. energy diagram for bulk and quantum well is shown in Fig. 1.1. In real quantum well structures, the barrier potential is finite and the wave-functions of the confined carriers leak out of the well towards the barrier (Fig. 1.2) [1]. Moreover, at each heterojunction, the joining of two different semiconductors results in creation of new energy states near the interface which lie in the forbidden energy gap of either semiconductor [49–51]. A band bending occurs near the interface depending on the band gap of the two materials and the doping level [2, 43, 44]. Figure 1.3 shows the band bending in case of an AlGaAs(n-doped)-GaAs heterostructure [2, 43]. Because of this electrons excited on the GaAs

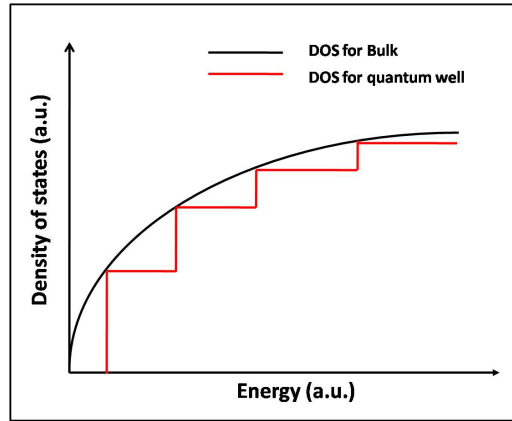


Figure 1.1: Density of states for bulk (3D) and quantum well (2D) as a function of energy.

side will move towards the interface and holes will move away. As can be seen a triangular well is formed in the conduction band near the interface and can confine the electrons [27, 52, 53]. If the AlGaAs is p-type doped the resulting band bending is shown in Fig. 1.4 and will result in trapping of holes in the triangular well formed at the interface. These trapped electron or holes have very high in-plane mobility, which can be of the order of $10^6 \text{cm}^2 \text{V}^{-1} \text{s}^{-1}$ [43, 54]. Devices like Metal Oxide Semiconductor Field Effect Transistor (MOSFET) and High Electron Mobility Transistor (HEMT) have made use of this high mobility for increased efficiency [41, 42].

Surface is defined as the place where the bulk material is truncated and the three-dimensional periodicity of the solid is broken. A two-dimensional periodicity is observed near the surface [50, 55–57]. The changed periodicity on the surface and the dangling bonds change the electronic structure of the surface compared to the bulk three-dimensional material inside. Surface states are formed due to this changed electronic structure [50, 55, 56]. The wave functions of these surface states are localized near the surface and decay exponentially into the solid in contrast to the Bloch waves propagating in the bulk solid. This exponentially decaying wavefunction gives energy levels in the forbidden gap of the projected bulk band structure. Surface

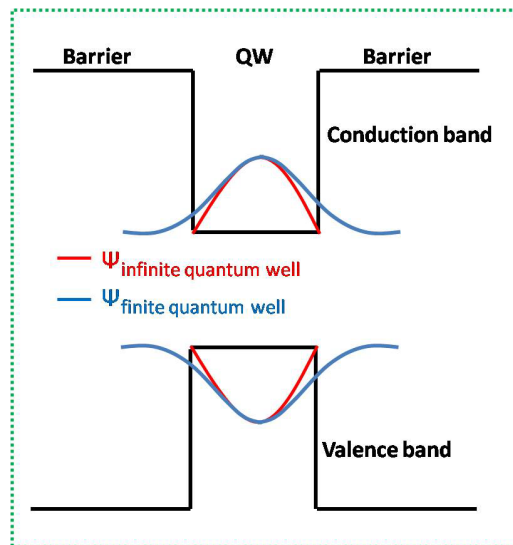


Figure 1.2: Tunneling of electron and hole wave-function in case of a finite and infinite quantum well.

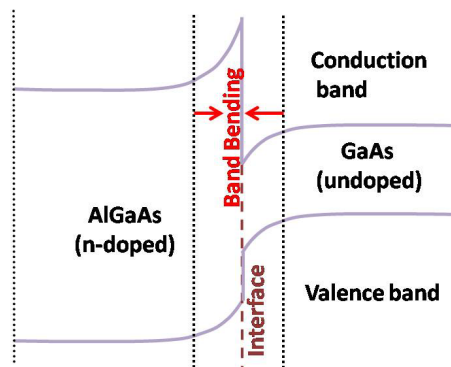


Figure 1.3: Band bending near interface in an AlGaAs-GaAs heterostructure. Al-GaAs is n-doped.

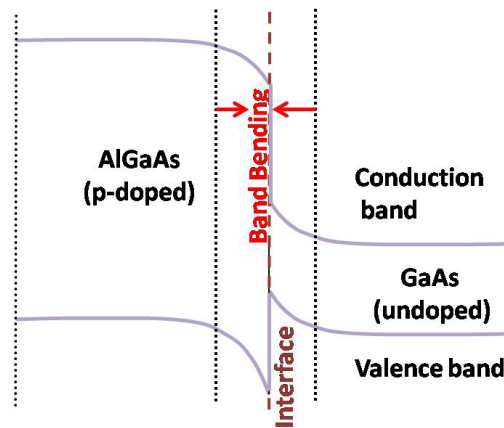


Figure 1.4: Band bending when the AlGaAs is p-doped in the AlGaAs-GaAs heterostructure.

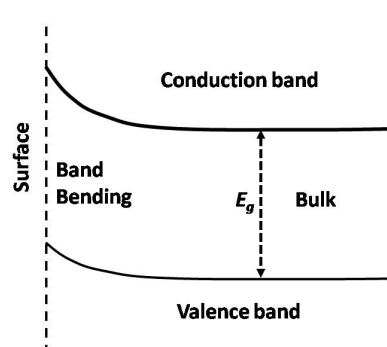


Figure 1.5: Band bending diagram near surface states in case of n-type doped semiconductor. The band bending becomes flat away from the surface.

states at the semiconductor surfaces shows donor or acceptor behaviour. Thus these states become charged. For surface region as a whole to remain electrically neutral the charged surface states produce a space-charge layer beneath the surface. This will result in band bending near the surface depending on whether the surface is donor like or acceptor like. Figure 1.5 shows the band bending near the surface in case of n-type doped semiconductor. The band bending is such that any excited or injected holes will be pushed towards the surface and electrons will move away from the surface.

In GaAs like semiconductor materials, the depth of surface states is a few nm

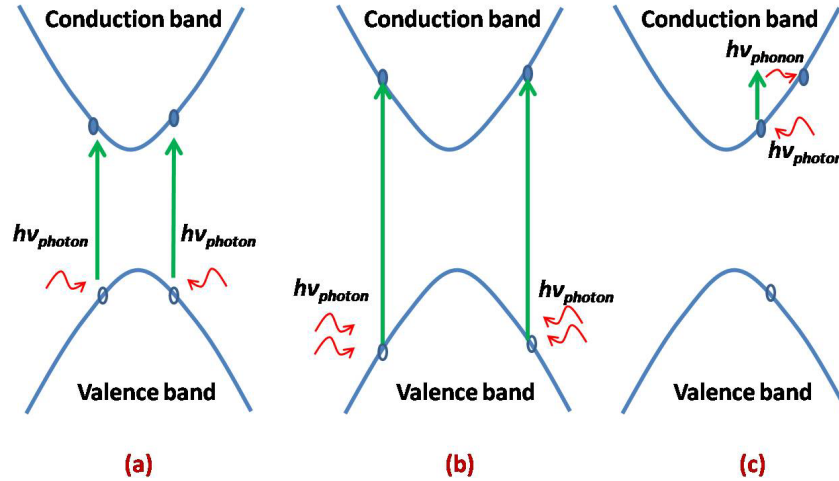


Figure 1.6: Carrier excitation mechanism (a) band to band absorption by a single photon (b) band to band absorption of two photons (c) free carrier absorption within band.

[50, 57]. The surface states start affecting the carrier dynamics in semiconductor quantum well once they are in close proximity with the quantum well [36, 58, 59]. The carriers can tunnel out of the quantum wells under the built-in electric field created due to the surface. This provides a faster alternative non-radiative recombination path [36]. This property of surface states becomes useful for applications like fast photodiodes, fast saturable absorbers [15, 16, 60, 61].

Figure 1.6 shows the possible mechanisms for generating photo-induced carriers in a semiconductor. The photoexcited carriers generated by ultrafast pulses undergo several stages of relaxation before reaching equilibrium. These include thermalisation and carrier recombination [21, 22, 32, 62–64]. Thermalization occurs due to carrier-carrier scattering (Fig. 1.7(a)) and causes a rapid dephasing of the induced coherence. In GaAs the dephasing time has been reported to be of the order of tens of fs [21, 22, 32, 62–64].

Once the carriers thermalize, the population distribution is given by the Fermi-Dirac distribution. Subsequently, carriers exchange energy with the lattice through carrier-phonon scattering (Fig. 1.7(b)) and reach the band edge. This process does

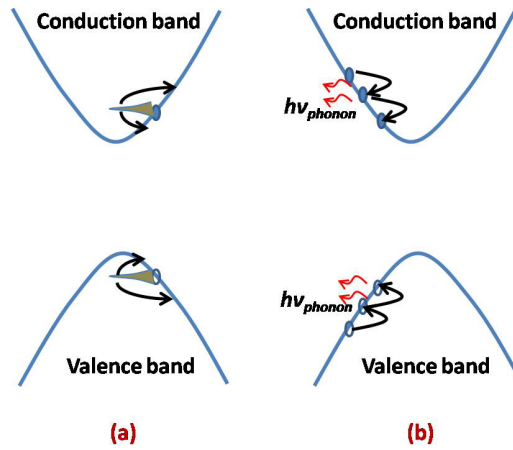


Figure 1.7: Carrier scattering (a) carrier-carrier scattering to thermalize to fermi-dirac distribution (b) carrier-phonon scattering .

not change the number of excited carriers. In GaAs this process takes several picoseconds [21,22,32,62–64]. Once the carriers reach the band edge, recombination becomes prominent. This reduces the excited carrier population. The electron and holes can recombine radiatively as shown in Fig. 1.8(a). For GaAs time scale for this radiative recombination is of the order of hundreds ps to nanoseconds (ns) [21, 22, 32, 62–64]. Carriers can also recombine non-radiatively within a few ps through the defect and surface states as shown in Fig. 1.8(b).

GaAsP/AlGaAs single quantum wells are in wide use as laser diodes [30, 65]. The doping of phosphorous shifts the emission to shorter wavelengths as compared to GaAs/AlGaAs quantum wells. Surface quantum wells of GaAsP/AlGaAs have been used as surface emitters [66, 67]. However, not much information is available for the ultrafast relaxation dynamics of these quantum wells. AlGaAs-GaAs heterostructures are a well studied material [46, 53, 68]. Time resolved photoluminescence measurements have been carried out at low temperatures using a streak camera with time resolution of ~ 30 ps [27]. Under photoexcitation the photoluminescence peak from the 2DEG shows a blue shift which recovers as the carriers recombine. The formation of 2DEG is reported to be ~ 50 ps and the decay to be in the range

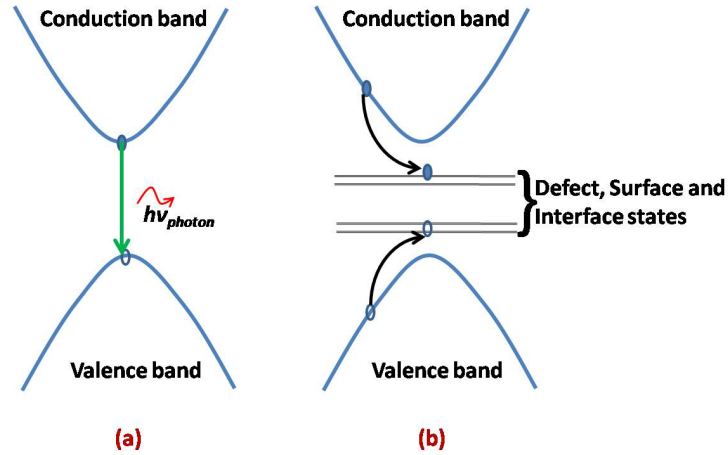


Figure 1.8: Carrier recombination (a) band to band radiative recombination (b) defect and surface recombination.

of 0.5 ns to a few ns [27]. Carrier dynamics at several temperatures and wavelengths have been studied using transient reflectivity [46,48]. However, not many room temperature studies on the ultrafast dynamics of AlGaAs-GaAs heterostructures have been reported. Thus, the results of this thesis will fill some of these information gaps.

1.3 Organisation of the thesis

In this thesis, the effect of surface and interface states has been studied using pump-probe transient reflectivity technique in III-V based semiconductor structures. **Chapter 2** describes the samples and experimental techniques used in this thesis. Pump-probe transient reflectivity at room temperature and at low temperature has been described in detail. Discussion on photoluminescence and photorefectance has also been included which has been used to characterize the sample. In **chapter 3**, a discussion on the various process which modify the refractive index of GaAs under photoexcitation has been done. The relative contribution of these processes to the change in the refractive index at different carrier densities has been evaluated. Also

the behavior of all these processes with intensity has been shown. This is followed by showing results on transient reflectivity signal from bulk GaAs.

Chapter 4 shows the carrier dynamics work performed on a $\text{GaAs}_{0.86}\text{P}_{0.14}/\text{Al}_{0.7}\text{Ga}_{0.3}\text{As}$ single quantum wells at room temperature. We have established that in a near-surface $\text{GaAs}_{0.86}\text{P}_{0.14}/\text{Al}_{0.7}\text{Ga}_{0.3}\text{As}$ single quantum well, photogenerated holes tunnel to the surface leading to a faster decay. Further, we have also demonstrated a coherent coupling between the quantum well states and surface states. This could lead to applications based on coherent manipulation of the tunneling carriers. **Chapter 5** shows the carrier dynamics measurements done on an $\text{Al}_{0.7}\text{Ga}_{0.3}\text{As}$ -GaAs heterostructure at low temperature. Low temperature Cw photoluminescence measurements are also discussed to characterize the various peaks. Time-resolved reflectivity has been performed at different wavelengths and temperature to study the carrier dynamics in $\text{Al}_{0.7}\text{Ga}_{0.3}\text{As}$ -GaAs heterostructure at low temperature. **Chapter 6** involves study of transient reflectivity measurements on $\text{Al}_{0.7}\text{Ga}_{0.3}\text{As}$ -GaAs heterostructure at room temperature. The 2DEG formation is clearly visible at low temperature from time resolved photoluminescence measurement. At room temperature carrier dynamics of 2DEG is difficult because of absence of photoluminescence. In this work we have shown that using transient reflectivity, the contribution of individual layer carrier dynamics from multilayer structure. Similar study on two-dimensional hole gas has been shown in this chapter. The dependence of recombination time in 2DEG forming in an $\text{Al}_{0.7}\text{Ga}_{0.3}\text{As}$ -GaAs heterostructure on the number density of photoexcited carriers has also been measured and discussed in this chapter. **Chapter 7** summarize the main results obtained in this thesis and future scope of the work done for this doctoral work.

1.4 Summary

In this chapter, the motivation for the research problems investigated in this thesis has been discussed. The chapter wise organisation is also described.

Chapter 2

Experimental Techniques

2.1 Introduction

This thesis deals with carrier dynamics of III-V semiconductor nanostructures in picosecond and sub-picosecond time scales. The main aim of this thesis is to study the effect of surface and interface on the carrier dynamics of nanostructures. Therefore, near-surface quantum wells and heterostructures have been selected for this study. Ultrafast carrier dynamics was investigated using femtosecond pump-probe transient reflectivity [20, 69, 70]. This technique has been chosen due to two reasons: first, the substrate layers of all samples were highly absorbing at the wavelengths of interest and second, transient reflectivity measurements, unlike the more popular photoluminescence measurements, can be performed at any temperature with the same degree of accuracy. This chapter gives the details of the samples used in this work, and a brief description of the transient reflectivity experiments as well as the photoluminescence and photorefectance techniques which were used to characterize the samples. The low temperature transient reflectivity experiments required more efforts to get reliable data, which have been described in detail.

2.2 Samples

All the quantum well and heterostructure samples used for this doctoral work have been grown by metalorganic chemical vapour deposition (MOCVD). In this technique, the precursors are ultra pure gaseous compounds of the materials to be deposited. The deposition occurs via a chemical reaction at the substrate surface. The gas pressure and temperature as well as the substrate temperature are precisely controlled to deposit an epitaxial layer of the desired material onto a semiconductor wafer. Multiple layers with good crystalline quality can be grown. The samples used in this study were provided by the Semiconductor Physics and Devices Lab, RRCAT.

These include $\text{GaAs}_{0.86}\text{P}_{0.14}/\text{Al}_{0.7}\text{Ga}_{0.3}\text{As}$ single quantum wells and $\text{Al}_{0.7}\text{Ga}_{0.3}\text{As}$ - GaAs heterostructures. The layer structure of all the samples is shown in Fig. 2.1. The single quantum wells consisted of a $\text{GaAs}_{0.86}\text{P}_{0.14}$ quantum well layer sandwiched between two $\text{Al}_{0.7}\text{Ga}_{0.3}\text{As}$ layers. The thickness of the quantum well was 11 nm. Two different quantum well structures were used. In one of the quantum well sample the thickness of the top $\text{Al}_{0.7}\text{Ga}_{0.3}\text{As}$ layer was 5 nm (Fig. 2.1(a)) and in the second structure the top layer thickness was 50 nm (Fig. 2.1(b)). Two different AlGaAs - GaAs heterostructures were also studied. Both had an n-type GaAs substrate with an undoped 250 nm thick GaAs layer grown over it. The $\text{Al}_{0.7}\text{Ga}_{0.3}\text{As}$ layer in one sample was n-doped with a thickness of 600 nm (Fig. 2.1(c)). In the second sample the $\text{Al}_{0.62}\text{Ga}_{0.38}\text{As}$ was p-doped and had a thickness of 650 nm (Fig. 2.1(d)). Since the samples, whether quantum wells or the heterostructures, were grown on n-doped GaAs substrates, reference measurements were also done on the bare n-doped GaAs substrates and undoped GaAs deposited on n-doped GaAs substrate.

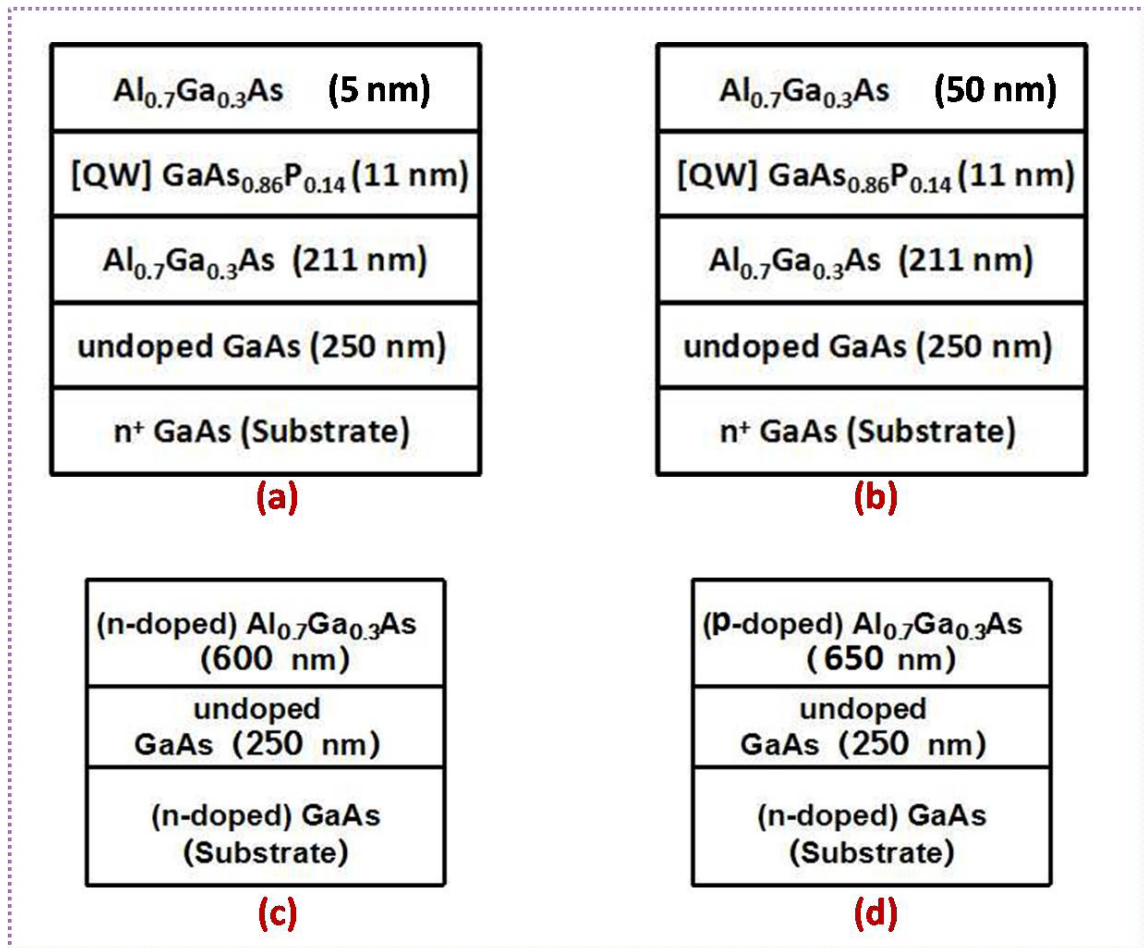


Figure 2.1: Layer structure of samples (a) near-surface quantum well (NSQW) (b) buried quantum well (BQW) (c) AlGaAs(n-doped)-GaAs heterostructure (d) AlGaAs(p-doped)-GaAs heterostructure.

2.3 Characterization

To ensure that the samples are of good quality and to determine the lowest resonances, photoluminescence (PL) and photorefectance (PR) spectra of samples were measured. Since these are standard techniques a brief description is provided below.

2.3.1 Photoluminescence

Photoluminescence (PL) spectrum is a powerful optical tool for characterizing semiconductors [1, 71]. It can be used to determine band gaps and also to detect presence of impurities and defects. A semiconductor material absorbs light of energy higher than its band gap, creating an electron hole pair. The excited electrons (holes) usually relax down to the edge of the conduction band (valence band) from where they recombine radiatively. This constitutes the photoluminescence emission. The photon emitted upon recombination corresponds to the energy difference between the valence and conduction bands, and is hence lower in energy than the excitation photon. In bulk semiconductors the photoluminescence spectrum allows determination of the bandgap. Further, the variation of photoluminescence strength with respect to input pump intensity can give information about whether the recombination is free carrier or excitonic in nature [72, 73]. In nanostructures, due to the quantum confinement, the energy levels become discrete and it is possible to have photoluminescence emission corresponding to recombination of more than one pair of electron-hole states (from discrete energy levels).

The schematic for photoluminescence measurement used in this thesis is shown in Fig. 2.2. The excitation source can be chosen between a He-Ne laser at 632.8 nm, a He-Ne laser at 543 nm and a diode laser at 405 nm. The sample is mounted in a closed-cycle optical cryostat which can go down to a temperature of 10 K. The emitted PL is collected using a suitable lens combination and focused on to a fiber

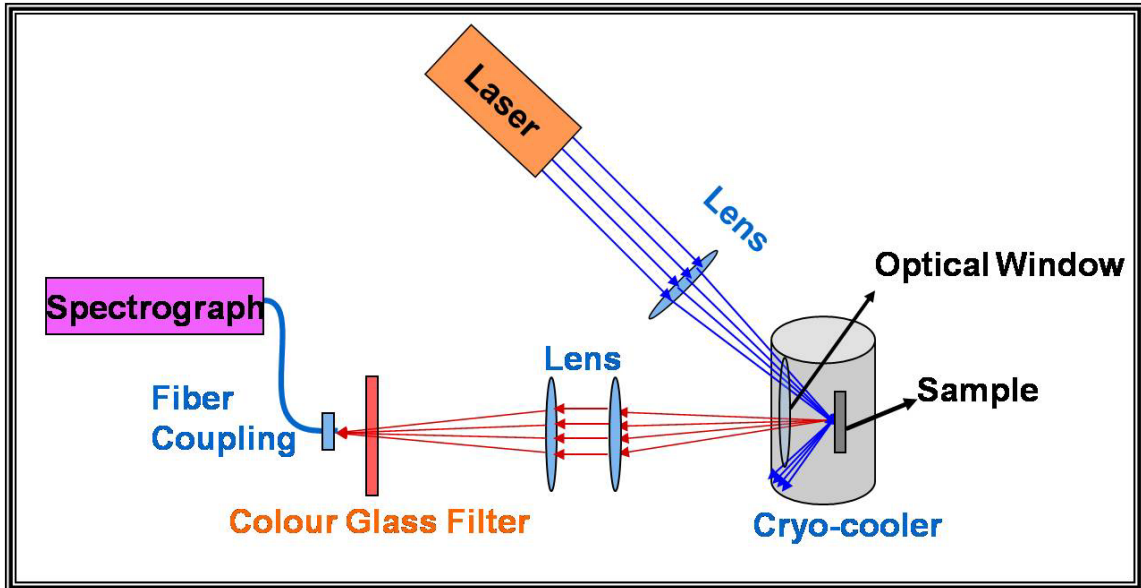


Figure 2.2: Schematic showing photoluminescence(PL) measurement setup.

-coupled spectrograph. Appropriate filters are used for blocking the scattering of the pump laser.

2.3.2 Photoreflectance

Photoreflectance (PR) is also an extremely valuable technique for optical characterization of semiconductor structures [74, 75]. Photoreflectance involves the measurement and interpretation of changes in the optical response (reflectivity) of a sample by modulating its electric field. This field is caused by photoexcited electron-hole pairs created by a pump source which is modulated in time. The measurement procedure results in sharp derivative-like spectral features at the wavelengths where inter-band transitions are present. The PR spectrum reveals the features of the structure from the different resonances present in the sample. The setup schematic is shown in Fig. 2.3. PR results reported in this work were provided by the Semiconductor Physics and Devices Lab, RRCAT.

once again before being directed to the sample via beam splitter (BS2) and mirror M3 (Fig. 2.4). This configuration prevents delay stage movement induced misalignment of probe beams in both vertical and horizontal planes. Since the beam passes twice through the retroreflector, a movement of d distance by the retroreflector makes the laser pulse travel an additional $4d$ distance and a corresponding time delay is introduced with respect to the pump beam. The time matching between pump and probe laser pulses is done by a second harmonic autocorrelator technique by using a beta barium borate (BBO) crystal. Both pump and probe beams are then focused and spatially overlapped on the sample by lens L3. The angle between the two beams is kept approximately 10 degrees. The size of pump beam is controlled by a telescopic lens arrangement in the pump beam path using lens L1 and L2. Lens L2 is kept on a linear manual translation stage for beam diameter control. On the sample, the size of probe beam is nearly $25 \mu\text{m}$ and pump beam size is $\sim 50 \mu\text{m}$. The pump to probe intensity ratio is kept at least 1:5. The reflected probe beam from sample is detected using a wide area silicon photodiode. The change in the sample reflectivity for the probe beam measured as a function of the pump probe delay gives information on the evolution of the photo-generated carriers excited in the sample by the pump beam.

To probe the true carrier dynamics it is essential that the excited carrier density must be kept as low as possible. In such conditions, the relative change in reflectivity ($\Delta R/R$) is expected to be less than the order of 10^{-3} . Phase sensitive detection technique can provide sufficiently high signal-to-noise ratio for such measurements. For this, the pump beam is time modulated using a mechanical chopper. The reflected probe beam is detected by a photodiode and lock-in-amplifier combination. The chopper provides the reference signal to the lock-in-amplifier. The changes in the probe beam due to the pump beam have the same modulation frequency and are enhanced by the lock-in-amplifier. The normalised transient change in reflectivity ($\Delta R/R$) at various pump-probe delay is calculated by taking ratio of the in-phase

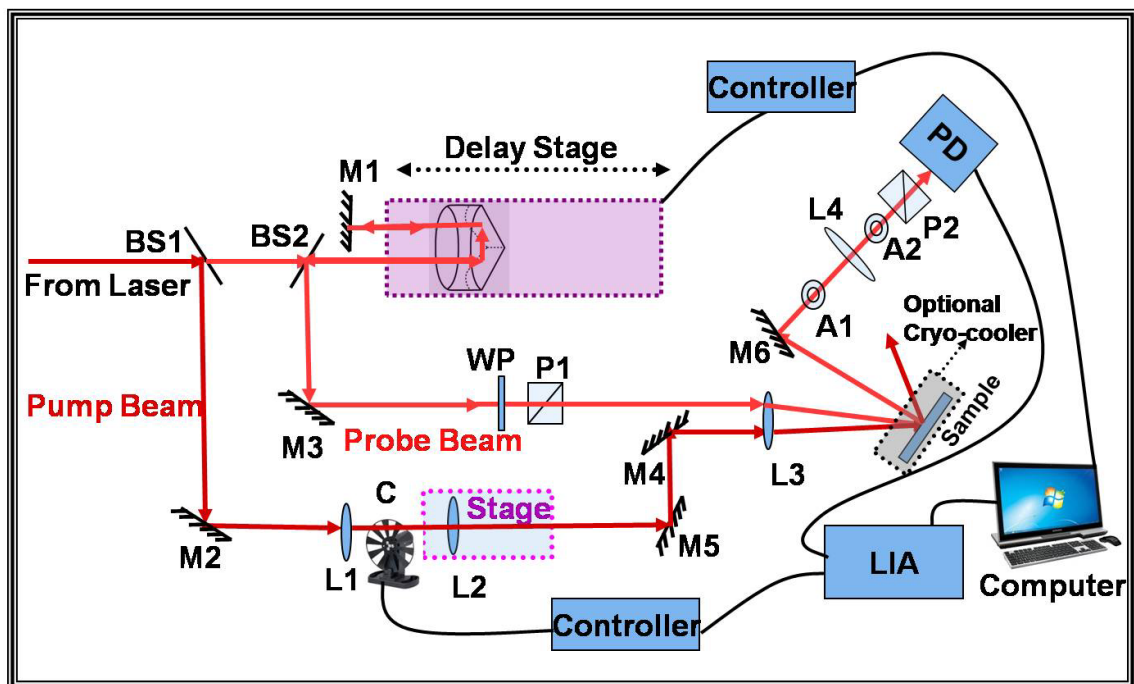


Figure 2.4: Time-resolved degenerate pump-probe reflectivity setup. The laser used is femtosecond laser. (BS-Beam splitter, C-Chopper, L-Lens, WP-Waveplate, M-Mirror, PD-Photodiode, P-Polarizer, A-Aperture and LIA-Lock-in-amplifier).

signal and the average reflected probe power [69]. Apertures A1 and A2 are placed in the path of reflected probe beam towards photodiode to prevent the scattering of the pump beam from the sample reaching the photodiode (Fig. 2.4). Further, the probe beam polarization is made orthogonal to the pump beam polarization with help of a half wave plate and a polarizer (WP and P1). This is done to minimize coherent artifacts in the transient reflectivity signal. The experiment is performed using a customized software which controls the delay stage movement and acquire the data from the lock-in-amplifier at each delay. This software was developed by Laser Electronics Support Division, RRCAT.

2.5 Establishment of low temperature transient reflectivity measurements

Some studies in this work required transient reflectivity measurements at low temperatures. For such measurements the sample was placed in an in-house developed closed-cycle cryostat which could go down up to 40 K. The cryostat was provided by Cryo-engineering and Cryo-module Development Division, RRCAT. A heavy vertical stand was custom designed to place the cryostat above the experimental table in order to minimize the effect of vibrations. This setup was used to measured transient reflectivity of the near-surface GaAsP/AlGaAs single quantum well. However the initial low temperature scan were found to be erratic and the data showed modulation within a scan of pump-probe delay of few hundreds of ps. So, before the transient reflectivity measurements could be done, the source of these modulations had to be determined. Figure 2.5(a) and (b) show two successive scans each at room temperature and 50 K respectively.

Performing the measurements with the cryostat in on and off conditions, it was confirmed that these modulations were not being caused by the cryostat vibrations.

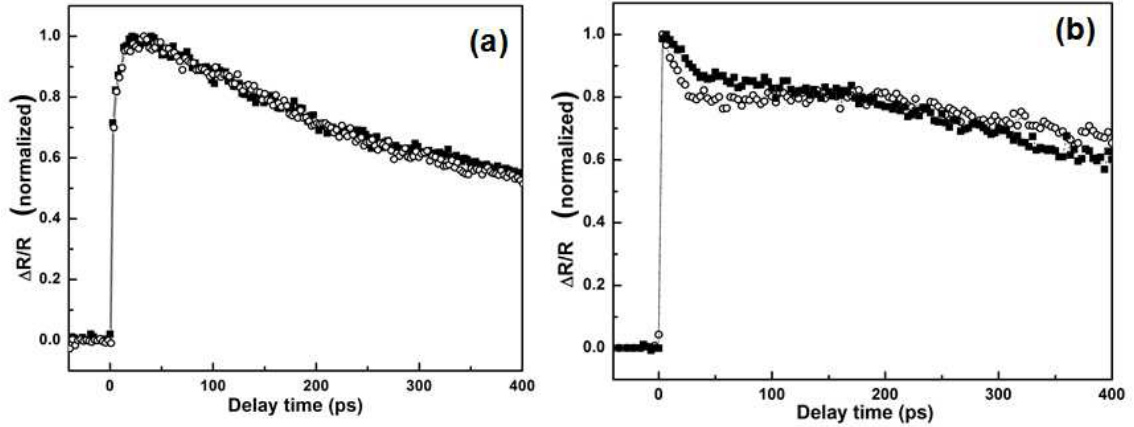


Figure 2.5: (a) Two representative scans of transient reflectivity signal from GaAsP/AlGaAs quantum well at room temperature (300 K) under identical conditions. The data was always repeatable within the experimental errors. (b) Two representative scans of transient reflectivity signal ($\Delta R/R$) of GaAsP/AlGaAs quantum well at 50 K. The time evolution of the signal was different on each scans.

A search of literature revealed that similar oscillations in transient reflectivity were reported from $\text{La}_{0.5}\text{Sr}_{1.5}\text{MnO}_3$ at low temperature and has been attributed to some kind of memory effect [76]. However, the origin of the oscillations could not be established conclusively. Further, periodic modulations were reported in the linear reflectivity of ZnO at low temperature [77]. Therefore, the linear reflectivity behavior of quantum well in the same setup was checked by measuring the probe reflectivity as a function of time. It was found that the linear reflectivity was varying periodically. The transient reflectivity experiment measures $\Delta R/R$ under the assumption that linear reflectivity (R) remains constant. Any variation in R could cause the observed modulation in $\Delta R/R$.

In order to confirm that the high power of the femtosecond laser was not the cause of the modulations, the linear reflectivity was also measured using a continuous wave low-power He-Ne laser at 632.8 nm. The same oscillatory behaviour was observed. In ZnO the oscillations in the linear reflectivity had been attributed to a continuously growing space charge layer [77]. To check whether this explanation was applicable

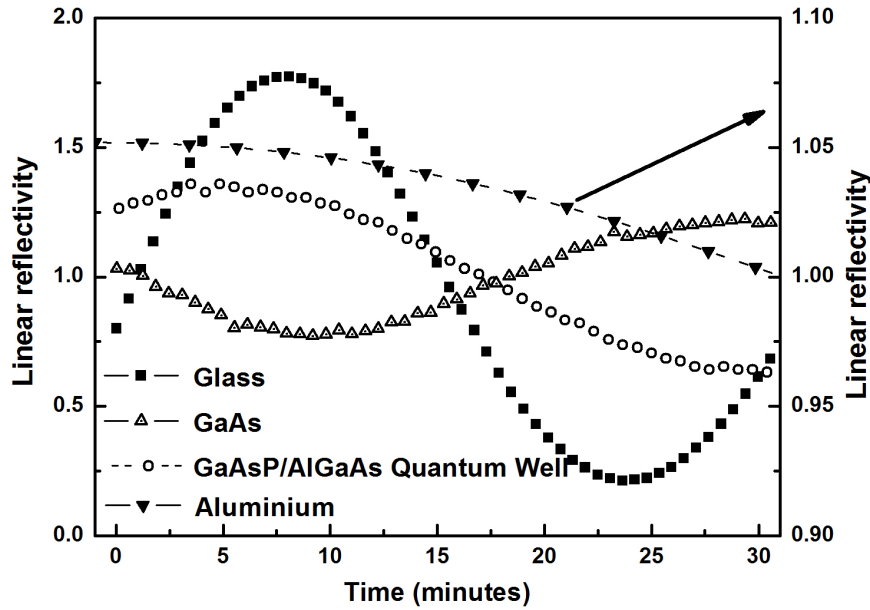


Figure 2.6: The variations in the linear reflectivity from various materials at 50 K in the cryostat. The incident He-Ne laser power was 0.8 mW. For ease of viewing, the reflected signals have been scaled by suitable multiplier.

here also, measurements in the same setup were done on various materials, namely glass plate (insulator), a bulk GaAs wafer (semiconductor) and a thin aluminium plate (metal). The surface of all these samples were of optical quality. In all cases, the linear reflectivity showed similar modulations as shown in Fig. 2.6. The observation of similar periodic variations in the low temperature linear reflectivity of different kinds of materials implies that the oscillations have a common origin independent of the nature of the material but strongly dependent on the sample temperature.

Recalling that the vacuum level in the cryostat is typically in the order of $\sim \times 10^{-6}$ millibar, it is possible that enough residual water vapour and gases are present to condense and form a continuously growing film on the sample surface. In the reflectivity measurement interference between the reflection from the top and bottom interfaces of this growing film can give rise to the observed modulations.

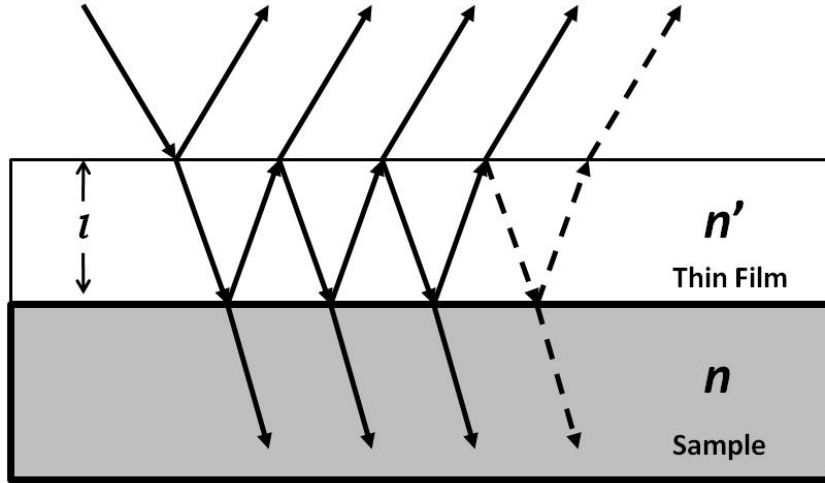


Figure 2.7: Schematic of multiple reflection from a thin film-substrate system. l is the thickness of thin film. n' and n are the refractive index of the thin film material and the sample respectively.

In order to confirm whether this phenomenon will explain the observed behavior, we model the effect of a continuously growing thin film on the reflectivity of the sample. Let l be the thickness of the thin film growing on the sample at any time t (as shown in Fig. 2.7). The net reflectivity from the film and the sample at any given time is [78,79]

$$R(t) = \frac{R_1 + \Omega(t)^2 R_2 + 2\Omega(t)\sqrt{R_1 R_2} \cos(4\pi n' l(t)/\lambda)}{1 + \Omega(t)^2 R_1 R_2 + 2\Omega(t)\sqrt{R_1 R_2} \cos(4\pi n' l(t)/\lambda)}, \quad (2.1)$$

where R_1 is the reflectivity of the air and thin film interface and R_2 is the reflectivity of the thin film and sample interface. n' and n are the refractive indices of the thin film and sample materials at the wavelength of the light used [80,81]. The absorption loss per pass, Ω , is $\exp(-\alpha l(t))$, where α is the linear absorption coefficient of the thin film material. For a growing film l will vary with time. l will be given by gt where $g = dl/dt$ is the growth rate of the film. Figure 2.8 shows the calculated reflectivity oscillations using Eq.2.1 at experimental wavelength of 632.8 nm for different values

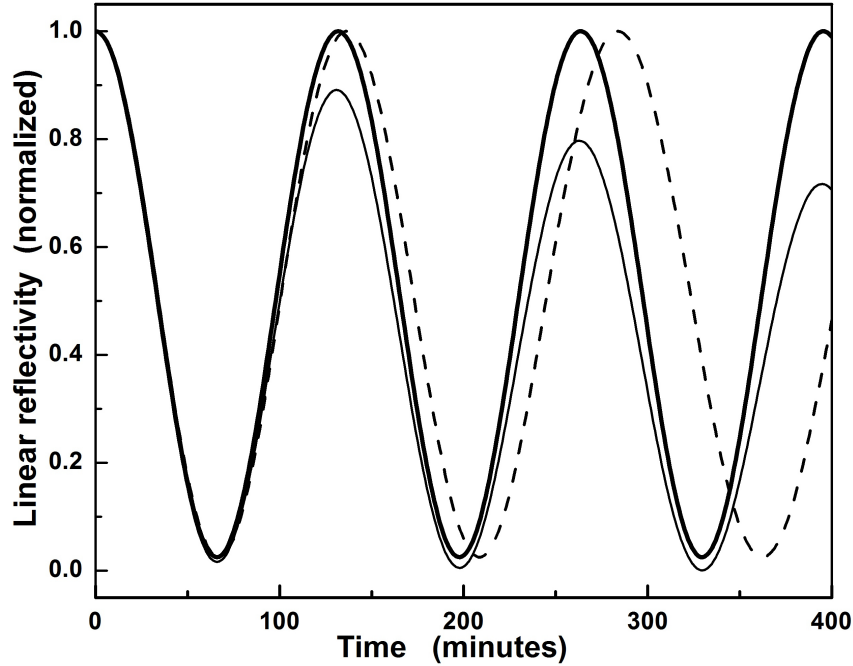


Figure 2.8: The calculated variation of linear reflectivity from a sample and a thin film on its top surface with time using Eq.2.1: thick line - constant g and no absorption in the film ($\alpha = 0$), thin line - constant g with finite absorption in the film and dashed line - linearly decreasing g and $\alpha = 0$.

of n' , g and α . We see from Fig. 2.8, for a given growth rate and n' of a non-absorbing thin film, the period as well as the magnitude of oscillations remains constant with time. This can be explained as follows: if either the sample or the film is a poor reflector, then $R_1 R_2 \ll 1$ and the denominator Ω can be taken to be nearly 1 with this approximation and assuming that the film thickness increases linearly with time, the above equation can be approximated to

$$R(t) = A + B \cos \left[\frac{4\pi n' g t}{\lambda} \right], \quad (2.2)$$

where $A = R_1 + R_2$ and $B = 2\sqrt{R_1 R_2}$. Thus, the reflectivity of a non-absorbing thin film with constant growth rate and n' will have constant amplitude as well as constant time period.

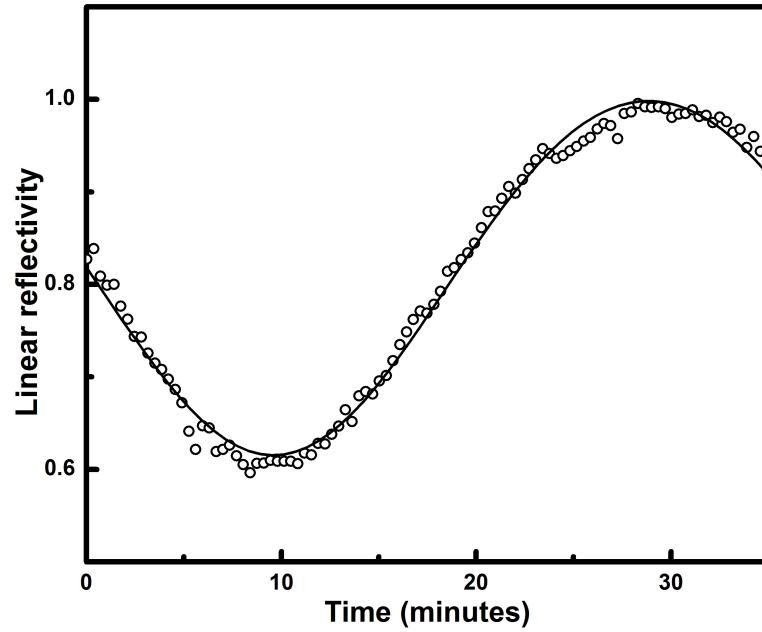


Figure 2.9: The variation of the measured linear reflectivity of bulk GaAs sample. The calculated curve is the best fit with Eqn. 2.1 neglecting any absorption in the film. For ease of viewing, the reflected signal has been normalized by dividing it with its maximum value. The refractive index of the GaAs used in fitting as well as the best fit parameters are given in Table 1.

Assuming the growing thin film on our samples to have constant growth rate, constant refractive index and no absorption, we fit the experimental data using Eq.2.1 to have an estimate for the refractive index and growth rate of the film. Figure 2.9 shows the measured linear reflectivity of GaAs along with the best fit using Eq.2.1. Table 2.1 shows the estimated refractive index and growth rate of the thin films condensing on different samples derived from these fittings.

In case of cryo-vacuum condensation of gases, the crystalline structure and density of the condensed film have been shown to depend on temperature and ambient atmosphere [82,83]. However, our results show that material and surface quality of the sample on which the gases are condensing will also affect the growth rate and refractive index of the thin film. Thus, the estimated refractive index and growth rate of the films are expected to vary with the underlying sample.

Material	n	k	$R(\%)$	n'	g (nm/min)
Aluminium	1.37	7.6	89	1.42	2.25
Glass	1.54	0	4	1.34	8
GaAs	3.3	0.2	29	1.15	7

Table 2.1: The estimated values of refractive index n' and growth rate g in nm/min of the film condensing on different materials. Approximate values of real and imaginary part of refractive index n and k used in the calculation is also listed in the table along with average reflectivity R . The wavelength is 632.8 nm.

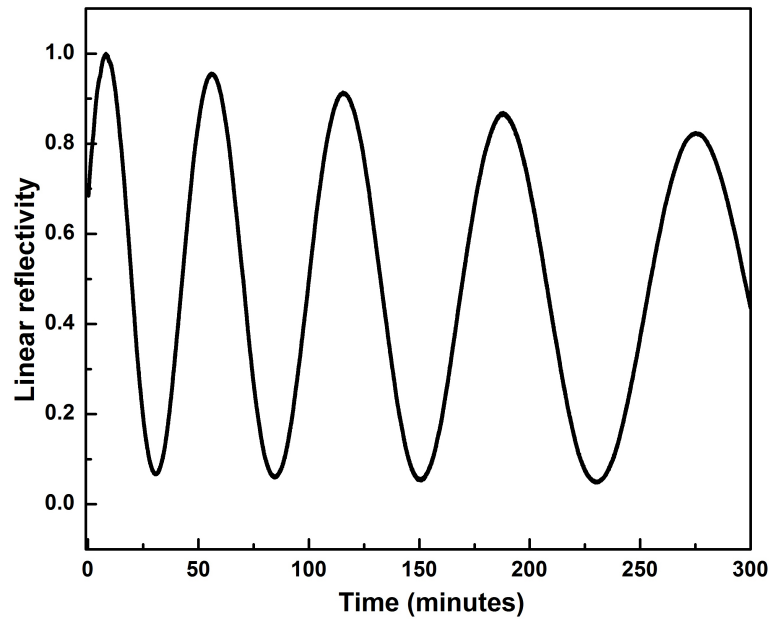


Figure 2.10: Measured time dependence of the linear reflectivity of a glass plate in a optical cryostat at temperature 50 K in much longer time of observations. For ease of viewing, the reflected signal has been normalized by dividing it with its maximum value.

Figure 2.10 shows the measured time dependence of linear reflectivity measured from the glass surface over a long observation period. Although the variations in the period of oscillations and the magnitude can be neglected over one cycle, the long time observation clearly shows an increase in the time period as well as changes in the magnitude of oscillations. Similar changes in the period of oscillations as well as the magnitude have been found in the linear reflectivity of all the samples. In Fig. 2.8, we have also shown the simulated changes in the reflectivity of the sample-thin film structure for two cases: in one case the film has finite absorption and in the other case the growth rate decreases linearly with time. The observed changes in the magnitude and period of oscillations in the linear reflectivity of the sample shown in Fig. 2.10 can be explained if we assume the thin film to have finite absorption and reduction in growth rate as it grows. It is expected that as the condensation starts, the amount of residual gas present in the chamber reduces and this can lead to reduction in the growth rate of the film. Thus, the observed oscillatory behavior in the linear reflectivity is consistent with our model of condensation of a thin film on the samples surface. In such thin film formation the growth rate should depend strongly on the temperature of the sample. It is expected that as the temperature of the sample increases the growth rate should reduce and hence the period of oscillations should increase. Figure 2.11 shows the temperature dependence of period of oscillations on the reflectivity of GaAs sample. Clearly the time period of reflectivity oscillations increases with increase in temperature, supporting the formation of thin film on the material under study.

Having understood the cause of modulations in the linear reflectivity, it was essential to suppress these oscillations to get the proper transient reflectivity signal. The chamber volume of cryostat was nearly 0.02 m^3 and the total volume along with the vacuum bellows was $\sim 0.5 \text{ m}^3$. The vacuum system consisted of a diffusion pump with a liquid nitrogen trap and backed by rotary pump and resulted in a vacuum

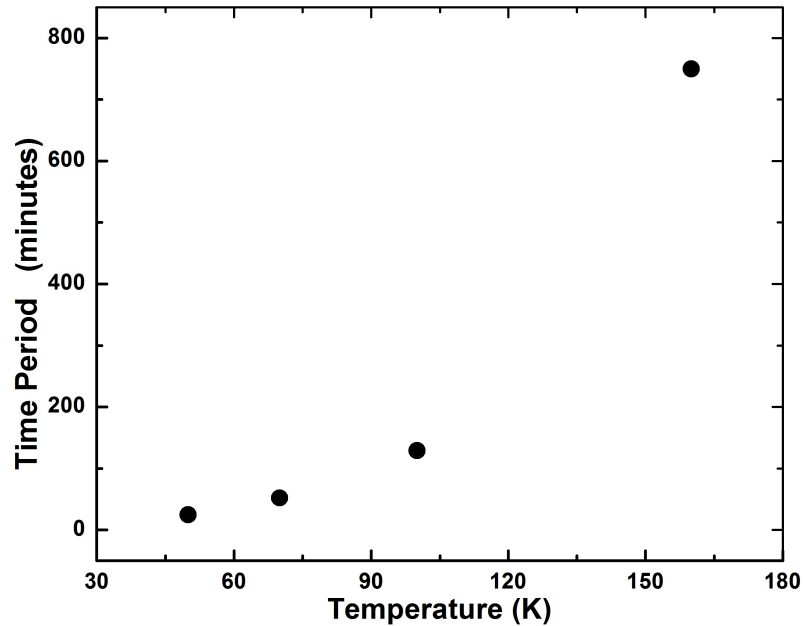


Figure 2.11: The temperature dependence of period of linear reflectivity oscillations measured from bulk GaAs.

level of $\sim 5 \times 10^{-6}$ mbar. In order to reduce the amount of residual gases, the cryostat was conditioned by purging with nitrogen and baking under vacuum. This improved the vacuum level to nearly 1×10^{-6} mbar. The reflectivity under various stages of conditioning is shown in Fig. 2.12.

Purging with nitrogen removes some of the residues. This results in increase of the time period of oscillation in the reflectivity, but the magnitude of oscillations remains the same. This shows that the same material is condensing under various stages of conditioning. What helped the most in reducing condensation on the sample surface, as shown in Fig. 2.12, was the mounting of a metal shield around the sample with through holes for optical beams. This is because a large fraction of the residual gases condenses on the shield and does not reach the sample inside. Figure 2.13 shows two representative scans of the transient reflectivity curve of the quantum well sample at 50 K after the cryostat is conditioned and with the metal shield in place. It is clear that with the slow oscillations in linear reflectivity suppressed, the transient

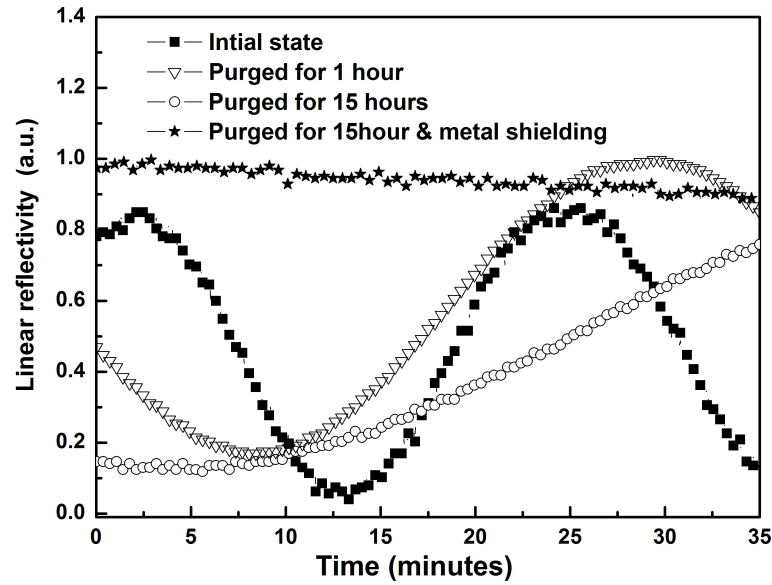


Figure 2.12: Reflectivity signal for glass at 50 K under different nitrogen purging times as well as with an additional metal shielding around the sample. All signals have been scaled by suitable multiplier for ease of viewing.

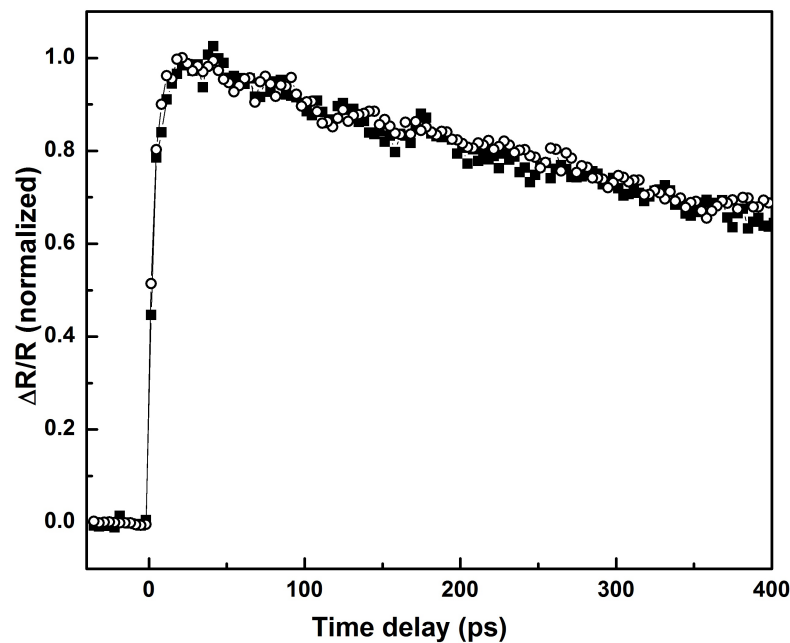


Figure 2.13: Two representative scans of transient reflectivity of GaAsP/AlGaAs quantum well at 50 K after conditioning the cryostat and with the metal shield around the sample.

reflectivity signal becomes repeatable and reliable. As a further check, similar measurements were made in other commercial cryostats which had metallic shields. It was found that the reflectivity modulations appeared if the vacuum conditions degraded and disappeared once the vacuum improved. We believe that the reflectivity oscillations reported earlier could be due to this same phenomenon [76,77]. Since the process of film growth can occur for any material, the precautions discussed above are important for reflection based experiments on any sample.

2.6 Summary

In this chapter, the details of the samples studied in this thesis and the experimental techniques developed for the same have been described. Standard degenerate pump-probe transient reflectivity experiment was set up for these studies. Earlier authors, in their work, have reported modulations with time in both linear and transient reflectivity at low temperatures. However, the cause could not be identified. In this work we have demonstrated that all these effects arise due to condensation on the sample surface. An effective method of preventing this effect has been demonstrated.

Chapter 3

Transient reflectivity in GaAs

3.1 Introduction

The main work in this thesis involves carrier dynamics studies in III-V semiconductor nanostructures based on time-resolved pump-probe reflectivity measurements. Upto moderate carrier densities, the excited carriers in the sample generated by the absorption of the pump pulse cause a transient change in its refractive index. This, in turn, induces a time dependent change in reflectivity, which is probed by a weak probe pulse [69, 84]. This transient refractive index change in these materials can be caused due to several phenomena e.g. band filling, bandgap renormalization, free carrier etc [85–95]. The relative importance of these depends on the excitation photon energy and excited carrier density. As discussed in chapter 2, all the quantum well and heterostructure samples used in the work are grown on a GaAs substrate. At the photon energies used for transient reflectivity measurements in this thesis work, there is always a large photo carrier density generated in the GaAs substrate. For example, the carrier density in GaAs substrate can be much higher than that generated in the quantum well. Thus the contribution from the substrate (GaAs) to

the transient reflectivity can be a major one and has to be understood before any conclusions can be reached about the contribution from the refractive index change of the nanostructure deposited on top of it.

GaAs is a fairly well studied material and transient refractive index changes in the range of 10^{-2} to 10^{-4} have been reported without any permanent change [84,95]. The corresponding photoexcited densities lie in the range of 10^{15}cm^{-3} to 10^{17}cm^{-3} . However, the complete information in the wavelength region of our interest was not available. Further, for ease of analysis, we also wished to work in carrier density regime where the reflectivity change had a linear, rather than nonlinear dependence on the carrier density. Therefore, the refractive index change in GaAs was first calculated as a function of incident photon energy as well as carrier density. Intensity dependent transient reflectivity measurements were also performed to experimentally determine the regime for linear change of reflectivity. This chapter describes these results.

3.2 Calculation of photoinduced refractive index change in GaAs

For photoexcited carrier densities in the range of 10^{15}cm^{-3} - 10^{17}cm^{-3} , three main processes are responsible for the photoinduced refractive index change in GaAs. These are band filling, band gap renormalization and free carrier absorption [84–88, 95]. In this section we first calculate separately the effect of each process and estimate the combined effect.

3.2.1 Band filling

The band filling effect, also called the Burstein-Moss effect, results in a shift of the band edge as a result of excitation [85,95]. The electron and holes are fermions

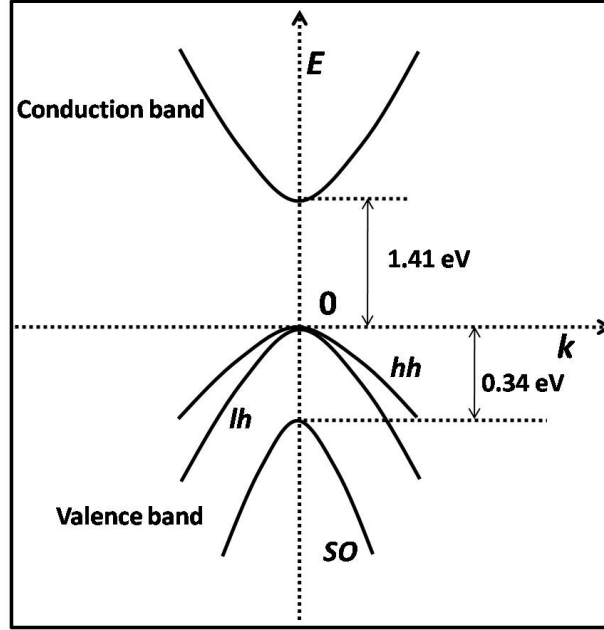


Figure 3.1: The band structure of GaAs at room temperature. *lh* stands for light hole and *hh* stands for heavy hole. *SO* is split-off band.

and obey Pauli's exclusion principle. After excitation, the electron in conduction band come down quickly to the band edge. Similarly excited holes also quickly accumulate at the top of the valence band. This reduces the states available for excitation near the band edge, thus effectively increasing the band gap. GaAs is a direct bandgap semiconductor and the conduction and valence bands are parabolic near the band edge. The band structure of GaAs is shown in 3.1 at $k = 0$. Here we have shown three direct band hole states in the valence band. Two of the hole states are degenerate at $k = 0$. These are called heavy holes and light holes. Light hole (*lh*) is having higher curvature and heavy hole (*hh*) has smaller curvature. The split off band (*SO*) has split off to lower energy due spin orbit coupling [26]. Near the band edge the absorption coefficient is given as [95]

$$\alpha_o(E) = \frac{C_{hh}}{E} \{E - E_g\}^{1/2} + \frac{C_{lh}}{E} \{E - E_g\}^{1/2} \quad (3.1)$$

Here, C_{hh} , C_{lh} is material parameter depending on type of hole state involved. E_g is band gap of GaAs and E is the photon energy at which $\alpha_o(E)$ is calculated.

Under photoexcitation, the band-edge will shift and therefore the absorption coefficient near band edge will also change. The change in absorption $\Delta\alpha_o(E)$ is given as [95]

$$\Delta\alpha(N, P, E) = \alpha_o(E)\{f_e(N, E) - f_h(P, E) - 1\}. \quad (3.2)$$

Here $\Delta\alpha_o(E)$ is change in absorption. $\alpha_o(E)$ is given by Eqn. 3.1. N and P is carrier density of photoexcited electrons and holes respectively. The filled electron states in conduction band is given by Fermi-Dirac distribution as $f_e(N, E)$ and filled hole states in valence band by $f_h(P, E)$. The distribution function $f_e(N, E)$ and $f_h(P, E)$ depends on photon energy (E), temperature (T) and excited carrier density (N or P). The corresponding change in refractive index due to change in absorption is given as [96]

$$\Delta n(N, P, E) = \frac{2c\hbar}{e^2} P \int_0^{\infty} \frac{\Delta\alpha(N, P, E')}{E'^2 - E^2} dE'. \quad (3.3)$$

Using Eqn. 3.3, the change in refractive index is calculated by using the values of various parameters from literature [85,95]. Figure 3.2 shows the calculated refractive index change at different photon energies for various excited densities. This change increases with increasing carrier density and is 10^{-3} for the lowest carrier density used ($6 \times 10^{15} \text{cm}^{-3}$). Figure 3.3 shows the intensity dependence of Δn for a few photon energies where the transient reflectivity measurement in nanostructure samples have been carried out. At all these photon energies, which are above GaAs band gap, Δn is positive. As can be seen, even for high excitation Δn varies linearly with carrier density, though the slope varies with photon energy.

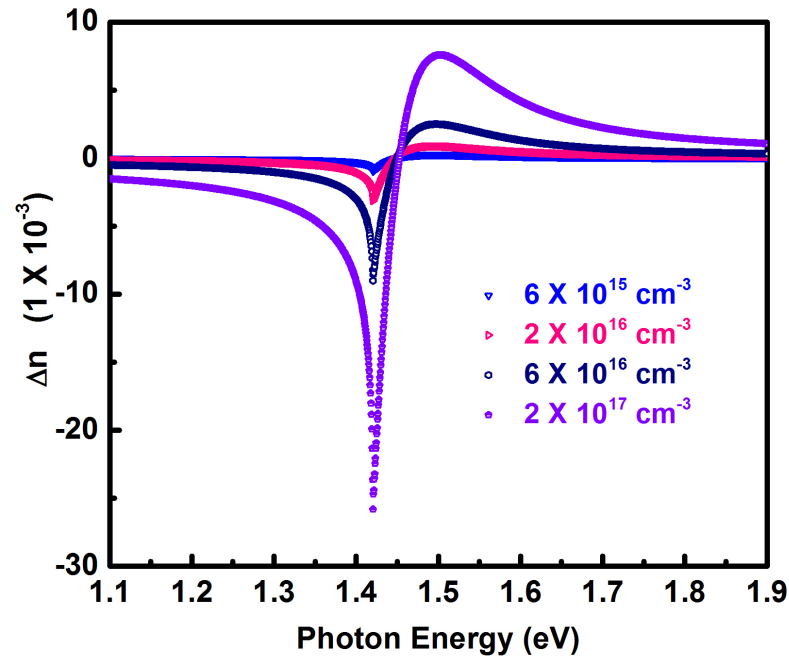


Figure 3.2: Calculated change in refractive index as function of photon energy due to band filling effect in GaAs. The results are shown at four different carrier densities.

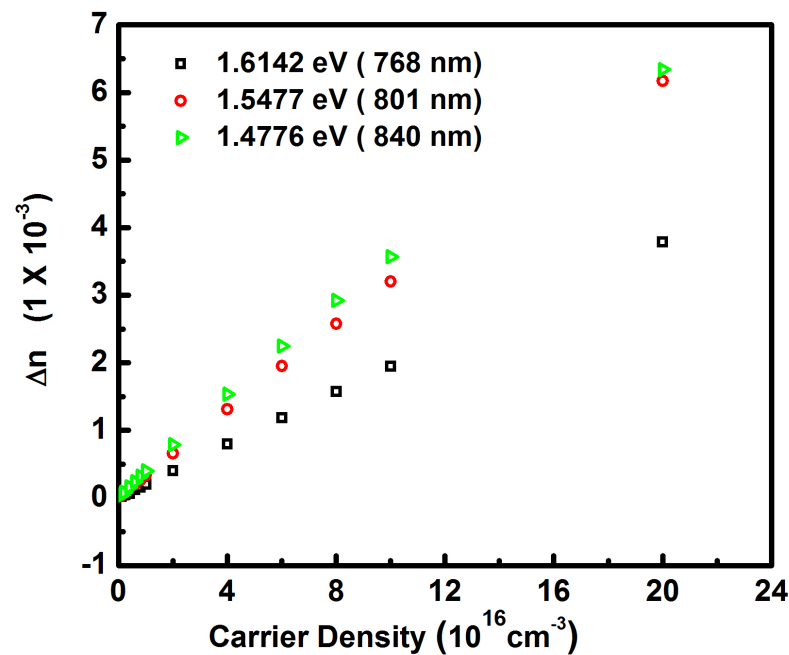


Figure 3.3: The change in refractive index due to band filling effect in GaAs as a function of carrier density at three different wavelengths.

3.2.2 Band gap renormalization

If the concentration of electrons in the conduction band is large enough, the electron wavefunction will start overlapping with each other. Then coulombic repulsion and Pauli's exclusion principle will cause electrons to repel each other and exchange effect will result in lowering of the electron energy. This will result in lowering of the conduction band in a highly excited semiconductor as compared to the unexcited semiconductor. Similarly, the valence band level will rise up due to the interaction among holes. The net effect of this lowering of conduction band and rising of valence band will result in band gap shrinkage in the highly excited semiconductor. This effect is called the band gap renormalization. The band gap reduction is proportional to average inter-particle distance. At lower density it is negligible.

An empirical model is available to estimate the band gap shrinkage as a function of carrier density [86–95]. Above a critical carrier density, N_{cr} , the reduction in band gap is given by [95]

$$\Delta E_g(N) = \frac{A}{\varepsilon_s} \left(1 - \frac{N}{N_{cr}}\right)^{\frac{1}{3}}. \quad (3.4)$$

where A is fitting parameter for given semiconductor material, ε_s is permittivity of semiconductor and N is excited carrier density. N_{cr} is critical density equal to 1.4 times Mott density [97]. N_{cr} for GaAs has been reported to be $5 \times 10^{16} \text{ cm}^{-3}$. The change in absorption $\Delta\alpha$ due to band gap renormalization is given as

$$\Delta\alpha(N, E) = \frac{C}{E} (E - E_g - \Delta E_g(N))^{1/2} - \frac{C}{E} (E - E_g)^{1/2}. \quad (3.5)$$

Here, C is material parameter for a given semiconductor, E_g is band gap and E is the photon energy where change in absorption is calculated.

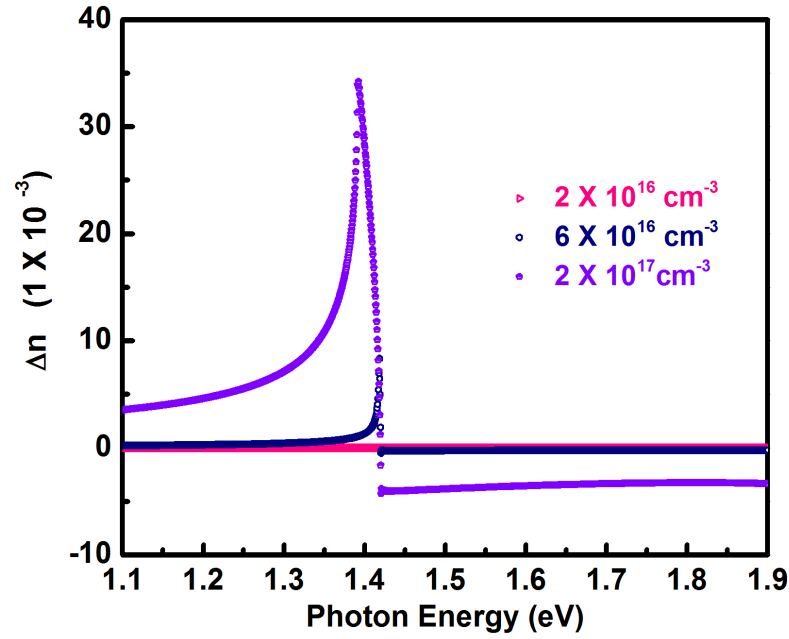


Figure 3.4: Calculated change in refractive index as function of photon energy due to band gap renormalization in GaAs. The results are shown at different carrier densities. The band gap renormalization starts to contribute above critical density which is $5 \times 10^{16} \text{ cm}^{-3}$ for GaAs.

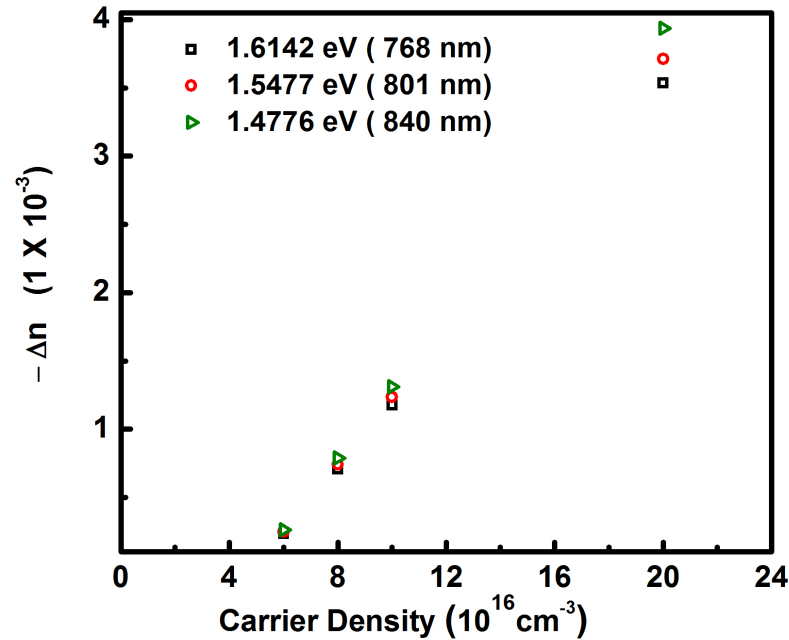


Figure 3.5: The band gap renormalisation induced change in refractive index in GaAs as a function of carrier density at three different wavelengths.

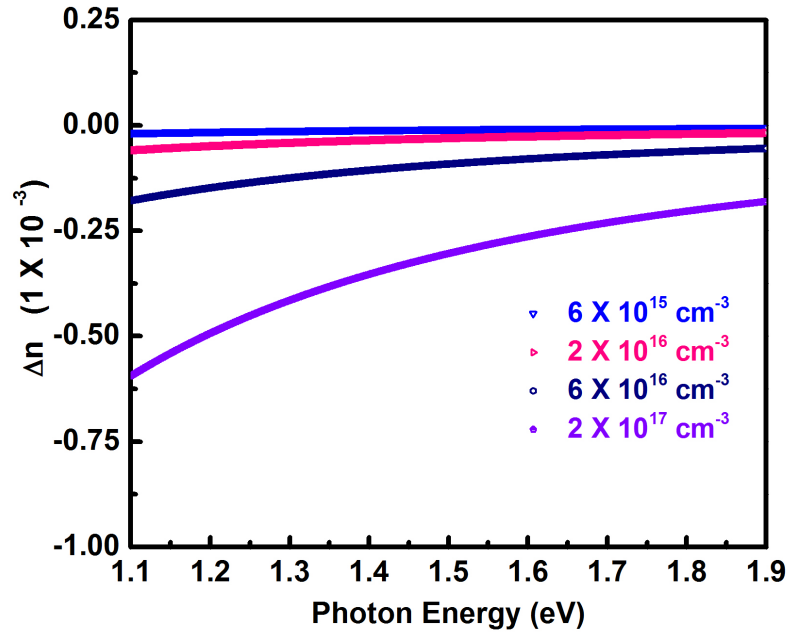


Figure 3.6: The refractive index change as function of photon energy due to free carrier absorption effect in GaAs. The results are shown at different carrier densities.

Figure 3.4 shows the results obtained for band gap renormalization effect in GaAs using Eqn. 3.5 calculated by taking required parameters for GaAs from literature [95]. For carrier densities greater than 10^{16} cm^{-3} , the magnitude of Δn is similar to that induced by band filling, though the sign is mostly opposite.

Figure 3.5 shows that the band gap renormalization induced change in refractive index (Δn) at three different wavelengths as function of carrier density. As can be seen that the effect starts to appear just after the critical density and becomes more dominant as we go on increasing the carrier density.

3.2.3 Free carrier absorption

The photoexcited carriers in semiconductors can further absorb the incident light and move to a higher state in the conduction/valence band. Following the Drude

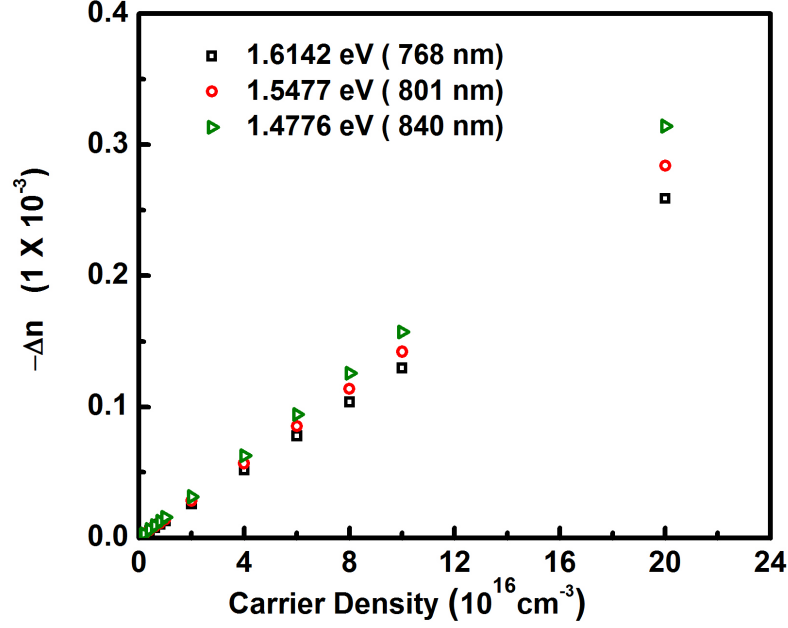


Figure 3.7: Change in refractive index due to free carrier absorption in GaAs as a function of carrier density at three different wavelengths.

model, the resultant change in refractive index is given as [94]

$$\Delta n = -\left(\frac{h^2 e^2}{8\pi^2 E^2 \epsilon_0 n}\right)\left(\frac{N}{m_e} + \frac{P}{m_h}\right). \quad (3.6)$$

Here h is Planck's constant, E is energy of photon. m_e and m_h are the respective effective mass of electrons and holes. The RHS shows that Δn is always negative. Figure 3.6 shows the calculated refractive index change for GaAs due to free carrier absorption. Here also the magnitude of Δn increases with increasing carrier density. However, the values are much smaller as compared to those from either band filling or band gap renormalization. Also, variation of Δn with carrier density for the same three photon energies, the magnitude of Δn increases linearly with carrier density (3.7).

Thus we see that, in a certain carrier density range, the refractive index change varies linearly with carrier density if each effect is considered separately. However

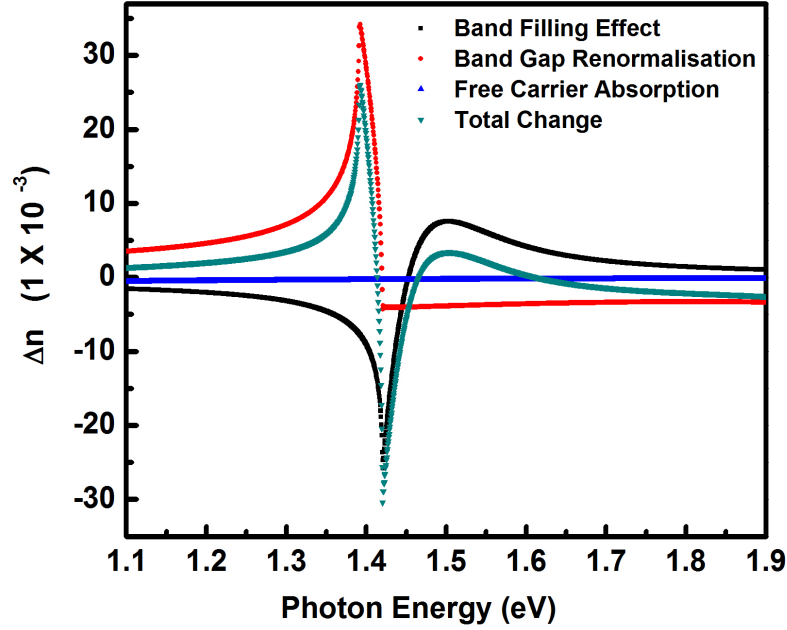


Figure 3.8: Calculated change in refractive index due to all three effects at carrier density $2 \times 10^{17} \text{ cm}^{-3}$ as function of energy due to combinations of effect in GaAs. All effects are shown individually and combined is also plotted.

the dependence on excitation photon energy is different for each process. In the next section we calculate the total change in refractive index due to these three process.

3.2.4 Combined effect of band filling, band gap renormalization and free carrier absorption

Figure 3.8 shows the calculated total Δn , at a carrier density of $2 \times 10^{17} \text{ cm}^{-3}$, due to all the three effects. For convenience of reference the three separate contribution are also shown. It is seen that around the band edge (1.41 eV) the variation with photon energy is more or less similar to that due to band filling. Figure 3.9 shows the total Δn for various carrier densities. Though the overall behaviour is similar to that of Fig. 3.2, crossover point from negative to positive shifts to higher energy as the carrier density increases. A more striking difference is seen if we look at Δn variation at a given photon energy. Figure 3.10(a) shows the total Δn for the same

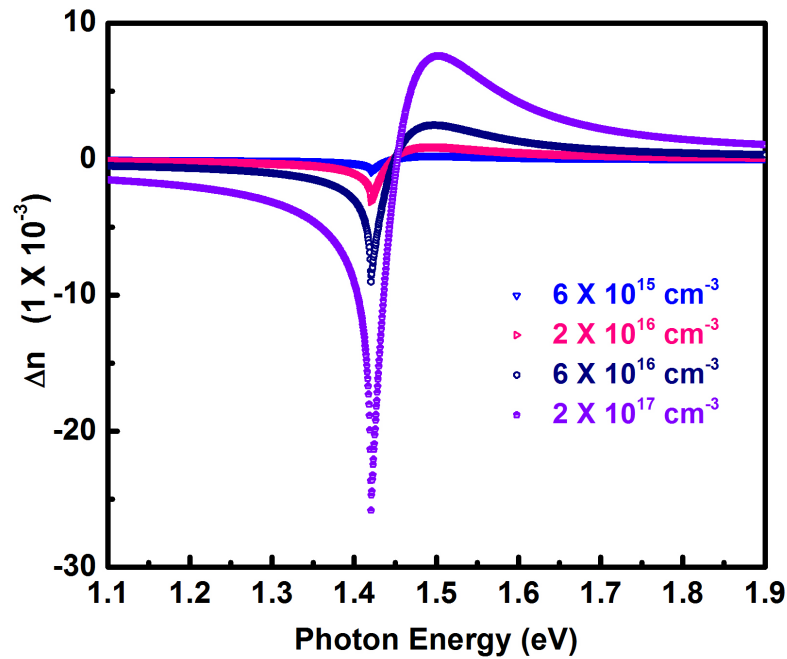


Figure 3.9: Calculated change in refractive index in GaAs as function of energy due to combinations of effect. The results are shown at different carrier densities.

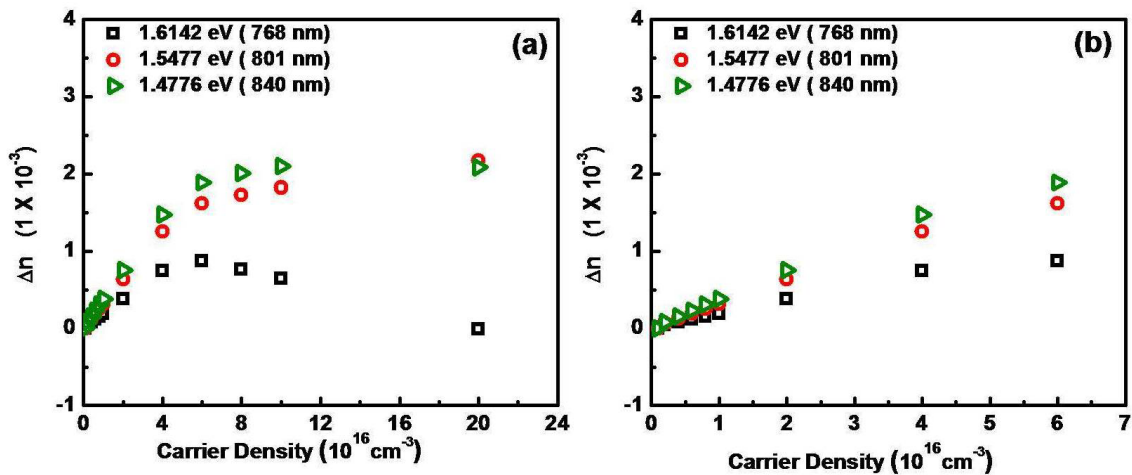


Figure 3.10: The change in refractive index (a) with carrier density at three different wavelengths in GaAs due to sum of all effects (b) the same refractive index change at zoomed scale which shows linear variation.

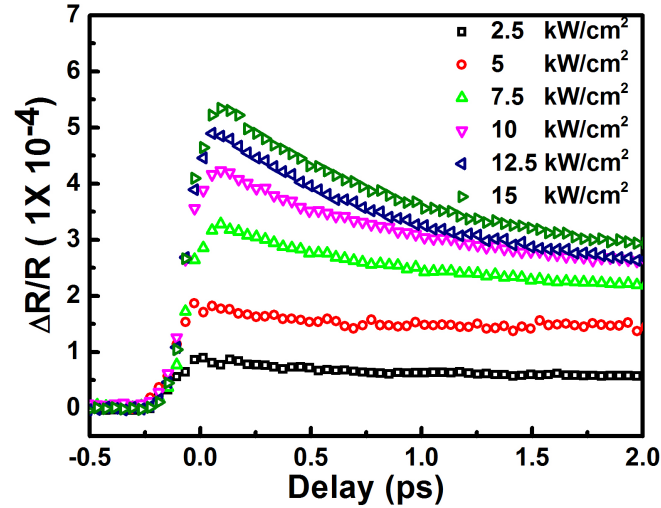


Figure 3.11: Transient reflectivity signal from GaAs at 768 nm at different pump intensity.

three photon energies as considered in 3.3, Fig. 3.5 and Fig. 3.7. We see that above $4 \times 10^{16} \text{cm}^{-3}$ the variation of Δn with intensity becomes nonlinear. We recall here that the critical density for band gap renormalization is $5 \times 10^{16} \text{cm}^{-3}$. Below this carrier density the total Δn is still linear as shown by the zoomed graph of Fig. 3.10(b). Thus it is safe to conclude that for carrier densities below $4 \times 10^{16} \text{cm}^{-3}$, the refractive index would arise mainly from band filling. The contribution from band gap renormalization is absent and that due to free carrier absorption is two orders of magnitude lower.

To confirm these calculations, we have carried out intensity dependent transient reflectivity measurement on GaAs at room temperature. These are described in the next section.

3.3 Transient reflectivity measurements on GaAs

Figure 3.11 shows the measured transient reflectivity of GaAs at 768 nm (1.6142 eV). For the measured linear reflectivity spectrum and the absorption coefficients

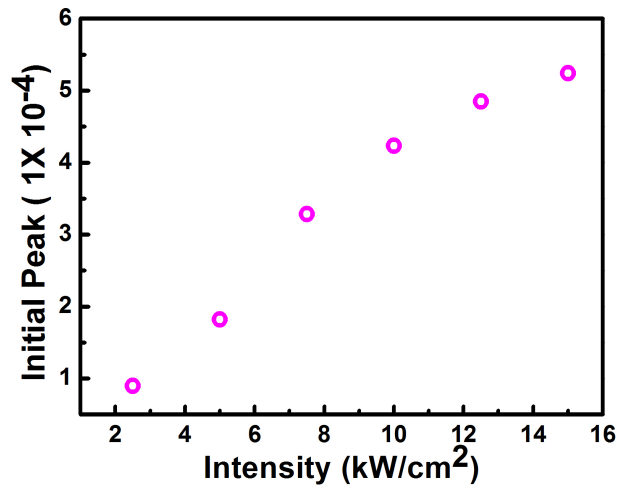


Figure 3.12: The initial peak (ΔR_{max}) of transient reflectivity signal from GaAs at 768 nm as function of pump intensity.

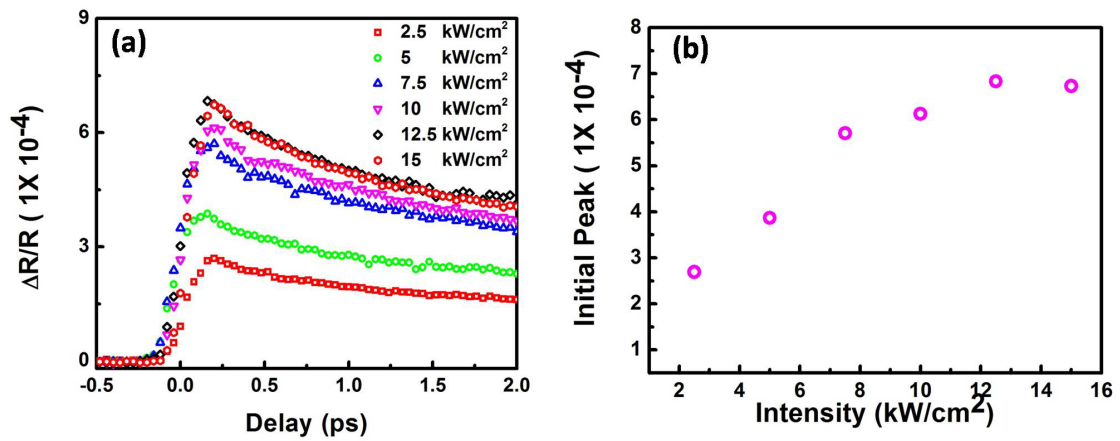


Figure 3.13: (a) Transient reflectivity signal from GaAs at 800 nm at different pump intensity. (b) The initial peak (ΔR_{max}) of transient reflectivity signal from GaAs at 800 nm as a function of pump intensity.

from literature, it is estimated that at this wavelength, at input pump intensity of 2.1 kWcm^{-2} corresponds to an excited carrier density of $1 \times 10^{16} \text{ cm}^{-3}$. The ΔR is positive as expected from Δn calculations of Fig. 3.9. The ΔR starts increasing as soon as the pump pulse arrives at the sample and reaches a maximum by ~ 200 fs. The magnitude of this maximum change is plotted as a function of input pump intensity shown in Fig. 3.12. It is observed that the ΔR_{max} starts saturating after 10 kWcm^{-2} . A similar behaviour is observed at 800 nm laser wavelength as shown in Fig. 3.13. Therefore transient reflectivity measurements in GaAs should be performed below this pump intensity.

However, all the samples used in this work have a top layer of $\text{Al}_{0.7}\text{Ga}_{0.3}\text{As}$. Between 700 nm to 800 nm (1.771 eV to 1.549 eV) $\text{Al}_{0.7}\text{Ga}_{0.3}\text{As}$ has a lower reflectivity (0.27 - 0.28) as compared to GaAs (.32 - .33). Therefore, the nonlinear behaviour start showing up at a slightly lower pump intensity ($\sim 8.5 \text{ kWcm}^2$). Therefore, all the transient reflectivity measurements described in this thesis, the pump intensity has been kept below $5\text{-}6 \text{ kWcm}^{-2}$.

3.4 Summary

In this chapter, the various physical processes responsible for photoinduced refractive index has been discussed briefly. The refractive index change in GaAs due to these processes has been calculated. The refractive index change ' Δn ' changes linearly with carrier density at low carrier densities ($\sim 10^{15} \text{ cm}^{-3}$). It is concluded that the most significant process is band filling at low carrier densities. The experimental pump intensity for linear regime in GaAs has been established by transient reflectivity measurements. In all the remaining measurements performed for this work, the pump intensity has been kept in this linear regime.

Chapter 4

Carrier Dynamics in Near-Surface Quantum Well

4.1 Introduction

Semiconductor quantum wells are used for many optical and optoelectronic devices like lasers, modulators and photodetectors [6, 7, 15, 16]. Their high efficiency arises mainly from the fact that photo-generated carriers are confined to a small region. Quantum wells can have a very high nonlinear optical response. However, in a typical quantum well, consisting of a thin epitaxial low band-gap material layer sandwiched between two high band-gap material layers, the recombination time of excited carriers is of the order of \sim ns. This restricts their use for ultrafast detectors or modulators. One way to make the optical response faster has been to introduce non-radiative recombination centers in the vicinity of the quantum well; thus providing an alternate faster decay channel for the excited carriers generated in the quantum well. An example is a near-surface quantum well where the barrier layer on one side of the quantum well is made very thin or completely removed [36, 37, 59, 98]. With such a

thin or nonexistent barrier layer, carriers can easily tunnel out from the quantum well and recombine non-radiatively at the surface [34, 37]. Near-surface quantum wells using III-V semiconductors have been used to make fast saturable absorbers, high power surface emitting lasers and all-optical switches for signal generation, temporal multiplexing and ultrashort pulse generation [15, 16, 37, 60, 61, 99–102]. Recently ultrafast all optical switching up to 10 Gbit per second has been demonstrated using InGaAs/InP surface quantum wells [37].

Some carrier relaxation studies in III-V surface quantum wells have been reported which shows the influence of surface states on carrier lifetime in quantum wells [36, 59, 103, 104]. Most of these studies have been at low temperature by either measuring the time-resolved photoluminescence directly or by studying the reduction in the CW photoluminescence. For example, in AlGaAs/GaAs and InGaAs/GaAs near surface quantum wells, it has been shown that the low temperature CW photoluminescence reduces as the top barrier thickness is reduced and disappear completely when the barrier thickness is ~ 5 nm [36, 59, 105]. This reduction in photoluminescence intensity is attributed to the increased tunneling of carriers from the quantum well to the surface states and subsequent non-radiative recombination there [36, 59, 103, 104]. Surface oxidation due to exposure to atmosphere has been reported to further enhance this tunneling efficiency [59].

In AlGaAs/GaAs near-surface quantum wells, time-resolved photoluminescence measurements have shown that the photoluminescence decay time at 10 K reduces from 130 ps for a 35 nm thick barrier layer to 100 ps for a 6 nm thick barrier [36]. In InGaAs/GaAs near-surface quantum wells, at 2K, the time-resolved photoluminescence decay time reduces from 220 ps at 16 nm barrier thickness to 28 ps at 9 nm barrier thickness [104]. In another study the time-resolved photoluminescence decay time at 12 K has been reported to be ~ 150 ps for an AlGaAs/GaAs quantum well with 8 nm thick barrier [105].

As already mentioned, all these reports are for low temperature. For any practical device room temperature operation is desirable. However, at room temperature, the non-radiative decay becomes stronger and photoluminescence correspondingly is much weaker. Therefore, we have selected the transient reflectivity technique to study the effect of surface states on the carrier dynamics in a GaAsP/AlGaAs single quantum well. Strained GaAsP/AlGaAs quantum well is one of the successful solutions for high-power performance in the 800 nm wavelength range [106–108]. The mode-locked vertical cavity surface emitting laser using the GaAsP/AlGaAs near-surface QW is one of the popular design due to the availability of a suitable and relatively inexpensive high-brightness pump source [30, 65]. However no systematic study of surface effects on the carrier dynamics is available for these quantum wells. We have selected a near-surface quantum well with a 5 nm thick top barrier. This ensures a strong interaction between the surface and quantum well states. It has been shown that the interaction with surface states leads to a sub-ps carrier lifetime which is the fastest reported in such quantum well structures.

4.2 Experimental details

Two GaAs_{0.86}P_{0.14}/Al_{0.7}Ga_{0.3}As single quantum well structures have been used in this study; a near-surface quantum well (NSQW) with a top Al_{0.7}Ga_{0.3}As barrier layer of 5 nm and a buried quantum well (BQW) with a 50 nm thick top barrier. The sample growth details have been given in chapter 2. The layer structures of the quantum wells is shown again in Fig. 4.1 for convenience.

The samples were first characterized by photoluminescence and photorefectance. As expected, only the BQW showed photoluminescence at room temperature. The spectrum is shown in Fig. 4.2. The broad peak can be resolved in three separate peaks corresponding to the three lowest transitions in the quantum well. Out of the three peaks, the one corresponding to the $e1 - hh1$ transition has the highest

$\text{Al}_{0.7}\text{Ga}_{0.3}\text{As}$ (d nm)
[QW] $\text{GaAs}_{0.86}\text{P}_{0.14}$ (11 nm)
$\text{Al}_{0.7}\text{Ga}_{0.3}\text{As}$ (211 nm)
undoped GaAs (250 nm)
n^+ GaAs (Substrate)

Figure 4.1: Layer structure of the single quantum wells. $d=5\text{nm}$ for near-surface quantum well (NSQW) and $d=50\text{ nm}$ for buried quantum well (BQW).

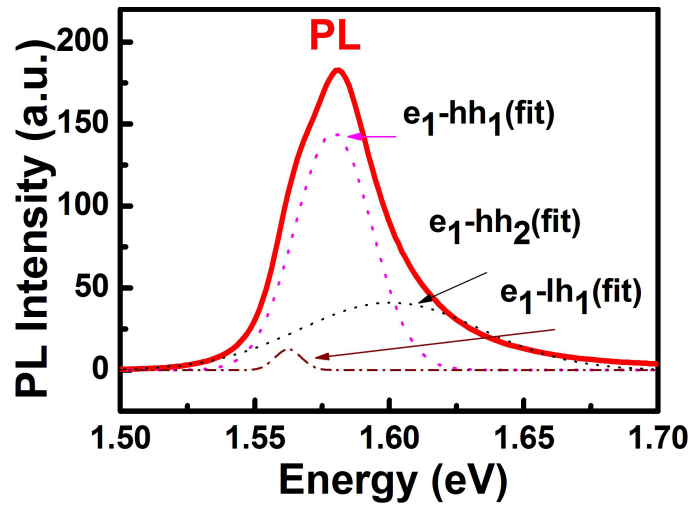


Figure 4.2: Photoluminescence (PL) spectrum of BQW at room temperature. The observed spectrum is resolved into three peaks shown by dashed and dotted lines. The transition corresponding to each peak is also indicated.

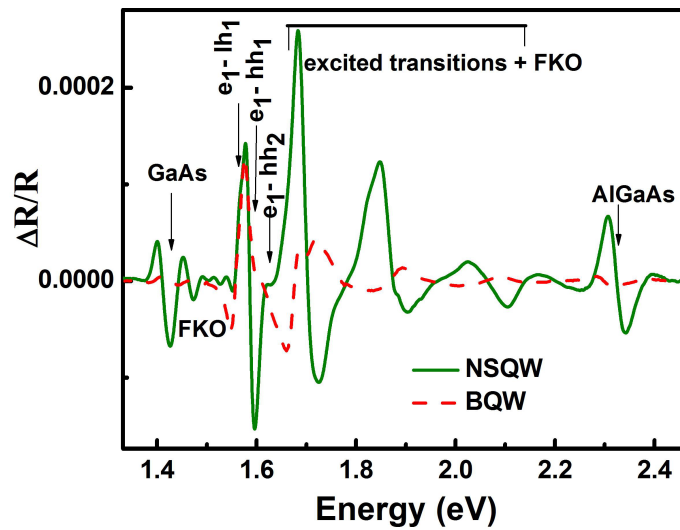


Figure 4.3: Photoreflectance spectrum of the NSQW and BQW. The energy levels of the GaAs substrate and barrier AlGaAs are also shown. FKO: Franz-Keldysh oscillations.

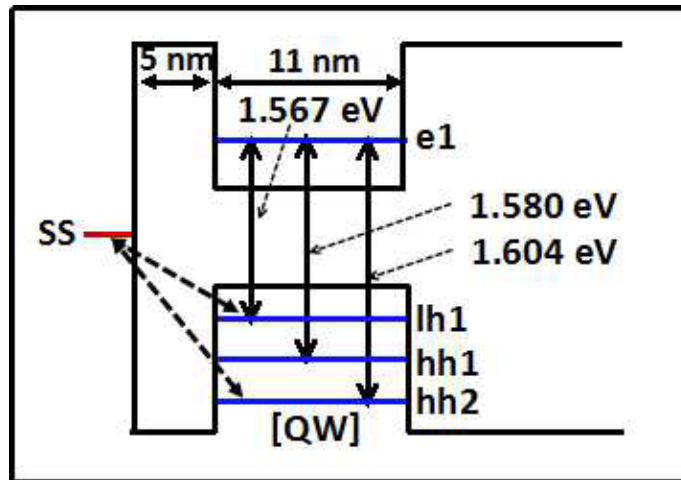


Figure 4.4: Energy levels: A schematic diagram showing the lowest energy levels and the transition energies in eV for the NSQW. The error in the energy of transitions is ± 2 meV estimated by the fitting of photoreflectance spectrum. *e1*: first electron level, *lh1*: first light hole, *hh1*: first heavy hole level, *hh2*: second heavy hole level, SS: surface state (approximate position). The energy levels of BQW are same except that the surface is too far away and the SS-hole transitions would be much less prominent.

intensity. The photorefectance spectra of both the samples were identical. The spectrum is shown in Fig. 4.3 with the identification of the various transitions. The corresponding energy level diagram (applicable to both samples) is shown in Fig. 4.4. For the NSQW, the possible position of the surface states is also indicated. It can be seen that the $e1 - lh1$ transition has the lowest energy as confirmed from both photoluminescence and photorefectance measurements. This is due to the tensile strain present in the sample [109].

The transient reflectivity measurements on these samples were performed at room temperature (23° C) in a standard degenerate pump-probe geometry described in chapter 2. The excitation laser was a ~ 70 fs, 82 MHz, Ti:Sapphire laser (Tsunami from Spectra Physics).

4.3 Transient Reflectivity

The transient reflectivity signal ($|\Delta R/R|$) for NSQW and BQW measured at a photon energy 1.577 eV is shown in Fig. 4.5. With a spectral width of 28 meV (FWHM) the laser beam excites the three lowest resonances $e1-hh1$, $e1-lh1$ and $e1-hh2$ of the NSQW. The time zero represents the arrival of the peak of the pump pulse on the sample. With the arrival of the pump pulse the $|\Delta R/R|$ increases, reaching a maximum near the end of the pump pulse. This can happen if the decay is not instantaneous so that even the later part of the pump pulse contributes to an increase in the signal [22]. This double decay behavior will also have a contribution arising due to the carriers excited either in the GaAs substrate or those trapped at the AlGaAs/GaAs interface [48, 110]. This is expected since, when the sample is excited at 1.577 eV, only a small part of the pump beam is absorbed by the thin quantum well layer. As a result more than 90% of the pump beam transmitted through the front surface of the sample reaches the GaAs which has a band gap of ~ 1.42 eV. The band gap of $Al_{0.7}Ga_{0.3}As$ is 2.07 eV, and it does not have any absorption at this

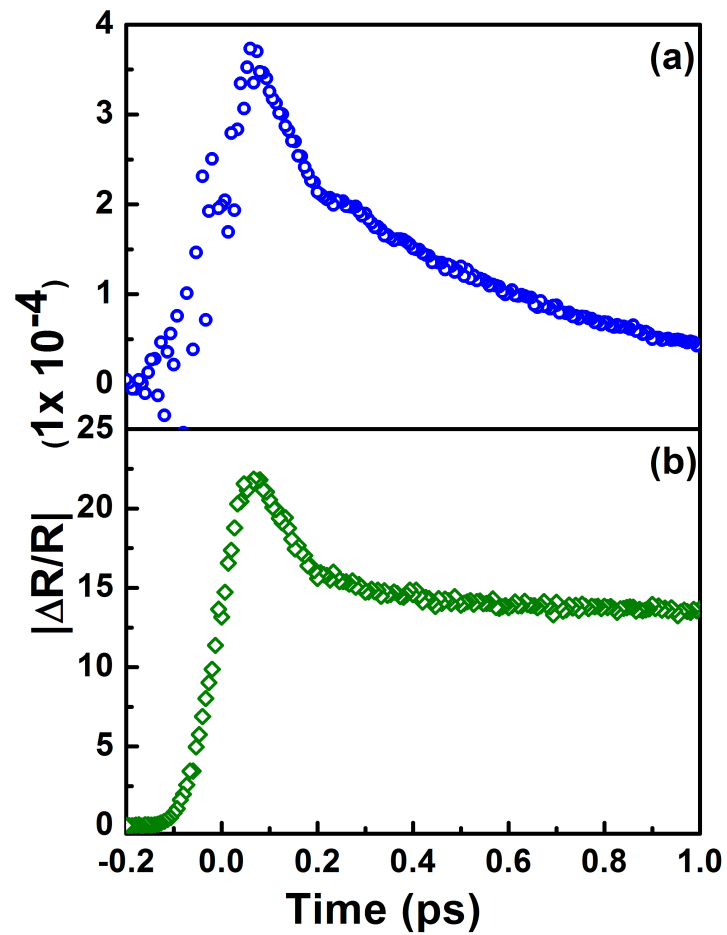


Figure 4.5: Transient reflectivity signal from (a) NSQW and (b) BQW. The laser photon energy is 1.577 eV and the pump fluence incident at sample was $26 \mu\text{Jcm}^{-2}$ (intensity was kept 2.1 kWcm^{-2}).

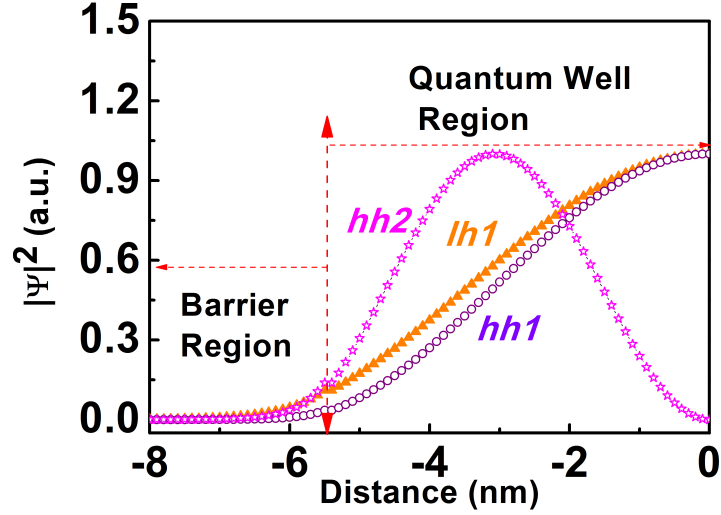


Figure 4.6: The wave functions corresponding to different hole states in the NSQW showing the higher tunneling of $lh1$ and $hh2$ as compared to $hh1$.

photon energy.

However, as can be seen from Fig. 4.5, the transient reflectivity recovery from the two quantum well samples is not exactly the same. For both the samples, the decay appears to have a fast and a slow component. By fitting a double exponential to the measured decay curves, the time constant for the first faster partial recovery has been found to be 40 fs for both the quantum wells. However, the slow component is markedly different, the time constant is estimated to be ~ 0.5 ps for NSQW and nearly 4 ps for BQW. The first fast decay is attributed to thermalization of photogenerated carriers [22,32] and is therefore the same for both quantum wells. In the second slower component the effect of proximity of surface states to the quantum well can be seen.

The calculated wave functions of the three lowest hole states are shown in Fig. 4.6. It can be seen that although all three wavefunctions tunnel out of the quantum well, the $lh1$ and $hh2$ tunnel to a much higher degree as compared to $hh1$. The higher tunneling of $lh1$ is due to its lower effective mass, whereas that of $hh2$ is

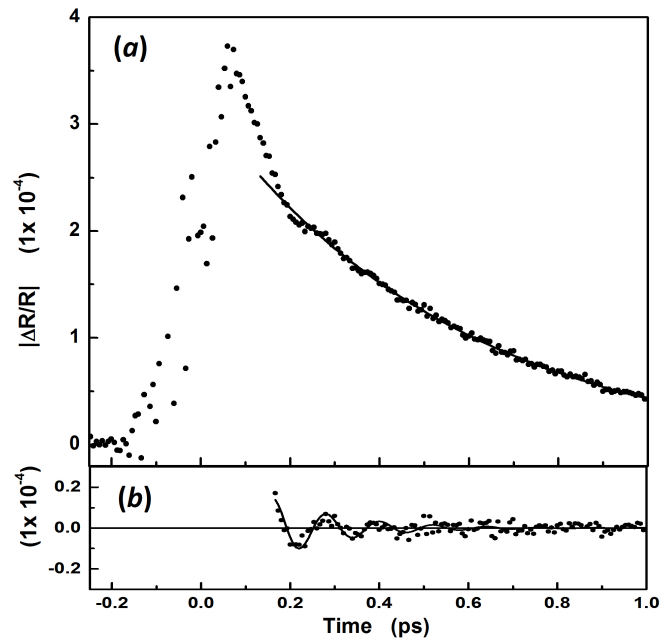


Figure 4.7: The transient reflectivity signal of NSQW. (a) The dots are the as measured $|\Delta R/R|$ and the line is the best fit to the data after 0.15 ps with a single exponential decay function. (b) The time dependence of \mathfrak{R} obtained from the experimental data. The solid line is the best fit to the data with F .

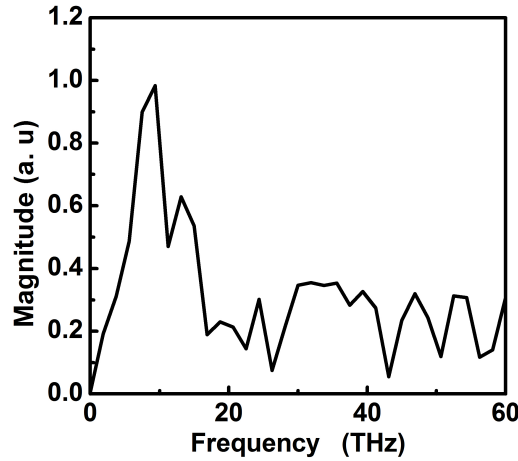


Figure 4.8: The FFT of the data after subtraction of the exponential decay function from experimental data (\mathfrak{R}).

due to its higher energy. Moreover, the space charge formation due to the surface termination results in an electric field near the surface. For NSQW, this electric field is estimated from the Franz-Keldysh oscillations in the photoreflectance spectrum to be $\sim 33 \text{ kVcm}^{-1}$ and is directed towards the surface. Thus it will assist in the movement of holes towards the surface. This tunneling of holes to the surface provides an alternate decay channel for the carriers. These results show that at room temperature the carrier decay time is 0.5 ps which is much shorter than the time-resolved photoluminescence decay times reported at low temperature. In the BQW, the surface is further away so that this process is not so effective and as a result the carrier lifetime in the quantum well is much longer.

A close observation of the $|\Delta R/R|$ curves of NSQW and BQW showed up another difference. In the NSQW a faint oscillation was observed superimposed on the slow exponential decay. This was investigated and determined to be a coherent effect. This analysis is described in the following section.

4.4 Coherent Coupling

The transient reflectivity curve of NSQW is shown again in Fig. 4.7(a). Faint oscillations can be seen starting from ~ 0.2 ps delay. To see the oscillations more clearly, the slow component fit was subtracted from the measured $|\Delta R/R|$ curve and the result is (denoted \mathfrak{R}) is shown in Fig. 4.7(b). We found that \mathfrak{R} could be fit well with a function, F , given by

$$F = A \cos\left(\frac{2\pi}{T}t + \phi\right) e^{-t/\tau}, \quad (4.1)$$

where A is the amplitude, T is the time period, ϕ is the phase and τ is the decay time of the oscillations. From the best fit we obtain the value of T and τ to be 120 ± 4 fs and 147 ± 10 fs respectively. Figure 4.8 shows the FFT of \mathfrak{R} showing a clear resonance at 8-9 THz. It may be recalled that the above data was taken at 1.577 eV where because of ~ 27.9 meV spectral width of the laser, all the three lowest transitions of the quantum well transitions were excited. We found that if the excitation laser energy was tuned away from 1.577 eV, the oscillations starts reducing. At a shift of ~ 20 meV the oscillations disappear completely. As example, the $|\Delta R/R|$ measured for the NSQW sample at 1.6 eV is shown in Fig. 4.9 and at 1.55 eV in Fig. 4.10. In both results, oscillations can not be seen.

This suggests that the oscillations occur only when the laser can excite all the quantum well transitions to some degree. For example, when the excitation is at 1.6 eV, $e1-lh1$ is not excited and when the excitation is at 1.55 eV $e1-hh2$ is not excited. We also made careful measurements at various photon energies on a sample of a single layer of AlGaAs on a GaAs substrate and a bare GaAs substrate. In neither case were the oscillations found to be present. Thus, it is confirmed that the oscillatory behavior observed in the transient reflectivity signal of NSQW involves quantum well levels and indicates the possibility of coherent coupling between them.

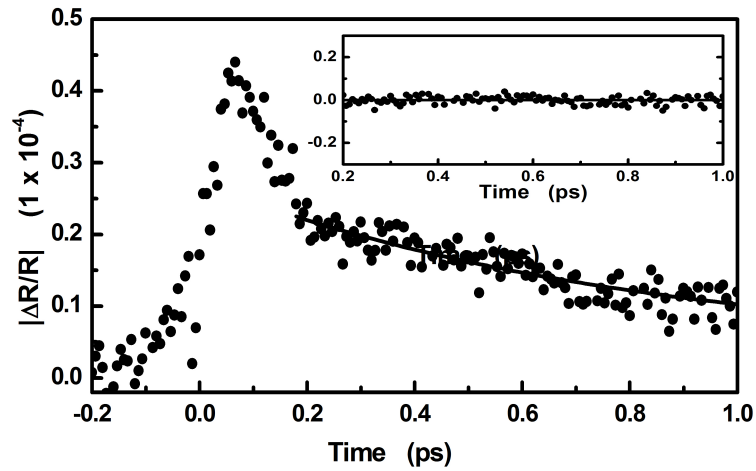


Figure 4.9: Same as Fig. 4.7 but for photon energy 1.6 eV. Inset shows the data after subtracting best fitted single exponential decay function.

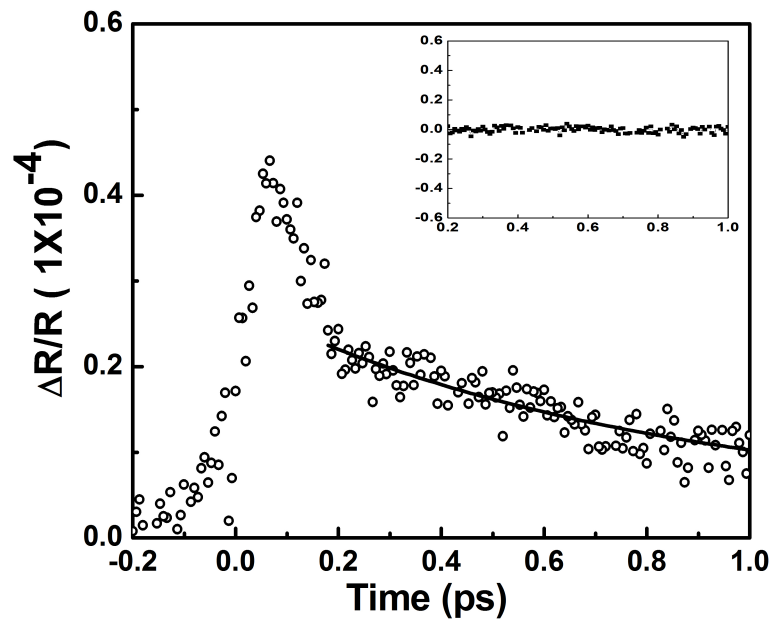


Figure 4.10: Transient reflectivity for sample NSQW at photon energy 1.55 eV. Inset shows the data after subtracting best fitted single exponential decay function.

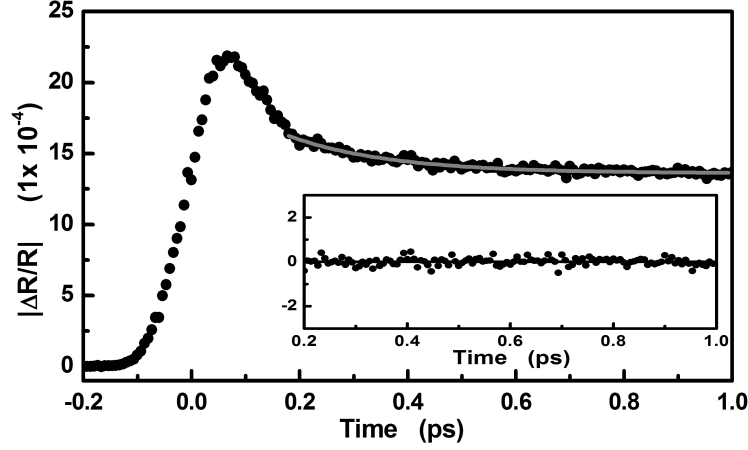


Figure 4.11: Same as Fig. 4.7 but for sample BQW at photon energy 1.577 eV. Inset shows the data after subtracting best fitted single exponential decay function.

In a three level system, carriers from two different levels can coherently coupled via a single third state [22]. This can lead to a beating in the coherent population of carriers and results in oscillations in the $|\Delta R/R|$ signal. Quantum beats have been reported in the transient reflectivity signal from an $\text{In}_x\text{Ga}_{1-x}\text{As}/\text{GaAs}$ strained single quantum well [38]. In this case the beating occurred due to the coherent coupling of light-hole and heavy-hole states with the electron state of the quantum well. In the present case there are three hole levels which can get coupled to the $e1$ state namely $lh1$, $hh1$ and $hh2$ (Fig. 4.4). The measured oscillation frequency (8-9 THz) matches with the energy difference between the levels $lh1$ and $hh2$ ($\sim 37 \pm 4$ meV). Thus it is possible that the interaction of $e1$ with levels $lh1$ and $hh2$ is generating the observed beating. The interaction of $e1$ with $lh1$ and $hh2$ should eventually result in emission of PL at corresponding energies. However, we could not record any PL emission from NSQW [111]. The typical time for electron-hole recombination (excitonic or free carrier) is of the order of nanoseconds. On the other hand the tunneling of holes from the quantum well to the surface state in the NSQW is expected to be in the

order of few hundreds of femtoseconds. The excited carriers tunnel to the surface states before recombining radiatively inside the quantum well [111]. Thus, in this case the interaction of $e1$ state to the hole states can not be the dominant mechanism which generates the observed oscillations.

Coherent beating in transient reflectivity has also been observed in asymmetric double quantum wells, super-lattices and multiple quantum wells [39,112,113]. In an asymmetric double quantum well with a sufficiently thin barrier, the states in the two wells are coupled due to tunneling of carriers from one well to the other. Although NSQW has only a single quantum well, its top barrier is thin (5 nm). As discussed above, the carriers excited in NSQW can tunnel to the surface. As soon as electrons and holes are excited inside the quantum well by the pump beam, the presence of surface electric field will also drive the holes to the surface. Although all the three hole states ($lh1$, $hh1$, and $hh2$) are excited the tunneling probabilities are different for each state as shown in Fig. 4.6. The two tunneling paths $lh1-SS$ and $hh2-SS$ can interfere and generate the observed beating in transient reflectivity signal from NSQW. This explains why coherent excitation of both $e1-lh1$ and $e1-hh2$ transitions (excitation energy 1.577 eV), which creates $lh1$ and $hh2$ hole populations, is required for observing the beating. On the other hand when the photon energy is tuned to 1.6 eV, only $hh1$ and $hh2$ states are populated. Since the tunneling probability of $hh1$ to the surface state is weak [111], beating between $hh1$ and $hh2$ is not observed. Same is the case for not observing beating between $hh1$ and $lh1$ when the photon energy is tuned to 1.55 eV. Our observation of quantum beats originating due to spatially separated holes and electrons is similar to that observed in Type-II quantum wells [40].

As discussed earlier in this chapter, the tunneling to the surface reduces with increasing top barrier layer thickness. This is confirmed by the transient reflectivity measurements on the BQW which has a top barrier layer of 50 nm. The same

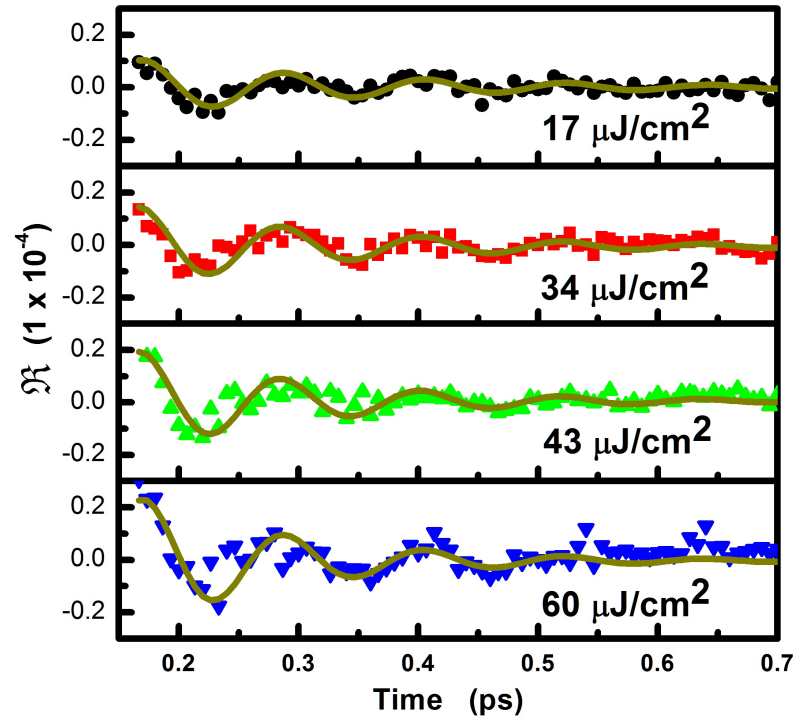


Figure 4.12: The dependence of the observed beating on the excitation fluence. Solid lines are best fit to the experimental data with the Eq.4.1.

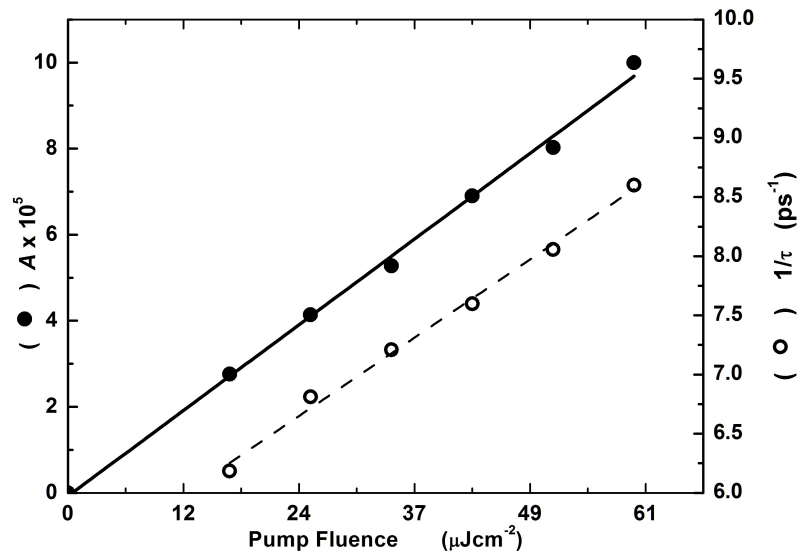


Figure 4.13: The dependence of beating oscillations on the pump fluence. Solid circles is the amplitude (A) and open circles are the $1/\tau$. The lines are the linear best fit to the data.

subtraction of slow exponential decay was applied to the BQW data of Fig. 4.5(b) and no oscillations were observed (Fig. 4.11). We have also measured the transient reflectivity of the NSQW at 1.577 eV and various pump fluences (Fig. 4.12). We find that the oscillation time period is independent of pump fluence. This is expected since the period of oscillations depends on the energy gap between $lh1$ and $hh2$ and is not expected to change for the pump fluences used in the present case [114]. With increasing pump fluence we observe a linear increase in both the amplitude of oscillation and the dephasing rate ($1/\tau$) (Fig. 4.13). As pump fluence increases, the number of excited carriers and hence the number of carriers tunneling to the surface increases. This leads to the observed increase in the amplitude of oscillations. It is known that the increased carrier-carrier scattering at higher carrier densities reduces the coherence time [114]. The observed increase in the dephasing rate with increasing pump fluence in NSQW suggests that the inter sub-band carrier-carrier scattering is the main cause for the observed dephasing.

4.5 Conclusion

Using transient reflectivity measurements, we have shown that in a near-surface GaAs_{0.86}P_{0.14}/Al_{0.7}Ga_{0.3}As single quantum wells, the room temperature carrier decay can be of the order of sub-ps. This fast decay occurs due to the tunneling out of photo-generated holes from the quantum well to the surface and subsequent non-radiative recombination with surface states. As a result, the slower radiative recombination becomes less probable and the photoluminescence disappears. We have also demonstrated for the first time, the occurrence of tunneling assisted coherent beating if the right combination of quantum well states are excited. The observed beating signal has a period of 120 ± 6 fs. This demonstration of a coherent interaction between surface and quantum well states even at room temperature could lead to possibility of coherent manipulation of carriers tunneling to surface.

Chapter 5

Carrier Dynamics in an AlGaAs-GaAs Heterostructure at low temperature

5.1 Introduction

The transient reflectivity results of chapter 4 showed that the surface states can play strong role in the carrier dynamics of semiconductor quantum wells. In this chapter, we investigate the effect of buried interfaces on the carrier dynamics. In order to avoid any ambiguity from carriers generated in multiple layers, an AlGaAs-GaAs heterostructure sample with a single interface between the GaAs and AlGaAs layers has been used. This structure is similar to that on which the single quantum well samples (used in the work reported in chapter 4) were grown.

In any AlGaAs-GaAs heterostructure, an electric field is developed at the interface due to the difference between the band gaps of GaAs and AlGaAs and any difference in doping. This built-in electric field causes band-bending resulting in a

triangular well at the interface [2,43,46]. Some of the photo-excited electrons (holes) generated in GaAs near the interface move towards it under the influence of built-in electric field and get trapped in the triangular well. Thus a two-dimensional electron (hole) gas is formed while the electrons (holes) are confined. In the sample used in this study, the AlGaAs layer is n-doped while the GaAs buffer layer is undoped. This will result in free electrons getting trapped in the triangular well and forming a two-dimensional electron gas (2DEG). The built-in field in an AlGaAs heterostructure is typically $\sim 30\text{-}40 \text{ kVcm}^{-1}$ and the extent of the resultant triangular well is about 10 nm [46,53,68]. The 2DEG systems are of great interest as they provide high mobility electrons where the carrier density and mobility can be controlled by selecting suitable doping level and structure design. AlGaAs-GaAs, in particular, is very popular semiconductor heterostructure which has been widely used in devices like metal-oxide semiconductor field effect transistors and high electron mobility transistors [1-3].

The dynamics of two-dimensional electron gas has mostly been studied by time integrated and time resolved photoluminescence at low temperatures [27,53,115–119]. In the photoluminescence from AlGaAs-GaAs heterostructures, a peak, which is red shifted compared to the GaAs peak, has been identified as the photoluminescence from the carriers confined in the 2DEG. This peak usually overlaps the emission from the defect states but two can be separated by their intensity dependence. The peak position of two-dimensional electron gas photoluminescence spectrum shows a blue shift with increasing carrier density [53,53,116] whereas the defect peak position remains constant. Time resolved photoluminescence measurements have been reported using femtosecond laser excitation and streak camera detection with a time resolution up to $\sim 20 \text{ ps}$ [27,115,117]. The two-dimensional electron gas photoluminescence peak position shows a blue shift on excitation. This blue shift recovers (red shifts) as the carriers recombine. The formation of two-dimensional electron gas in AlGaAs-GaAs heterostructure is reported to be $\sim 50 \text{ ps}$ [27,115,117] and the decay

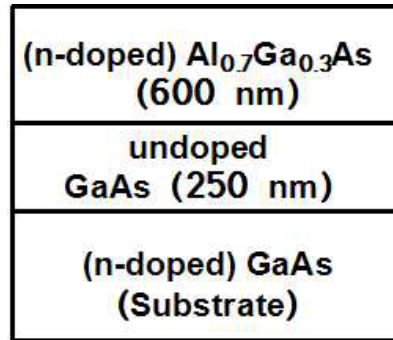
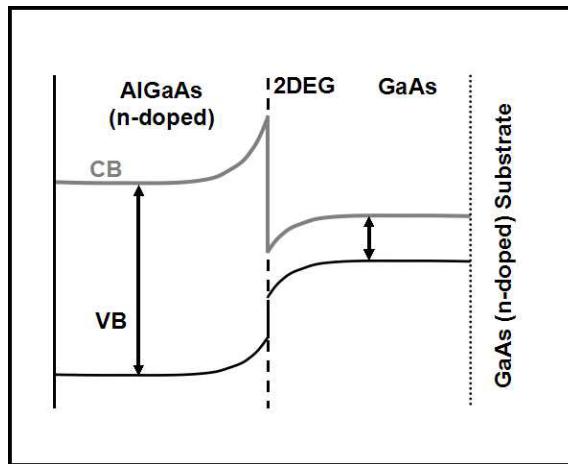
in range from 0.5 ns to a few ns [27,115,117]. However, the fact that the defect state and photoluminescence of two-dimensional electron gas are almost overlapping, does bring in some uncertainty in the time resolved photoluminescence measurements. Also the time resolution is limited by the streak camera to a few ps. The frequency up-conversion technique can have a much better time resolution. However, even at low temperature the photoluminescence intensity from two-dimensional electron gas in an AlGaAs-GaAs heterostructure is too low to permit time resolved measurement.

Transient reflectivity, on the other hand, does not have any of these drawbacks. It gives a reasonably large signal at room temperature as well as at low temperatures. The time resolution is limited only by the laser pulse width, so measurements with sub-ps time resolution are possible. A recent report on p-GaInP₂/TiO₂ heterostructure at room temperature using femtosecond pump white light continuum probe reflectivity has demonstrated that the drift of carriers to the interface is completed within the probe pulse width of 150 fs [120].

Degenerate transient reflectivity has been used to probe the low temperature carrier dynamics of the two-dimensional electron gas formed at the interface of an AlGaAs-GaAs heterostructure. The origin of different resonances is established with the help of the photoluminescence spectrum. In this chapter it has been shown that, in the AlGaAs-GaAs heterostructure, the two-dimensional electron gas formation is completed within ~ 200 fs.

5.2 Experimental details

The AlGaAs-GaAs heterostructure sample used for this work has composition Al_{0.7}Ga_{0.3}As-GaAs. The layer structure is shown in Fig. 5.1. Undoped GaAs of thickness 250 nm was grown on the n-type doped GaAs substrate (2×10^{18} cm⁻³). A 600 nm thick Al_{0.7}Ga_{0.3}As layer was grown on top of this undoped GaAs. The doping of Al_{0.7}Ga_{0.3}As layer was n-type with doping similar to the substrate. The

Figure 5.1: Sample structure of the Al_{0.7}Ga_{0.3}As-GaAs heterostructure.Figure 5.2: Band bending diagram of the Al_{0.7}Ga_{0.3}As-GaAs heterostructure. CB and VB are the conduction and valence bands respectively.

band bending near the interface is shown in Fig. 5.2. A piece of the GaAs substrate was used for some reference measurements for comparison.

Low temperature transient reflectivity measurements were carried out using the setup described in chapter 2. The excitation laser was Ti:Sa femtosecond oscillator (Tsunami, Spectra Physics) with a pulse width of ~ 100 fs and tuning range from 750 nm - 840 nm. The low temperature photoluminescence was measured using a commercial cryostat.

5.3 Results

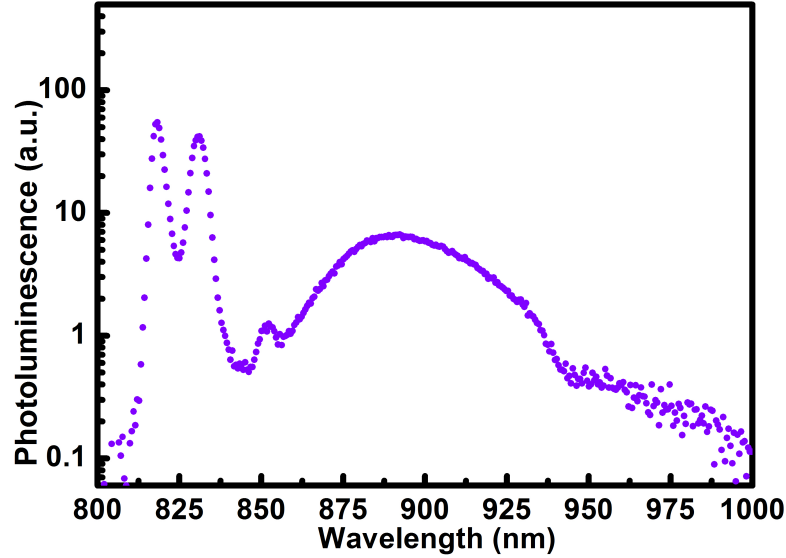


Figure 5.3: Photoluminescence spectrum of $\text{Al}_{0.7}\text{Ga}_{0.3}\text{As}$ -GaAs heterostructure at 11 K. Excitation wavelength is 632.8 nm.

5.3.1 Photoluminescence

Photoluminescence is a simple and effective method to determine the resonances present in the semiconductor sample. However, it is usually not possible to observe the photoluminescence at room temperature due to strong non-radiative decay. The photoluminescence spectrum of the heterostructure measured at 11 K is shown in Fig. 5.3. The spectrum shows various sharp and broad features in the range of 800 nm to 1000 nm. As the excitation is below the $\text{Al}_{0.7}\text{Ga}_{0.3}\text{As}$ band gap, the likely origin of all the observed photoluminescence peak is from various excitation and recombination in GaAs part of the heterostructure sample. However, mid-gap states of $\text{Al}_{0.7}\text{Ga}_{0.3}\text{As}$ can occur in this region. Thus to confirm any such contribution, the sample was excited with with 405 nm diode laser so that excitation is only inside $\text{Al}_{0.7}\text{Ga}_{0.3}\text{As}$ part. No photoluminescence emission was observed from the sample.

To identify the peaks present in the photoluminescence spectrum of the heterostructure sample, photoluminescence spectrum of similar bulk GaAs was also measured. The photoluminescence spectrum is shown in Fig. 5.4. Two broad peaks

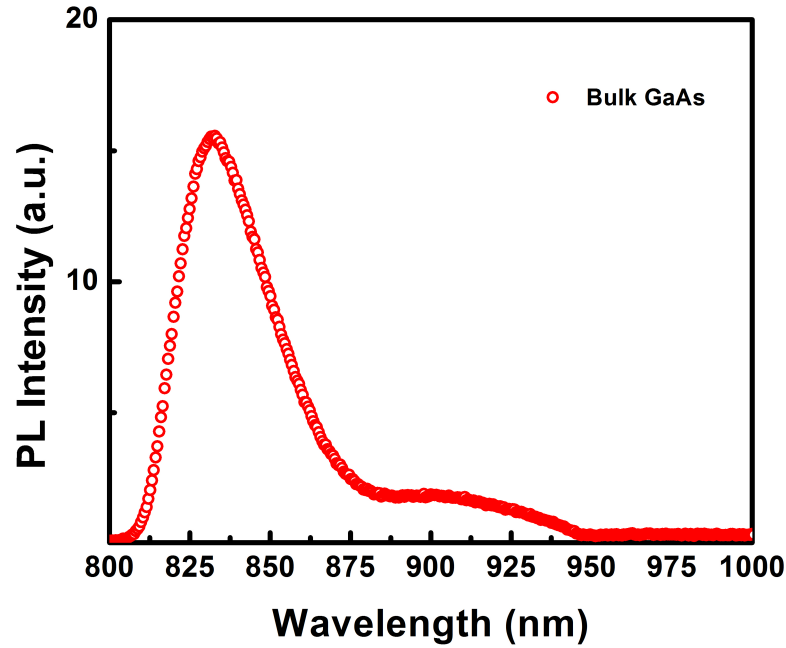


Figure 5.4: Photoluminescence signal measured from bulk GaAs at 11K. Excitation laser wavelength was kept at 632.8 nm.

are observed near 831 nm and at ~ 905 nm. In literature, such peaks have been assigned to donor-to-acceptor pair (DAP) at 831 nm and to defect state (~ 905 nm) [53, 115, 116, 119].

The PL spectrum of heterostructure and bulk GaAs is compared below 850 nm to identify the peaks observed in the $\text{Al}_{0.7}\text{Ga}_{0.3}\text{As}$ -GaAs heterostructure. The comparison at 11 K is shown in Fig. 5.5. One of the peaks observed in the heterostructure is similar to that observed in GaAs which is related to DAP. The other peak at around 817 nm is reported to be excitonic in nature [53, 115, 116, 119]. Since the transient reflectivity measurement is done at 40 K for studying the carrier dynamics, the photoluminescence spectrum at 40 K is also recorded. The photoluminescence spectrum from $\text{Al}_{0.7}\text{Ga}_{0.3}\text{As}$ -GaAs heterostructure along with photoluminescence from bulk GaAs is plotted in Fig. 5.6. The peak at 818 nm is related to excitonic and peak at 831 nm is related to DAP. The DAP peak is observed in both heterostructure

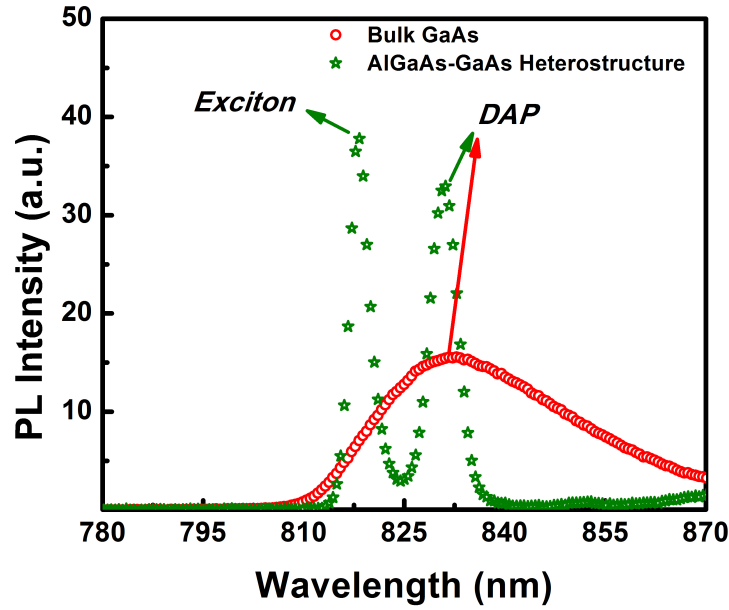


Figure 5.5: Photoluminescence signal from $\text{Al}_{0.7}\text{Ga}_{0.3}\text{As}$ -GaAs heterostructure showing PL from GaAs features at 11K. The photoluminescence from bulk GaAs is also shown at the same temperature. The excitonic and Donor to Acceptor (DAP) peaks are shown.

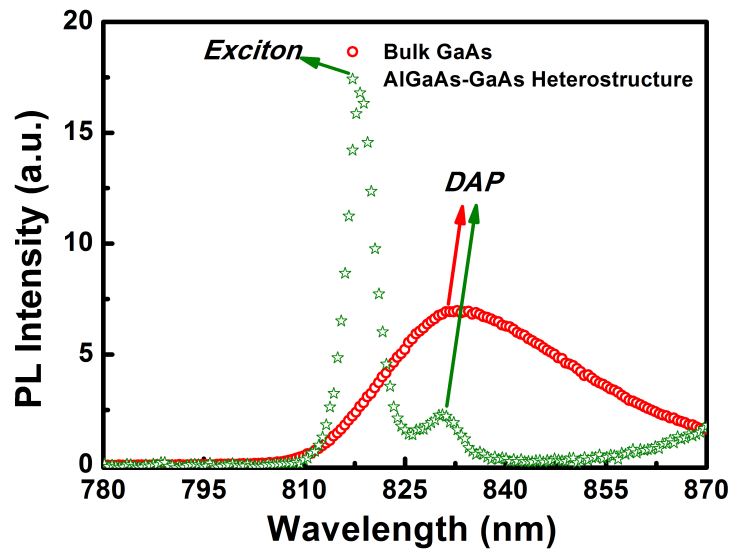


Figure 5.6: Photoluminescence signal from $\text{Al}_{0.7}\text{Ga}_{0.3}\text{As}$ -GaAs heterostructure showing PL from GaAs features at 40 K. The photoluminescence from bulk GaAs is also shown at the same temperature. The excitonic and Donor to Acceptor (DAP) peaks are shown.

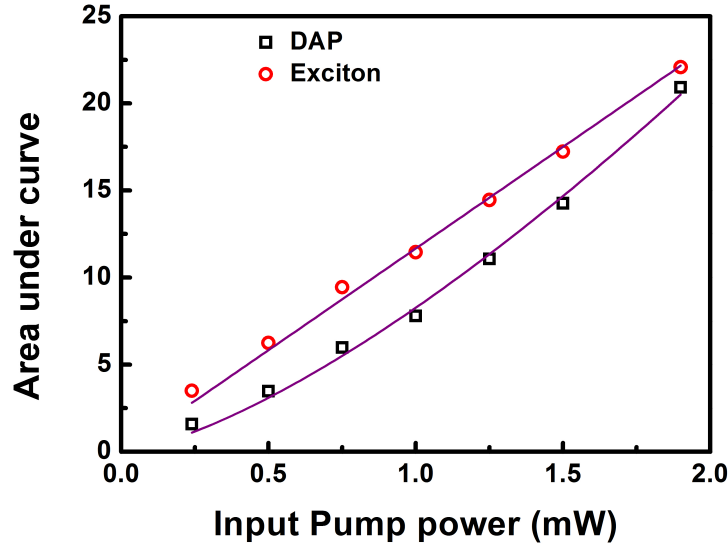


Figure 5.7: Area under curve plotted against input pump power for excitonic as well as DAP peak at 11 K. Solid line is fit to the curve using Eqn. 5.1. Excitonic recombination showed linear variation whereas DAP showed nonlinear variation with input pump power.

as well as bulk GaAs. The nature of recombination is confirmed by performing intensity dependent photoluminescence measurements on the heterostructure sample and plotting area under curve as a function of intensity for both peaks. The plot is shown in Fig. 5.7. The plot is fit to the Eqn. 5.1.

$$PL_{area} = AI^a. \quad (5.1)$$

A is arbitrary fit parameter and the value of fitting parameter a decides the nature of recombination. The plot shows linear dependence ($a = 1$) for the peak at 818 nm whereas it is nearly $a = 1.41$ for the peak at 831 nm. Since excitonic recombination is single particle recombination it shows linear and donor-to-acceptor pair recombination is many body interaction, which can show value of a from 1-2 [72]. Hence, in this heterostructure sample, excitonic formation is observed along with the donor-to-acceptor pair recombination.

Now, the peaks above 850 nm observed in the heterostructure sample have to be addressed. It has been found that two peaks are present as shown in Fig. 5.8 by fitting the spectrum to two peak gaussian function. One peak comes out to be at ~ 890 nm and another one at nearly 905 nm. Bulk GaAs has also showed peak at 905 nm which is attributed to defect state [53, 115, 116, 119]. The peak at 890 nm could be signature of two-dimensional electron gas formed near the interface [53, 115, 116, 119]. To confirm this, intensity dependent photoluminescence measurement was performed. The formation of two-dimensional electron gas is confirmed by intensity dependent photoluminescence measurement. The triangular well is formed due to built-in electric field which lowers with more and more excited electron-holes in the sample. Therefore, the band bending reduces and thus becomes more and more flat when photoexcitation intensity is increased. In such case photoluminescence observed from two-dimensional electron gas will be more blue shifted with carrier density which is effectively due to increased intensity. The photoluminescence peak position is plotted against excitation power for both two-dimensional electron gas and defect state. The result is shown in Fig. 5.9. The peak position related to two-dimensional electron gas shifts towards blue with intensity whereas the peak at ~ 905 remains at same place. This confirms the the formation of two-dimensional electron gas.

The different peaks observed in the photoluminescence spectrum of Al_{0.7}Ga_{0.3}As-GaAs heterostructure has been addressed. The two-dimensional electron gas formation is observed at low temperature. Exciton has also been observed in the photoluminescence spectrum of Al_{0.7}Ga_{0.3}As-GaAs heterostructure. The exciton is not observed in bulk GaAs where DAP recombination is dominant mechanism. The exciton formation in Al_{0.7}Ga_{0.3}As-GaAs heterostructure is due to confinement of electrons near the interface within the ~ 10 nm triangular well.

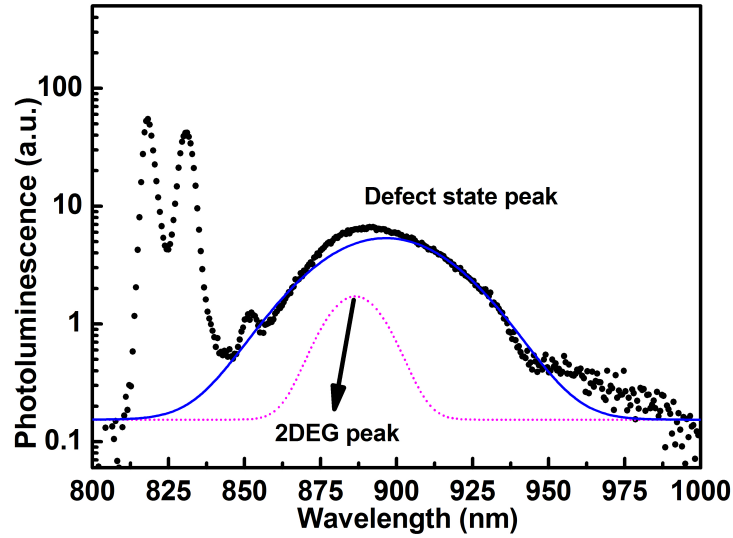


Figure 5.8: Contribution of 2DEG and defect state to the low temperature photoluminescence spectrum of the $\text{Al}_{0.7}\text{Ga}_{0.3}\text{As}$ -GaAs heterostructure at 11 K. The two peaks above ~ 840 nm are due to free carriers and DAP recombination as shown in Fig. 5.6. The broad peak below 870 nm can be resolved in two peaks. The peak at nearly 890 nm is attributed to 2DEG recombination and that at ~ 905 nm to the recombination from defect states.

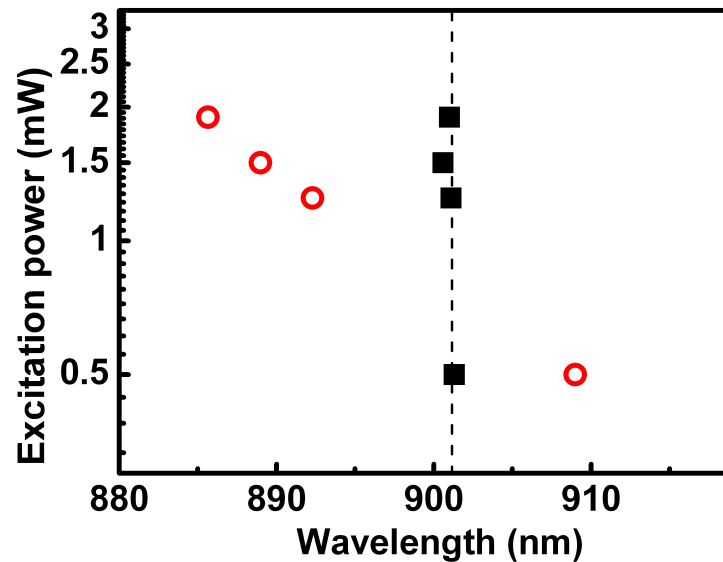


Figure 5.9: The variation of peak wavelength of two-dimensional electron gas and defect state peaks with excitation power at 11 K; circles - 2DEG peak and squares - defect state peak.

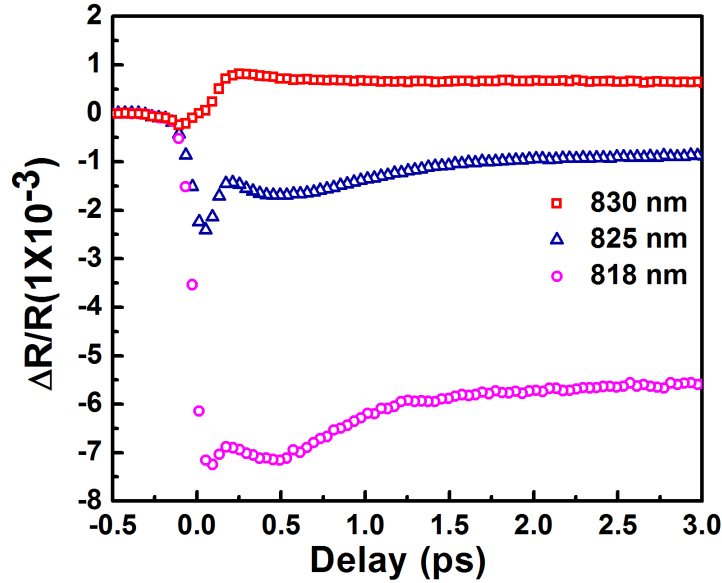


Figure 5.10: Transient reflectivity signal at 40 K measured on $\text{Al}_{0.7}\text{Ga}_{0.3}\text{As-GaAs}$ heterostructure at three different wavelengths.

5.3.2 Transient Reflectivity

The various peaks observed in the photoluminescence spectrum of the $\text{Al}_{0.7}\text{Ga}_{0.3}\text{As-GaAs}$ heterostructure show that there are several relaxation paths available to carriers generated in the GaAs layer e.g. excitonic or DAP recombination, two-dimensional electron gas formation etc. The relative probability of these recombination processes is highly temperature dependent. To study the ultrafast dynamics of these processes through transient reflectivity, measurements were carried out at different temperatures. At 40 K, three excitation wavelengths were used; the first was 818 nm which corresponds to the excitonic recombination, the second was 825 nm which corresponds to DAP recombination and the third was an intermediate 825 nm. In the last one, both recombination channels would be accessible due to the ~ 10 nm spectral width of the femtosecond laser. The recovery in transient reflectivity signal was partial till 150 ps. However, some interesting features were observed in the sub-ps region and therefore detailed investigations were done for this part of the

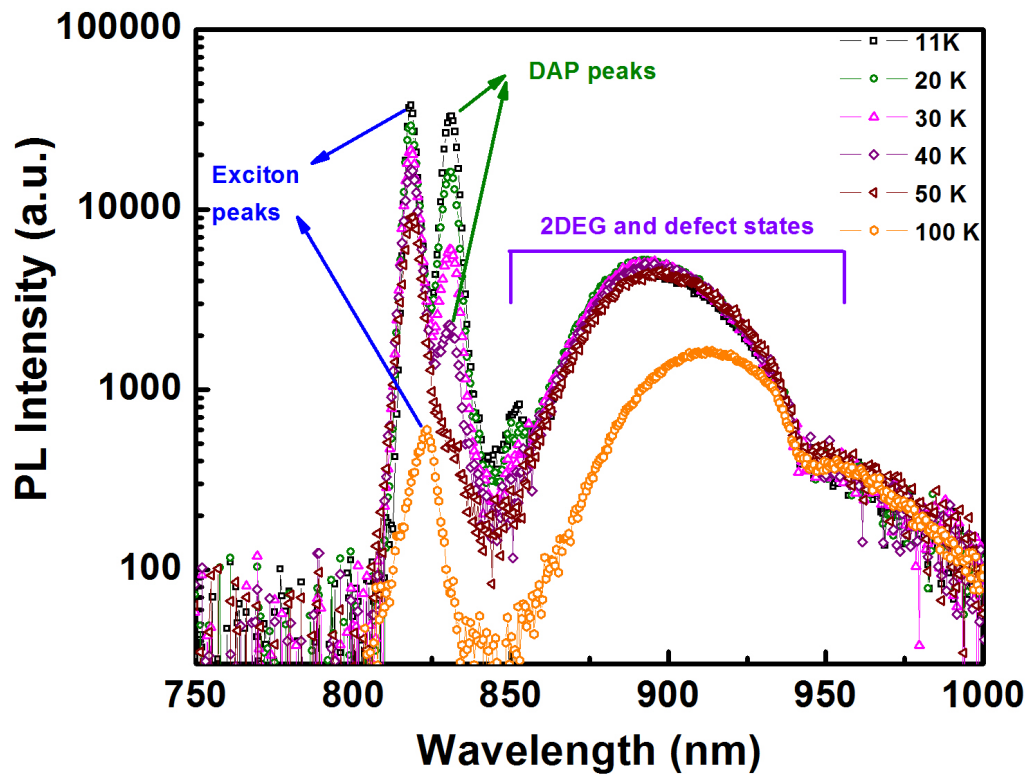


Figure 5.11: Photoluminescence spectrum of $\text{Al}_{0.7}\text{Ga}_{0.3}\text{As-GaAs}$ heterostructure measured at different temperatures. DAP peak becomes weaker with increasing temperature. It completely disappears at 100 K.

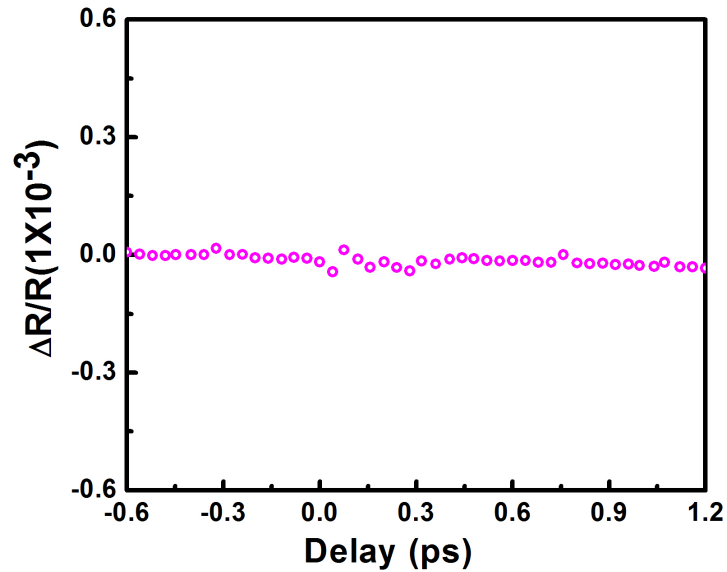


Figure 5.12: Transient reflectivity signal from $\text{Al}_{0.7}\text{Ga}_{0.3}\text{As-GaAs}$ heterostructure at room temperature at 890 nm. No transient signal is observed.

transient reflectivity. Figure 5.10 shows the early portion of the transient reflectivity at the three wavelengths. The signal at 818 nm and 825 nm showed modulations in the beginning (up to ~ 800 fs) which was absent at 830 nm. a likely explanation of these modulations comes by recalling that a built-in field is present near the interface of the heterostructure which can cause free carriers to drift towards it. This drift would thus be more prominent at 818 nm than at 830 nm where the stringer DAP recombination indicates less availability of free carriers.

The DAP recombination strength changes with temperature. The temperature dependent photoluminescence has shown that DAP recombination becomes very weak at 50 K and almost disappears at 100 K as shown in Fig. 5.11. At room temperature the DAP recombination is expected to be at 890 nm. Figure 5.12 shows the room temperature transient reflectivity measurement at 890 nm. No signal is observed and the transient reflectivity is nearly flat with pump-probe delay. To further confirm the role of DAP, the transient reflectivity measurement has been performed at 100 K and 830 nm and is shown in Fig. 5.13. A strong modulation

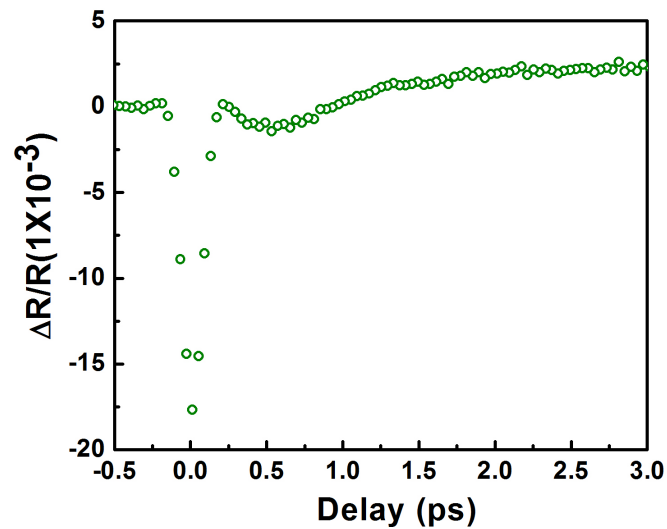


Figure 5.13: Transient reflectivity signal measured at 100 K from $\text{Al}_{0.7}\text{Ga}_{0.3}\text{As-GaAs}$ heterostructure at wavelength 830 nm.

is again observed. The photoluminescence spectrum shown in Fig. 5.11 shows that DAP peak is missing at 100 K as the DAP can ionise easily at higher temperatures. Thus, the carriers are not trapped by DAP and electrons drift towards interface and modulations are observed in the transient reflectivity signal measured at 100 K. As the temperature is increased further, free carriers will be more excited/present under photoexcitation. The transient reflectivity measured at room temperature at 800 nm is shown in Fig. 5.14. Strong sub-ps modulations can be observed again.

We propose the following explanation for these observations. A schematic of the proposed process is shown in Fig. 5.15. As soon as the femtosecond laser falls on the heterostructure, carriers will be generated in GaAs layer. The electrons will start moving towards the interface under the built-in electric field and get accumulated in the triangular well. This will increase the magnitude of change in refractive index as the carriers concentration is increasing in the well. On the other hand, The holes will move away from the interface. The width of the triangular well formed near the

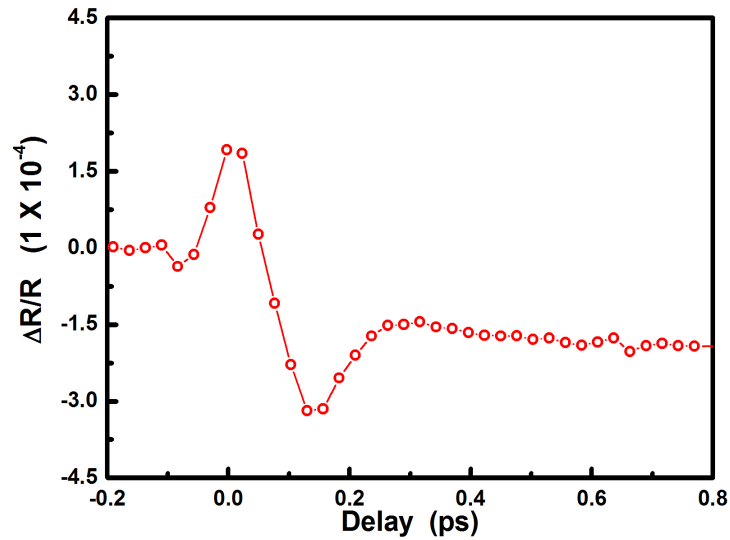


Figure 5.14: Transient reflectivity signal measured from $\text{Al}_{0.7}\text{Ga}_{0.3}\text{As}$ -GaAs heterostructure and GaAs at room temperature at 800 nm. The signal from heterostructure showed modulation.

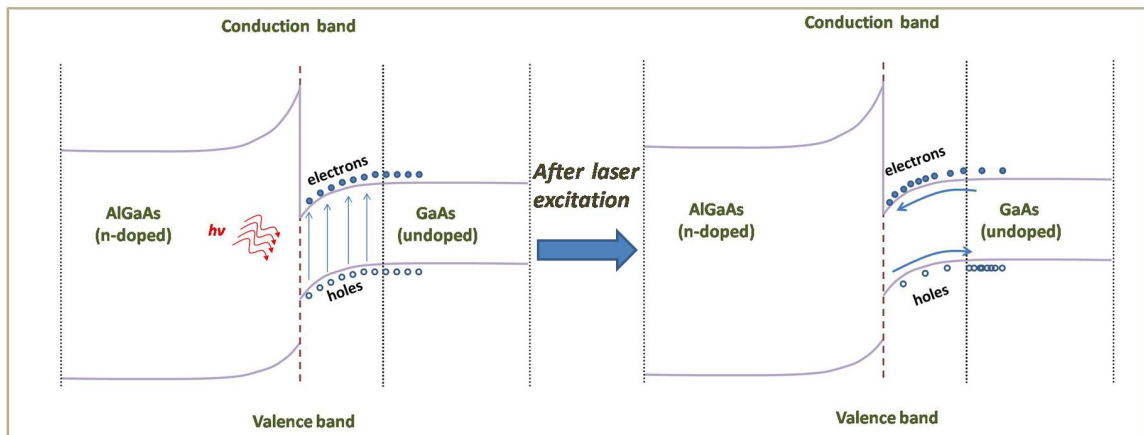


Figure 5.15: The figure shows that when femtosecond laser falls on the sample, electron hole pairs are generated in GaAs. Some of the excited electrons in conduction which are near the interface will move towards the triangular well and accumulate there. The holes will be moving away from the interface.

interface of Al_{0.7}Ga_{0.3}As-GaAs heterostructure is typically 10 -15 nm. The time for drift of electrons will be of few tens of femtoseconds under built-in field of $\sim 30\text{-}40$ kVcm⁻¹. The holes will move away but with a slower drift velocity. These two drifts with two different time scales result in the sub-ps modulations observed in measured transient reflectivity signal.

5.4 Conclusion

In this chapter it has been shown that sub-ps modulations in the transient reflectivity of an Al_{0.7}Ga_{0.3}As-GaAs heterostructure are indicative of carrier drift towards the interface. Since this carrier drift is an essential requirement for the formation of two-dimensional electron gas, we propose that the presence of these modulations is a signature of two-dimensional electron gas formation. This is an important result showing the advantage of transient reflectivity measurements over photoluminescence in carrier dynamics studies at higher temperatures. Our results show that in the Al_{0.7}Ga_{0.3}As-GaAs heterostructure the drift of photo-generated carriers starts immediately on excitation by the femtosecond laser pulse. The completion time of the drift process reduces with increasing temperature such that at room temperature it comes down to ~ 200 fs from nearly 800 fs at 40 K.

Chapter 6

Room Temperature Carrier Dynamics in AlGaAs-GaAs Heterostructures

6.1 Introduction

In the previous chapter it has been shown that the carrier dynamics in an AlGaAs-GaAs heterostructure has an ultrafast component of sub-ps time scale which indicates the drift of carriers and formation of two-dimensional electron gas. The room temperature measurement are important for heterostructures to be used as devices. Therefore, the formation and decay of two-dimensional electron gas and its dependence on the experimental parameters needs to be studied at room temperature. However, an issue with transient reflectivity is the interpretation of the results. Resonant excitation of the two-dimensional electron gas is not possible, as carriers have to be excited in bulk GaAs which subsequently forms two-dimensional electron gas. The energy levels of bulk GaAs and two-dimensional electron gas are very close to each other, so that unambiguous interpretation of dynamics becomes difficult.

Still a few transient reflectivity measurements have been reported at different temperatures [46, 48, 118]. In these studies it was proposed that a change in sign of the transient reflectivity can be used to identify the presence of 2DEG. For example in ref. [46, 48, 118] reported that in an AlGaAs-GaAs heterostructures, the transient reflectivity changed sign every 20 nm. This was attributed to the combined effect of electron cooling and bulk and 2DEG contributions to the transient reflectivity. It was also reported that the bulk GaAs contribution to the reflectivity (positive contribution) was absent at some wavelength and also with temperature at a given wavelength [48, 118]. The transient reflectivity was also reported to change sign with increasing intensity [48, 118]. However, no firm explanation was available for the observed sign changes. Based on the above observations, it was concluded by the authors that the 2DEG recovery is slower (1200 ps) compared to that in bulk GaAs (730 ps) which changed with intensity. It may be noted that these papers did not discuss much about the sub-ps dynamics of transient reflectivity whereas we have shown that this regime can have a characteristic signature of the 2DEG formation.

In this chapter we have investigated the room temperature carrier dynamics of 2DEG in an AlGaAs-GaAs heterostructure. We have been able to evolve a new and elegant technique which unambiguously differentiate between the 2DEG and bulk contributions to the transient reflectivity. This is achieved by choosing the appropriate wavelength to probe the sample based on the linear reflectivity spectrum. The details are described in the following section 6.3.1

6.2 Experimental details

In this study two AlGaAs-GaAs heterostructure samples have been used. Most of the measurements have been carried out on the same n-doped AlGaAs-GaAs heterostructure on which the low temperature studies described in chapter 5 were carried out. The second sample is a p-doped AlGaAs-GaAs heterostructure. The

layer structures of the two samples are shown along with the results in the following sections.

Room temperature transient reflectivity measurements were performed using the setup described in chapter 2. The excitation laser was a 100 fs, 80 MHz, Ti:Sapphire laser (MAITAI, Spectra Physics).

6.3 Transient reflectivity results

6.3.1 n-doped Al_{0.7}Ga_{0.3}As-GaAs heterostructure

Following the earlier work, we also started by measuring the room temperature transient reflectivity at different wavelengths. Figure 6.1 shows the transient reflectivity data at four wavelengths, all well above the GaAs band-gap. We also observed that the transient reflectivity signal changes sign as the wavelength is changed, being positive at 765 nm and 786 nm, and negative at 800 nm and 836 nm. As shown in earlier reports, the negative signal should correspond to carriers confined in the 2DEG and the positive signal to carriers in bulk GaAs [46, 48, 118]. However, as we have shown in chapter 5, the formation of 2DEG is also indicated by sub-ps oscillations in the transient reflectivity signal. An examination of Fig. 6.1 shows that though the appearance of modulations is dependent on the excitation wavelength it is apparently not correlated with the sign of the signal. They appear both for positive (at 786 nm) and negative (800 nm) signals. Since the source of photoexcited carriers is from GaAs part of the Al_{0.7}Ga_{0.3}As-GaAs heterostructure, we also performed measurements on GaAs to see the variation with wavelength. Figure 6.2 shows the TR signal for GaAs at three wavelengths. In all cases the transient reflectivity is positive. It recovers with two different time constants which correspond to intraband and interband relaxations [84, 100]. In the present study the excitation intensity is $\sim 2.1 \text{ kWcm}^{-2}$. The excited carrier density is of the order of $\sim 10^{15} \text{ cm}^{-3}$ as discussed

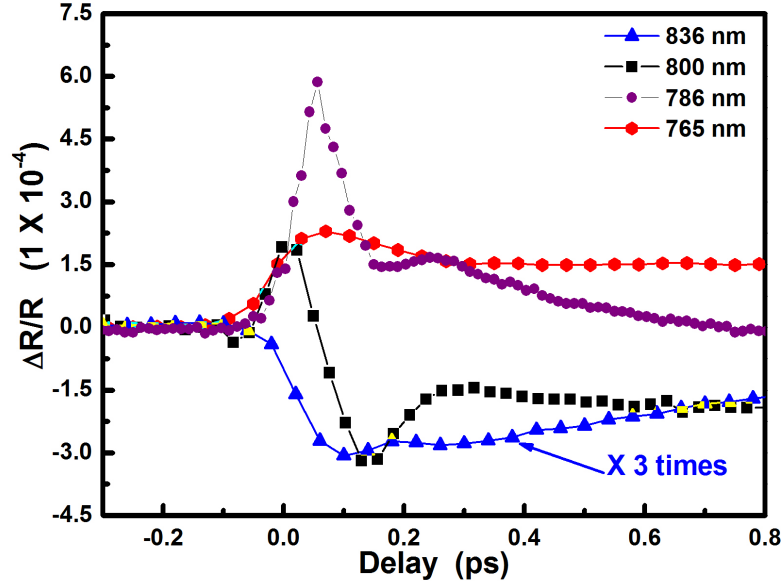


Figure 6.1: Transient reflectivity signal measured at different wavelengths for the n-type heterostructure. Note that the signal at 836 nm has been multiplied by three for clarity.

in chapter 3, the reflectivity change in GaAs is positive mainly due to band filling at this photoexcited carrier density [84,95].

Thus, it seems likely that, both the sign reversal and the sub-ps modulations arise due to the heterostructure, but their dependence on the excitation wavelength is not clear. However, it is to be noted that the heterostructure is a multilayer structure with layers of different refractive indices and the linear reflectivity itself would have a wavelength dependence due to interference from the partial reflections from each layer. Once the 2DEG forms, the heterostructure can be assumed to have three layers, namely the AlGaAs layer, the 2DEG layer and the GaAs layer as shown in Fig. 6.3.

The reflectance from this three layer structure at a given wavelength, λ , is [78, 79]

$$r = \frac{r_1 + r_2 e^{-2i\delta_1} + r_3 e^{-2i(\delta_1 + \delta_2)} + r_1 r_2 r_3 e^{-2i\delta_2}}{1 + r_1 r_2 e^{-2i\delta_1} + r_1 r_3 e^{-2i(\delta_1 + \delta_2)} + r_2 r_3 e^{-2i\delta_2}}, \quad (6.1)$$

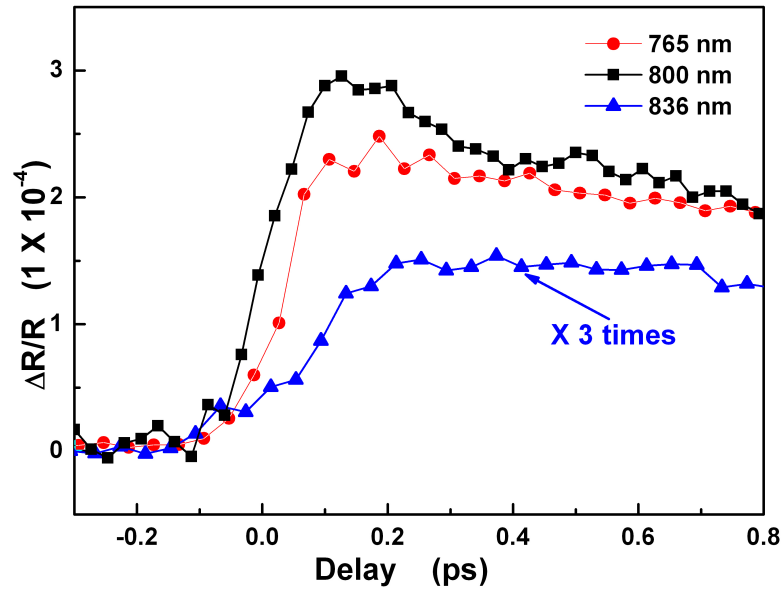


Figure 6.2: Transient reflectivity signal from bulk GaAs at three different wavelengths. Note that the signal at 836 nm has been multiplied by three for clarity.

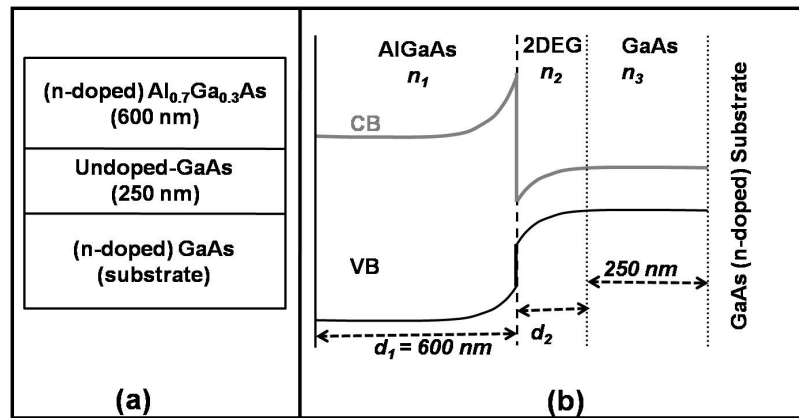


Figure 6.3: (a) Schematic of the n-type heterostructure. (b) The band bending diagram. n_1 , n_2 and n_3 are the refractive indices for AlGaAs, 2DEG region and GaAs respectively. d_1 and d_2 are the thickness of the top AlGaAs layer and the 2DEG layer respectively.

where n_1 , n_2 and n_3 are refractive indices of AlGaAs, 2DEG and GaAs respectively and $\delta_1 = 2\pi n_1 d_1/\lambda$ and $\delta_2 = 2\pi n_2 d_2/\lambda$. d_1 and d_2 are the thickness of AlGaAs and 2DEG layer respectively. r_1 , r_2 and r_3 are the reflection coefficients from the air-AlGaAs, AlGaAs-2DEG and 2DEG-GaAs interfaces respectively. The reflection coefficients r_i for $i = 1, 2$ and 3 are given by $r_i = (n_{i-1} - n_i)/(n_{i-1} + n_i)$ with $n_0 = 1$. In the wavelength range of 765 nm to 836 nm, the air to semiconductor reflectance (r_1) will be much higher than the other two reflectance values (r_2 and r_3), hence, $r_1 r_2 + r_1 r_3 + r_2 r_3 \ll 1$ [80]. Further, the terms containing the product $r_2 r_3$ can be neglected when compared to the other terms. With these approximations the total reflectivity from the heterostructure ($R = rr^*$) can be written as

$$R = r_1^2 + r_2^2 + r_3^2 + r_1 r_2 \cos(2\delta_1) + r_1 r_3 \cos[2(\delta_1 + \delta_2)]. \quad (6.2)$$

The refractive index and thickness of the 2DEG layer depend on the built-in electric field. Therefore values of n_2 and d_2 were determined by fitting Eqn. 6.2 to the reflectivity spectrum (Fig. 6.4) and slightly varying n_1 and n_3 around the reported values [80]. The best fit value for d_2 is 10 nm and is consistent with values reported for similar samples [27, 68].

In transient reflectivity measurements, when the pump pulse is incident on the sample, carriers are excited in the GaAs. Some of these carriers then drift to the interface due to the built-in electric field. Thus the refractive indices of both GaAs and 2DEG region are expected to change due to excitation by pump pulse. Assuming the pump induced change in refractive index at the probe wavelength (λ) in 2DEG and GaAs to be Δn_2 and Δn_3 respectively, the total change in the reflectivity of the sample (ΔR) can be written as,

$$\Delta R(\lambda, t) = \mathfrak{R}_2(\lambda) \Delta n_2(\lambda, t) + \mathfrak{R}_3(\lambda) \Delta n_3(\lambda, t), \quad (6.3)$$

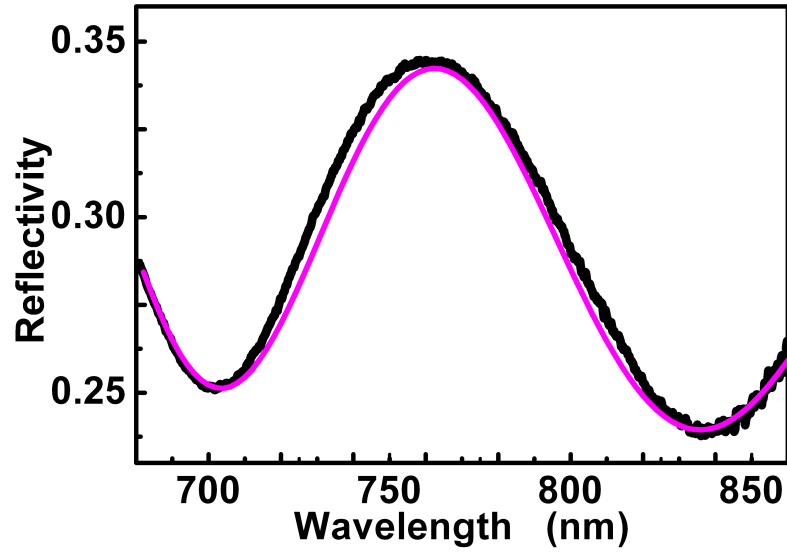


Figure 6.4: The linear reflectivity spectrum of the $\text{Al}_{0.7}\text{Ga}_{0.3}\text{As}(\text{n-doped})\text{-GaAs}$ heterostructure. Black line: measured linear reflectivity, pink thin line: best fit to data using Eqn. 6.2.

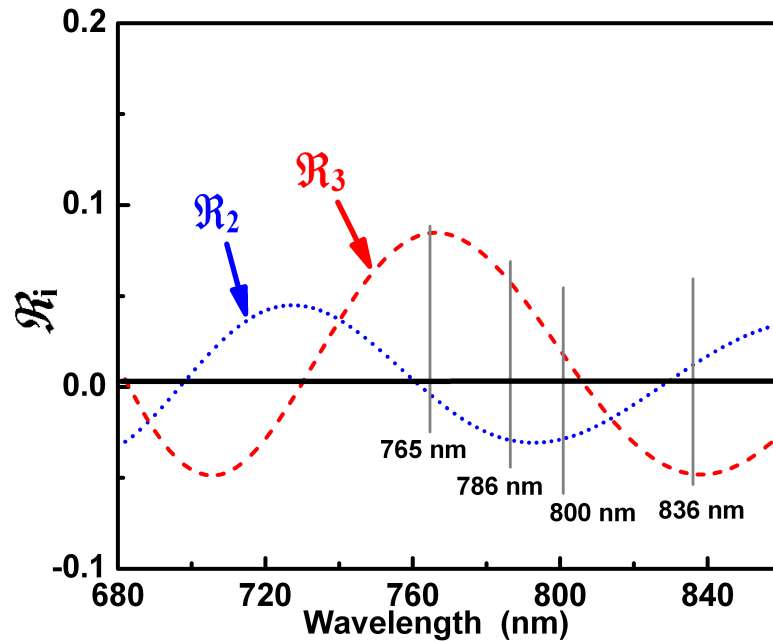


Figure 6.5: The calculated variation of \mathfrak{R}_2 (blue dotted line) and \mathfrak{R}_3 (red dashed line) with the wavelength of light. Vertical lines show the wavelengths at which the TR results are reported.

where $\mathfrak{R}_2 = \partial R/\partial n_2$ and $\mathfrak{R}_3 = \partial R/\partial n_3$. Note that Δn_2 and Δn_3 will change if the pump wavelength is changed as in non-degenerate pump-probe or pump-white light probe experiments. Any change in pump wavelength will change the excited carrier density due to variation in absorption coefficient resulting in changing the magnitude and behavior of Δn_2 and Δn_3 . However, for a given pump wavelength, \mathfrak{R}_2 and \mathfrak{R}_3 create an etalon like effect which is a function of the probe wavelength only. Using Eqn. 6.2 we can write,

$$\begin{aligned} \mathfrak{R}_2 = 2r_2 \frac{\partial r_2}{\partial n_2} &+ 2r_3 \frac{\partial r_3}{\partial n_2} + r_1 \cos(2\delta_1) \frac{\partial r_2}{\partial n_2} \\ &+ r_1 \cos[2(\delta_1 + \delta_2)] \frac{\partial r_3}{\partial n_2} \\ &- r_1 r_3 \sin[2(\delta_1 + \delta_2)] \frac{4\pi d_2}{\lambda} \text{ and} \end{aligned} \quad (6.4)$$

$$\mathfrak{R}_3 = 2r_3 \frac{\partial r_3}{\partial n_3} + r_1 \cos[2(\delta_1 + \delta_2)] \frac{\partial r_3}{\partial n_3}. \quad (6.5)$$

Figure 6.5 shows the variation of \mathfrak{R}_2 and \mathfrak{R}_3 in the wavelength range in which the experiments were performed. The oscillatory behavior of \mathfrak{R}_2 and \mathfrak{R}_3 causes the magnitude and sign of $\Delta R/R$ of the heterostructure to vary markedly with wavelength. In the above model we have assigned a well defined thickness to the 2DEG which can change a little depending on the number of carriers trapped in the 2DEG. Any dynamic change in 2DEG thickness will modify δ_2 . However, note that in expression for R (Eqn. 6.2), δ_2 comes only in the last term as $(\delta_1 + \delta_2)$ and $\delta_1 \gg \delta_2$. Thus the linear reflectivity will not be very sensitive to small variations in the thickness of 2DEG.

With this background, we try to understand the TR of the AlGaAs-GaAs heterostructure at the three different wavelengths shown in Fig. 6.6. At wavelengths near 765 nm, \mathfrak{R}_3 is positive and much higher than \mathfrak{R}_2 . Hence the TR near 765 nm will be dominated by the second term in Eqn. 6.3, $(\mathfrak{R}_3 \Delta n_3)$ and will be positive (Fig. 6.6). This is because the direct measurement on GaAs (Fig. 6.2) shows a positive

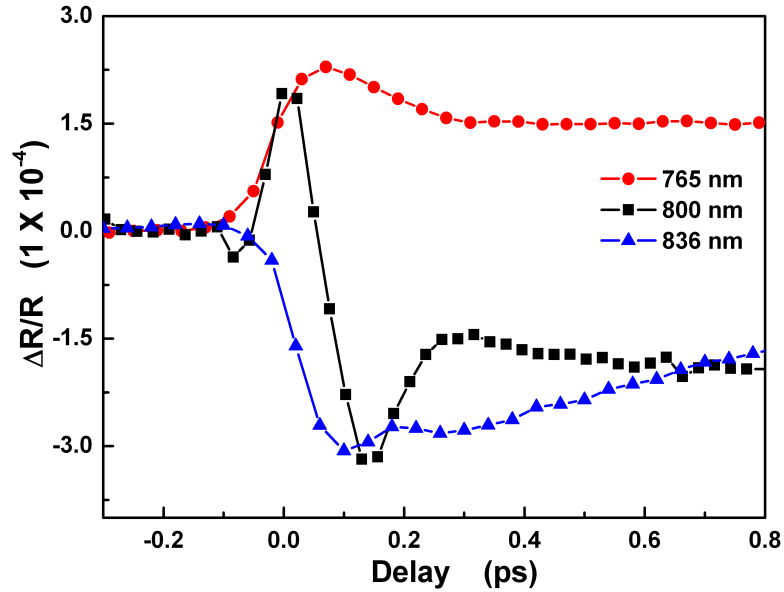


Figure 6.6: TR signal from $\text{Al}_{0.7}\text{Ga}_{0.3}\text{As}(\text{n-doped})\text{-GaAs}$ heterostructure at three different wavelengths. Note that the signal at 836 nm has been multiplied by three for clarity.

change which will be multiplied by \mathfrak{R}_3 at 765 nm which is also positive resulting in a positive response from heterostructure sample. For measurements near 836 nm once again \mathfrak{R}_2 is small and \mathfrak{R}_3 is much larger though negative. Thus the TR from the heterostructure sample would be expected to be similar to that of GaAs layer but with a change in sign. This is reflected in the results of the $\Delta R/R$ measurements at 836 nm (Fig. 6.6 and Fig. 6.2). It is to be noted that the excitation and probing are by femtosecond pulses which have a spectral FWHM of ~ 10 nm, so that even for peak wavelengths of 765 nm and 836 nm there will be a small contribution of the $\mathfrak{R}_2\Delta n_2$ term.

Now let us consider the third wavelength, 786 nm, where \mathfrak{R}_3 is positive, \mathfrak{R}_2 is negative and both of them have nearly the same magnitude. In this case, the TR from the AlGaAs-GaAs heterostructure sample will have contributions from both the AlGaAs and GaAs layers. Figure 6.7 shows the TR measured at 786 nm for both bulk GaAs sample and the AlGaAs-GaAs heterostructure samples. The transient

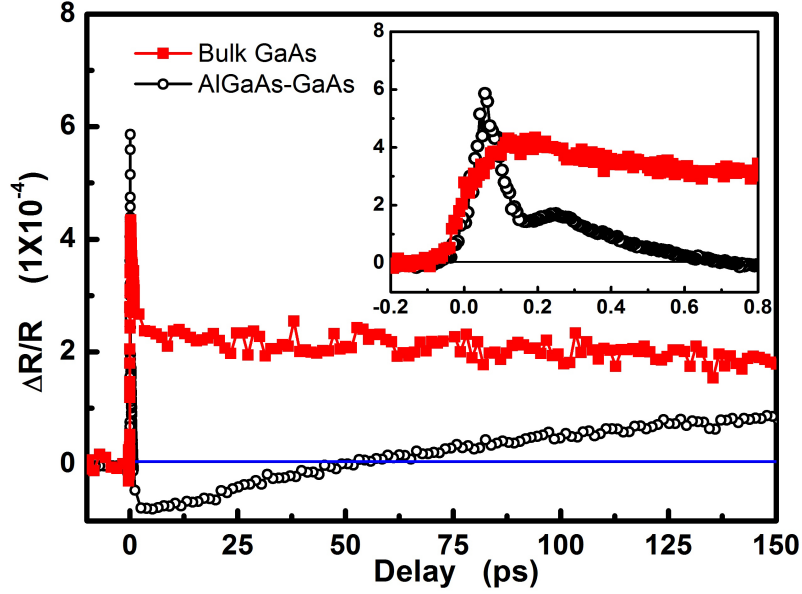


Figure 6.7: Transient reflectivity signal at 786 nm from bulk GaAs and $\text{Al}_{0.7}\text{Ga}_{0.3}\text{As}(\text{n-doped})\text{-GaAs}$ heterostructure sample. Inset shows the same TR signal zoomed near zero delay.

reflectivity curve from bulk GaAs is similar to that obtained at other wavelengths but that from the heterostructure is quite different. The transient reflectivity for the AlGaAs-GaAs heterostructure is initially positive, quickly goes negative and again becomes positive at ~ 50 ps. This can be explained using Fig. 6.5. At 786 nm there will be a contribution to the reflectivity from both the GaAs as well as the 2DEG layer. As the carriers are first generated in GaAs, the maximum initial change in refractive index will be in the GaAs layer which will be positive. As the carriers drift towards the interface to form the 2DEG, the negative contribution to the reflectivity will become dominant. Since the recombination time for the carriers in the 2DEG is much smaller than that of the carriers remaining in GaAs, the negative contribution to $\Delta R/R$ from the 2DEG reduces faster. This results in a positive signal again at ~ 50 ps.

With this multilayer model, the behavior of transient reflectivity from AlGaAs-GaAs heterostructure can be explained with a change in refractive index which is

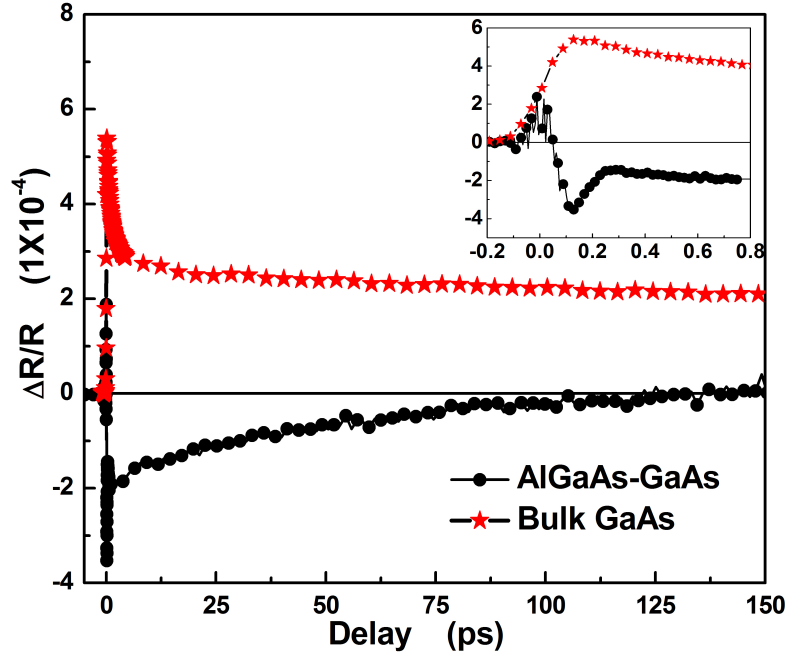


Figure 6.8: Transient reflectivity from bulk GaAs and $\text{Al}_{0.7}\text{Ga}_{0.3}\text{As}(\text{n-doped})\text{-GaAs}$ measured at 800 nm. Note that the $\Delta R/R$ for the heterostructure sample recovers much faster. Inset shows the same TR signal zoomed near zero delay.

always positive for both GaAs and 2DEG. Due to the layered structures the contributions from different layers add with different phases. This results in negative or positive changes in the total transient reflectivity measured for the heterostructure.

Next we consider the results at 800 nm (Fig. 6.8). Similar to the 786 nm case, the initial value is slightly positive due to the high density of carriers excited in GaAs, but it becomes negative quickly. At this wavelength \mathfrak{R}_3 is much smaller than \mathfrak{R}_2 . The subsequent dynamics is thus solely due to relaxation of the carriers in 2DEG and can be analyzed directly without the need to consider the relaxation of carriers in GaAs. This is confirmed by the fact that there is no signal at 150 ps even though carriers are still present in GaAs layer (Fig. 6.2).

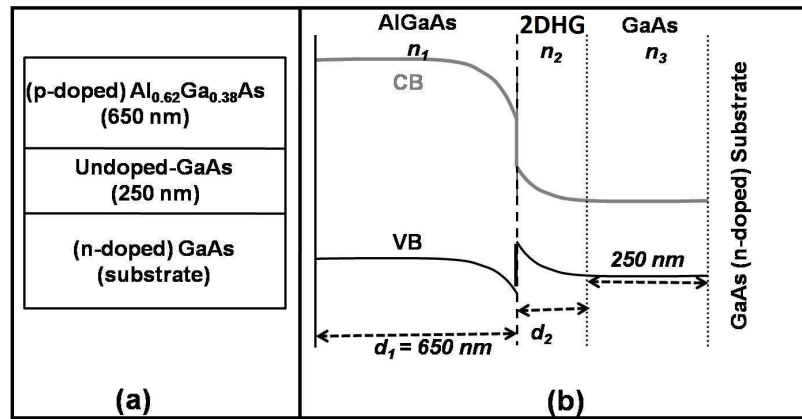


Figure 6.9: (a) Schematic of the p-type heterostructure. (b) The band bending diagram. The refractive indices for AlGaAs, 2DHG region and GaAs n_1 , n_2 and n_3 respectively. The thickness of the 2DHG layer is obtained by the same technique as used for 2DEG in case of n-type heterostructure.

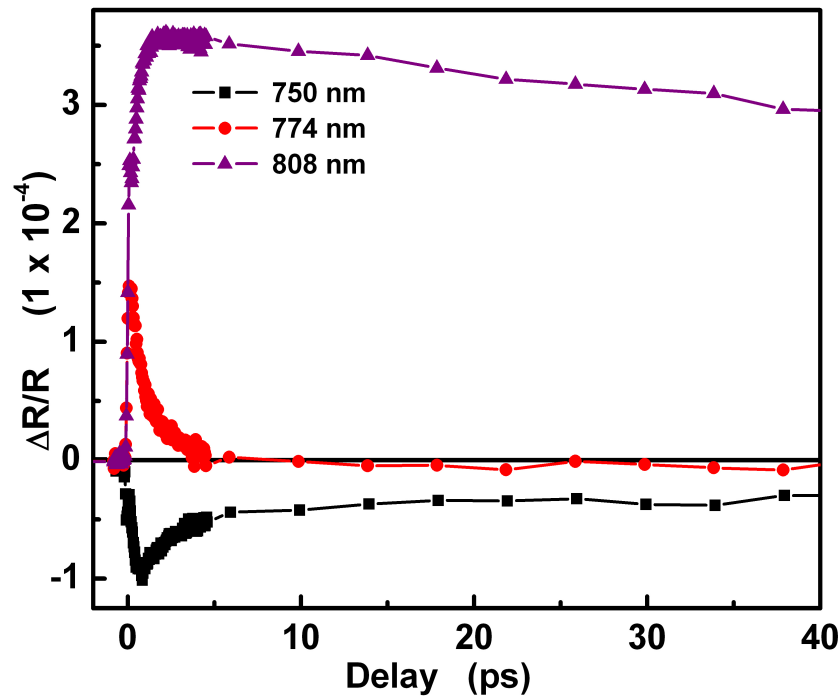


Figure 6.10: Transient reflectivity from $\text{Al}_{0.62}\text{Ga}_{0.38}\text{As}$ (p-doped)-GaAs heterostructure at different wavelengths. Note that the $\Delta R/R$ recovers to zero for 774 nm.

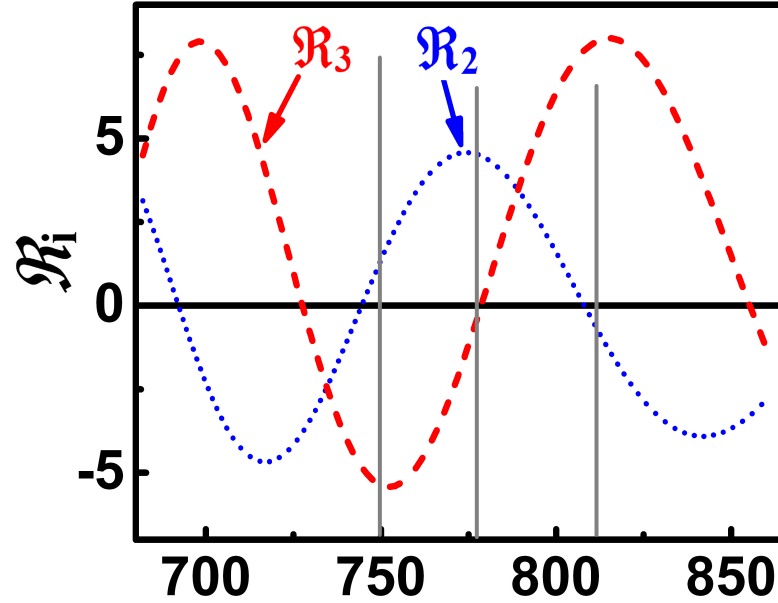


Figure 6.11: The wavelength dependence of \mathfrak{R}_2 and \mathfrak{R}_3 for the $\text{Al}_{0.62}\text{Ga}_{0.38}\text{As}$ (p-doped)-GaAs heterostructure (similar to Fig. 6.5 for the n-doped heterostructure).

6.3.2 p-doped $\text{Al}_{0.7}\text{Ga}_{0.3}\text{As}$ -GaAs heterostructure

To confirm our model, we have performed similar experiments on another $\text{Al}_{0.62}\text{Ga}_{0.38}\text{As}$ (p-doped-GaAs heterostructure having a two-dimensional hole gas (2DHG) at the interface. The top layer thickness in this sample is 650 nm and rest of the structure is same as that of the first sample. Once again, the TR measured at 808 nm and 750 nm shows a behavior similar to that of GaAs expect for a sign change in case of 750 nm (Fig. 6.10). This matches the behavior expected from Eqn. 6.3 with the corresponding wavelength dependence of \mathfrak{R}_2 and \mathfrak{R}_3 as shown in the Fig. 6.11. At 774 nm the transient measurement should be directly probing carrier dynamics in 2DHG since \mathfrak{R}_3 is very small at this wavelength. Since \mathfrak{R}_2 is positive the measured transient reflectivity is also positive at this wavelength. The measured decay time is 1.3 ps for 2DHG which is much faster than 2DEG decay. This variation in decay time will be discussed later in this chapter.

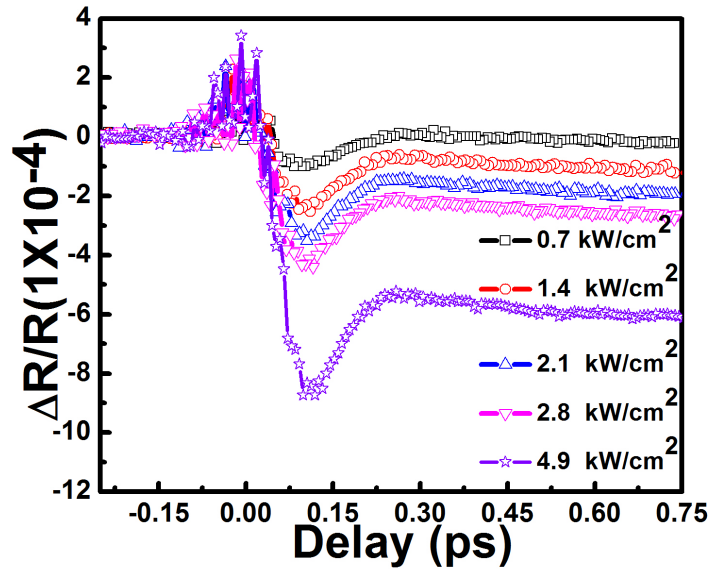


Figure 6.12: Time resolved reflectivity change within 1 ps for the $\text{Al}_{0.7}\text{Ga}_{0.3}\text{As-GaAs}$ n-type heterostructure at different pump intensities. Excitation wavelength is 800 nm.

6.4 Dynamics of 2DEG with carrier density

Having developed the technique to directly measure the carrier dynamics of the two-dimensional electron gas, we have studied the effect of carrier density on the 2DEG carrier dynamics. Figure 6.8 shows that measurement performed at 800 nm gives the dynamics of carriers in 2DEG. We performed measurements on $\text{Al}_{0.7}\text{Ga}_{0.3}\text{As-GaAs}$ heterostructure at 800 nm at different intensity. Fig. 6.12 shows the decay at different intensities. The Fig. 6.12 shows that as soon as carriers are excited within pump pulse, the carriers start to drift under built-in electric field. It reaches a local peak within 200 fs. The peak position does not change very strikingly different with pump excitation. Thus, the initial features are not changing with intensity as initially the carriers drift under built-in electric field which will be same at all intensities unless the carriers has accumulated near the interface.

After that the electric field and carrier separation will be modified which is re-

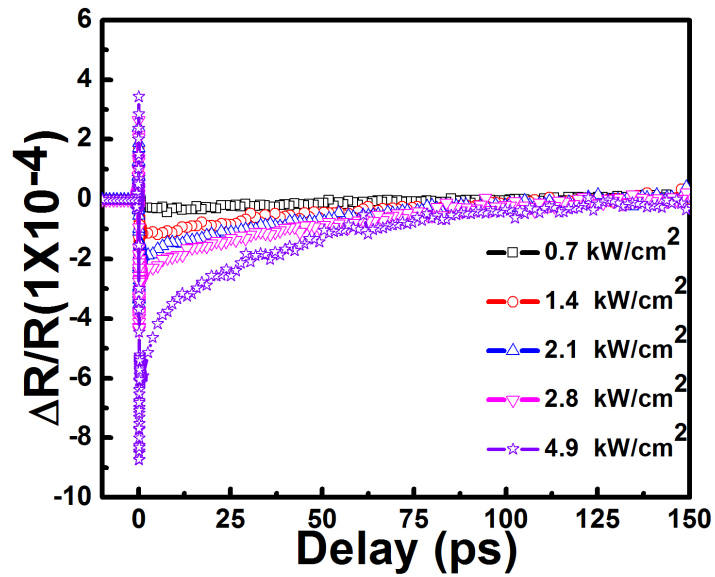


Figure 6.13: Full time resolved reflectivity curves from Al_{0.7}Ga_{0.3}As-GaAs n-doped heterostructure at 800 nm at different pump intensities. The signal recovers almost completely in 150 ps.

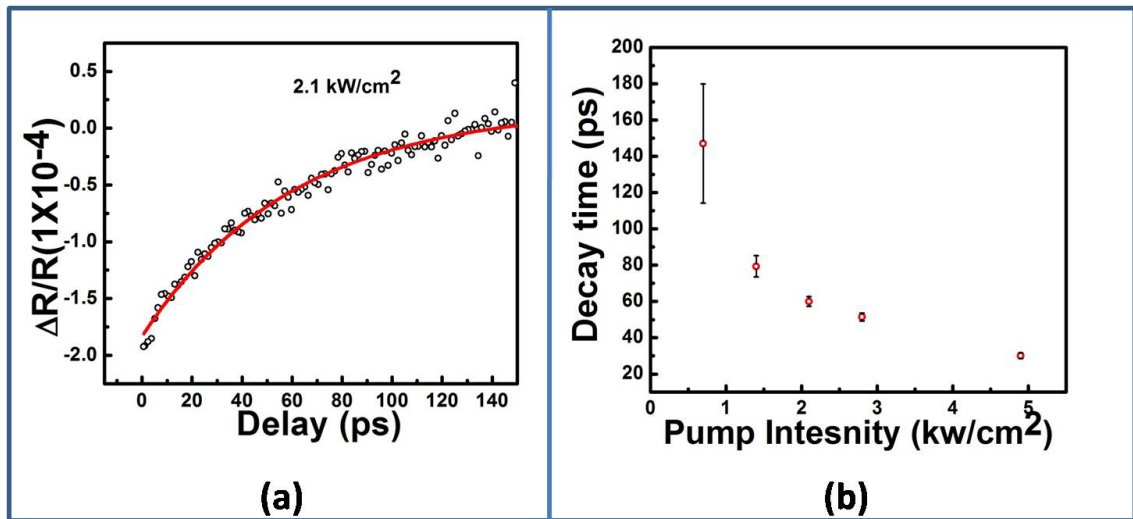


Figure 6.14: (a) Single exponential fit to transient reflectivity curve at pump intensity of 2.1 kW cm^{-2} which gives a recover time constant of 59.8 ps. The wavelength kept is 800 nm. Similar fit are done at other pump intensities. (b) Dependence of transient reflectivity recovery time on pump intensity for the n-doped heterostructure. Error bars are estimated from the fitting error.

flected in the recovery of the transient reflectivity signal. The longer recombination is given in Fig. 6.13 with intensity. At all intensities the signal recovers completely within 150 ps. The recovery seems to be faster with pump intensity. The single exponential decay time at various intensities plotted in Fig. 6.14. The inset shows the fitting of the transient reflectivity for longer delay time with single exponential decay. It is observed that with increasing carrier density the recombination time decreases. To understand physically the exact behavior of such decrease in decay of transient reflectivity, we performed intensity dependence transient reflectivity measurement on GaAs. The transient reflectivity on GaAs showed double exponential decay having shorter decay time within ps and one longer decay time within few hundreds of ps measured at 786 nm as shown in Fig. 6.15. The data is fitted with double exponential as shown in inset of Fig. 6.15(a) and Fig. 6.15(b) at pump intensity of 2.1 kW cm^{-2} . The shorter decay time goes on increasing with pump intensity as shown in Fig. 6.15(a). The longer is in the range of few hundreds of ps and fluctuating. This shows that the variation of decay time obtained from $\text{Al}_{0.7}\text{Ga}_{0.3}\text{As-GaAs}$ heterostructure is totally opposite to the behavior obtained from GaAs.

We come back to the band bending diagram of triangular well formed near the interface of $\text{Al}_{0.7}\text{Ga}_{0.3}\text{As-GaAs}$ shown in 6.3(b). As soon as carriers are excited, carriers move under built-in electric field and an induced electric field is formed near the interface due to excited carriers as shown in Fig. 6.16. The induced field lowers the confining potential in the triangular well. The well becomes shallower as we go on increasing the carrier density by photo-excitation and the decay time becomes faster.

To confirm this further, we performed the intensity dependent measurements at 786 nm on $\text{Al}_{0.7}\text{Ga}_{0.3}\text{As-GaAs}$ heterostructure. As can be seen from Fig. 6.5, at this wavelength contributions from both GaAs and 2DEG carriers will be there. The GaAs contribution will be positive and that of 2DEG will be negative. We could

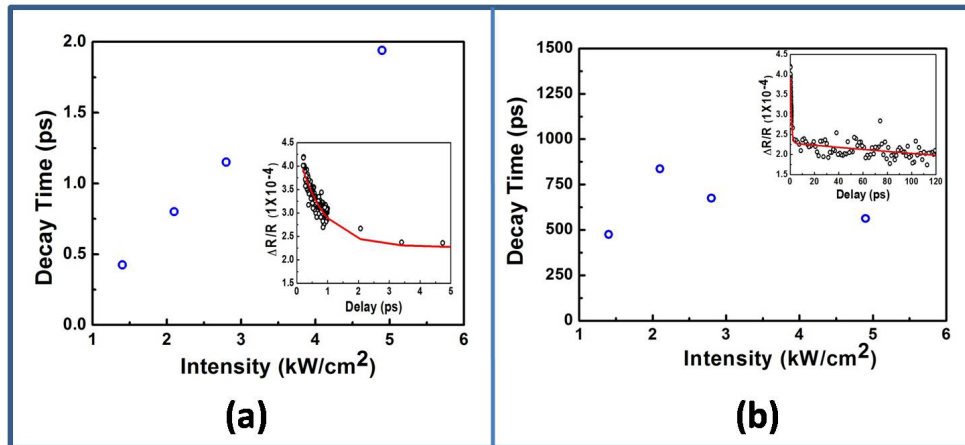


Figure 6.15: (a) Shorter decay time obtained from double exponential decay fit to the transient reflectivity curve from GaAs at different pump intensity. (b) The second decay time which is obtained from double exponential decay fit to the transient reflectivity curve from GaAs at different pump intensity. The inset in both (a) and (b) shows one of the fit at pump intensity of 2.1 kW cm^{-2} . The wavelength kept is 786 nm.

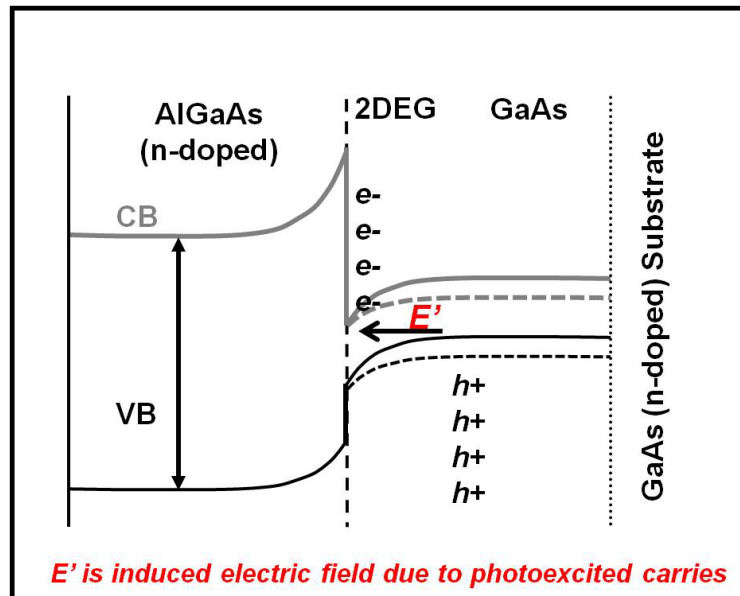


Figure 6.16: Change in band bending with photoexcited carriers in the $\text{Al}_{0.7}\text{Ga}_{0.3}\text{As}$ (n-doped)-GaAs heterostructure. The triangular well formed near the interface become shallow with photoexcitation. CB and VB are the conduction and valence bands respectively.

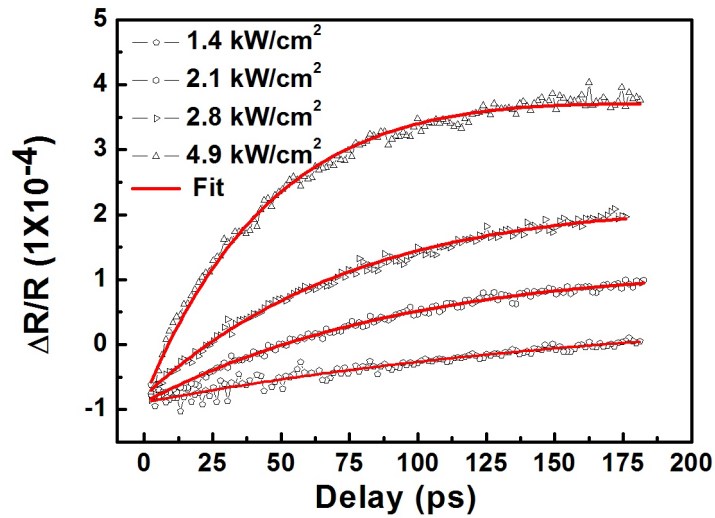


Figure 6.17: Time resolved reflectivity from Al_{0.7}Ga_{0.3}As(n-doped)-GaAs heterostructure at 786 nm at different pump intensity. The data is fit to a two exponential decay with opposite sign.

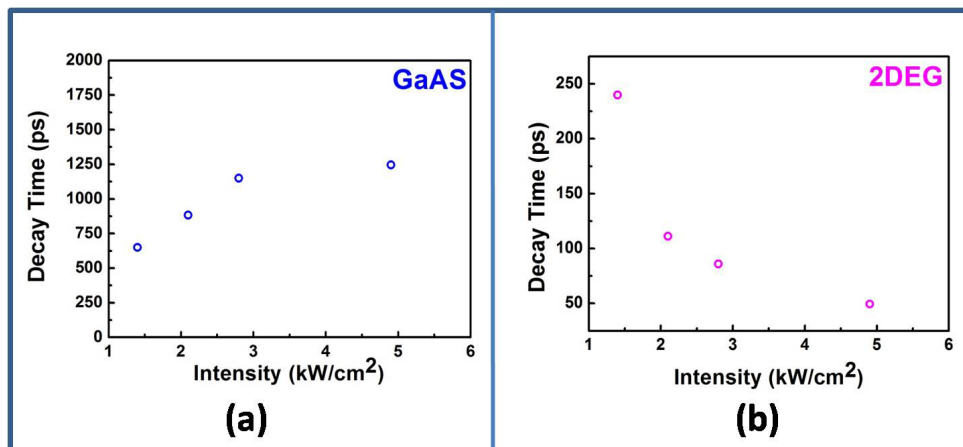


Figure 6.18: (a) Recombination time vs pump intensity for GaAs contribution obtained from double fit of transient reflectivity from Al_{0.7}Ga_{0.3}As(n-doped)-GaAs heterostructure at 786 nm as shown in Fig. 6.17. (b) Recombination time vs pump intensity for the two-dimensional electron gas contribution.

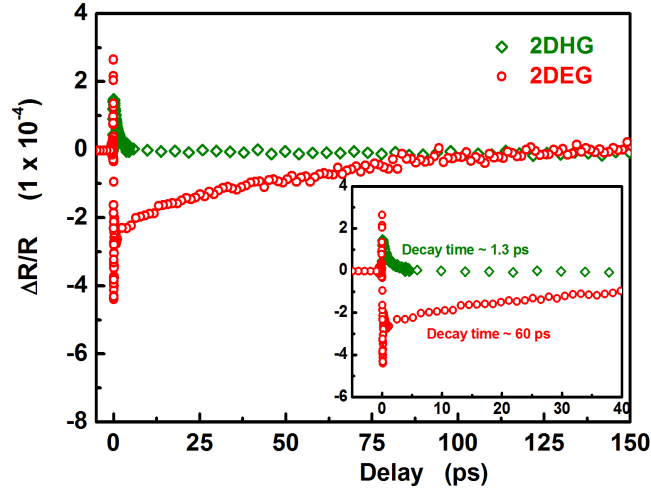


Figure 6.19: Transient reflectivity signal from 2DHG and 2DEG. The measurements has been performed at 774 nm on AlGaAs(p-doped)-GaAs heterostructure to measure the decay of 2DHG and at 800 nm on AlGaAs(n-doped)-GaAs heterostructure sample for measuring the decay of 2DEG. The inset shows the same data at zoomed scale.

fit the transient reflectivity at 786 nm to a two-exponential decay with one positive and one negative term as shown in Fig. 6.17. The intensity dependence of the two decay times extracted from the fit is shown in Fig. 6.18(a) and Fig. 6.18(b). The decay time corresponding to the negative term shows decrease with increasing pump intensity (Fig. 6.18(b)), similar to behavior at 800 nm (Fig. 6.14(b)). The decay time corresponding to the positive term (Fig. 6.18(a)) in similar range and behavior similar to that shown in Fig. 6.15(b). This observation confirms both our model as well as the fact that as the triangular well becomes shallower, the carrier decay faster.

Now we come back to the results shown in Fig. 6.8 and Fig. 6.10. The transient reflectivity signal corresponding to 2DHG decay in AlGaAs(p-doped)-GaAs heterostructure sample (774 nm) and 2DEG decay in AlGaAs(n-doped)-GaAs heterostructure sample (800 nm) have been shown again in Fig. 6.19. The decay constant of 2DHG is found to be nearly 1.3 ps and that of 2DEG is much longer at ~ 60

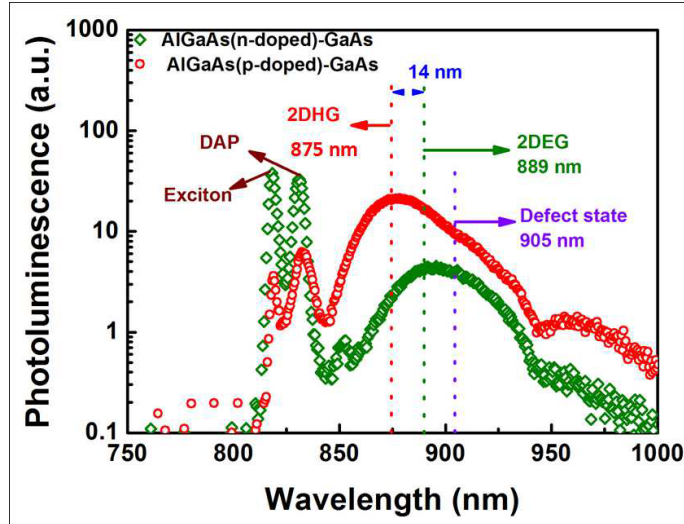


Figure 6.20: Photoluminescence spectrum of AlGaAs(p-doped)-GaAs heterostructure and AlGaAs(n-doped)-GaAs heterostructure sample. The photoluminescence peak from exciton, DAP and defect state comes nearly at same position for both samples. The 2DHG peak is blue shifted by nearly 14 nm compared with 2DEG peak.

ps. This can be understood as follows. A comparison of the low temperature photoluminescence spectra of the two samples shows that the 2DHG peak is blue shifted compared to the 2DEG peak while other peaks (DAP, defect, exciton etc.) are at the same position in both the samples as shown in Fig. 6.20. From the intensity dependence studies of photoluminescence we have already seen that the 2DEG peak shows a blue shift at higher intensities (Fig. 5.9). The decay time also reduces with increasing intensity showing that the triangular well depth decreases with increasing intensity (Fig. 6.14(b)) By analogy with Fig. 5.9 and Fig. 6.14(b) we can conclude that the triangular quantum well in the AlGaAs(p-doped)-GaAs heterostructure is much more shallow (less band bending) than that in the AlGaAs(n-doped)-GaAs heterostructure sample. This leads to much shorter carrier decay time in the former.

Coming back to the technique of choosing suitable wavelength based on linear reflectivity, there is one precaution which must be observed. The analysis leading to Fig. 6.5 assumes the dispersion in the wavelength range under consideration is

very low. In other words, the model assumes that there are no material resonances nearby. In semiconductors, the magnitude and sign of the refractive index change due to effects like band filling and band gap renormalization varies very sharply near any resonance. This would add to the phase changes due to multilayer reflection shown in Fig. 6.5 and leads to a very fast variation in the sign of transient reflectivity as a function of wavelength. A re-look at the low temperature data of chapter 5 shows this very clearly. There the wavelengths used were 818 nm, 825 nm and 830 nm. As per Fig. 6.5 the transient reflectivity should have been negative at all these wavelengths and should have come due to the GaAs contribution only. However as we have seen the signal is negative only at 825 nm and 818 nm, while it is positive at 830 nm. Further, we have established that the transient reflectivity signal at 825 nm as well as 818 nm shows the signature of two-dimensional electron gas formation (modulation in the early part). This is consequence of the laser wavelength being near excitonic and/or the DAP resonance of GaAs.

6.5 Conclusion

In this chapter we have described the development of a new technique to overcome the major problem faced in the interpretation of transient reflectivity measurements of multilayered semiconductor nanostructures. This technique enables one to isolate the contribution to the carrier dynamics from any individual layer by choosing an appropriate probe wavelength. This is a consequence of the wavelength dependence of the phase change experienced by the beam in the reflection at each layer. As long as the operating wavelength is kept well away from material resonance, a simple analysis of linear reflectivity spectrum is sufficient to identify the required wavelength.

Using this technique we have been able to measure the intensity dependence of carrier dynamics in the 2DEG. We have shown that with increasing carrier density, the decay time reduces very fast with an almost exponential like decay. For example,

for an $\text{Al}_{0.7}\text{Ga}_{0.3}\text{As}$ (n-doped)-GaAs heterostructure sample the decay time is nearly 60 ps at 2.1 kWcm^{-2} excitation intensity and $\sim 20 \text{ ps}$ at 4.9 kWcm^{-2} . In contrast for $\text{Al}_{0.62}\text{Ga}_{0.38}\text{As}$ (p-doped)-GaAs sample where a 2DHG layer is formed at the interface, the decay time is much shorter, being 1.3 ps at 2.1 kWcm^{-2} .

This work has also served to clarify the observation of earlier authors who had reported a sign change in transient reflectivity as function of wavelength, temperature as well as intensity with no clear physical explanation. As we have shown that, when away from any resonance, the sign of transient reflectivity can be effected by the phase change due to multilayer reflection. On the other hand, if the wavelength is near some resonance, the sign of the transient reflectivity would be hard to predict. However, modulations in the early part of transient reflectivity signal provide a clear indication of carrier drift towards the interface and get confined there.

Chapter 7

Conclusion and Future Scope

The motivation of this thesis was to study the effect of surface and interface states on the room temperature ultrafast carrier dynamics of III-V semiconductor two-dimensional nanostructures. The effect of surface has been explored by studying $\text{GaAs}_{0.86}\text{P}_{0.14}/\text{Al}_{0.7}\text{Ga}_{0.3}\text{As}$ single quantum wells whereas $\text{Al}_{0.7}\text{Ga}_{0.3}\text{As}$ (n-doped)-GaAs and $\text{Al}_{0.62}\text{Ga}_{0.38}\text{As}$ (p-doped)-GaAs heterostructure samples have been used to study the effect of interface states. These samples do not show any photoluminescence at room temperature, and are deposited on substrates which are highly absorbing at the wavelengths of interest. Therefore, femtosecond laser based pump-probe reflectivity measurements were carried out to study the ultrafast dynamics. During the course of this work, a couple of new methodologies were developed to analyze the transient reflectivity data. This has enabled the observation of some interesting phenomenon. The main conclusions from this work and future scope are described below.

Near-surface quantum wells can show interesting phenomena arising from an increased interaction of the quantum well states with the surface states. A well known phenomenon is the quenching of photoluminescence is attributed to the increased

non-radiative decay facilitated by the tunneling of carriers out of the quantum well to the surface. For a better understanding of the tunneling process, further investigations into the tunneling process are required. Another area of interest is to explore the possibility of coherent interactions similar to those observed in super-lattices. In this work we have studied both incoherent as well as coherent processes in a near-surface single quantum well and that too at room temperature.

We have demonstrated that in a near-surface $\text{GaAs}_{0.86}\text{P}_{0.14}/\text{Al}_{0.7}\text{Ga}_{0.3}\text{As}$ single quantum well the photo-generated holes tunnel out of the quantum well and undergo a very fast non-radiative recombination at the surface. We estimate a carrier lifetime of 0.5 ps which is possibly the fastest lifetime reported in III-V single quantum wells. It is worth pointing out that these lifetime estimates have been obtained despite the presence of a large photo-carrier population is generated in GaAs substrate.

An even more interesting result was the observation of coherent beating between two of the quantum well to surface state transitions. The beating had a period of ~ 120 fs and a dephasing time of ~ 150 fs. This, to the best of our knowledge, is the first demonstration of tunneling assisted coherent beating. This novel process opens up the possibility of switching the coherent interaction by generating photo-induced carriers in the AlGaAs layer using a third ultrafast laser pulse at a suitable wavelength. Thus further investigation of this tunneling assisted coherent beating would be worth pursuing.

Like the surface states, the buried interfaces between two layers of any heterostructure also play a significant role in the carrier dynamics. In an AlGaAs-GaAs heterostructure, the band bending at the interface can lead to formation of a narrow triangular quantum well. Excited carriers (electrons or holes) generated in the GaAs layer can drift to the interface and get trapped in this triangular well. This trapped electron (or hole) population has a very high in-plane mobility and behaves like a two-dimensionally confined electron (or hole) gas. Here also, a direct look at the drift

of carriers towards the interface and their subsequent decay has been difficult. To a great extent, this was due to the interference from the large number of carriers generated and recombining within the GaAs layer. A few earlier studies have reported the dependence of transient reflectivity on various experimental parameters like excitation and probe photon energy, excited carrier density and sample temperature. However, these did not give a full explanation of the observed dependence.

In this work we have demonstrated two ways in which the information on two-dimensional electron gas carrier dynamics can be obtained directly and unambiguously. The first clue comes if the excitation photon energy is near a resonance of the GaAs layer like exciton or DAP recombination. In this case, a modulation in the early part of the transient reflectivity is a signature of the drift towards the interface. This provides an easy way to estimate the time required by the electrons (or holes) to move towards the interface to form two-dimensional electron gas. For example in an $\text{Al}_{0.7}\text{Ga}_{0.3}\text{As}(\text{n-doped})\text{-GaAs}$ heterostructure the required time for electrons to drift is estimated to be ~ 800 fs at 40 K and ~ 200 fs at 300 K. This observation has been possible in this sample because this drift time is about two orders of magnitude shorter than the decay time of carriers in the two-dimensional electron gas. For example at room temperature and at a pump intensity of 2.1 kWcm^{-2} the decay time of electron in the 2DEG is about 60 ps. In samples where the built-in field is lower, the carrier drift time and decay time could be comparable and these modulations would not be so prominent. This was shown by our measurements on another sample which was a $\text{Al}_{0.62}\text{Ga}_{0.38}\text{As}(\text{p-doped})\text{-GaAs}$ heterostructure in which a two-dimensional hole gas is formed at the interface. In this sample the hole drift and decay time are comparable (~ 1 ps) and modulations are hardly noticeable.

The development of the second technique was motivated by a major problem faced in the interpretation of degenerate transient reflectivity results for such heterostructures. This is due to the fact that the only a fraction of the photo-generated

carriers in GaAs contribute to form the two-dimensional electron gas and the transient reflectivity can have a major contribution from the carriers remaining in bulk GaAs. We have demonstrated that it is possible to isolate the contributions of individual layers by suitably choosing the excitation wavelength. This utilizes the fact that the reflectivity spectrum of a multilayer sample will have an etalon like modulations. Thus away from sharp resonances, it is possible to find a wavelength where the refractive index change of one particular layer provides the dominant contribution to the transient reflectivity. This model can well explain the results of earlier reports. Using this technique we have studied the 2DEG and 2DHG decay in the above mentioned heterostructure samples. We have shown that the carrier lifetime in the two-dimensional electron gas reduces as the triangular quantum well becomes more shallow. This understanding of the two-dimensional electron gas formation and decay leads to a possibility of fast optical control of a two-dimensional electron gas based device by a ultrashort laser pulses.

References

- [1] Peyghambarian, N., Koch, S. W., and Mysyrowicz, A. *Introduction to Semiconductor Optics*. Prentice Hall Series in Solid State Physical Electronics, (1993).
- [2] Davies, J. H. *The Physics of Low-Dimensional Semiconductors*. Cambridge, (1998).
- [3] Weisbuch, C. and Vinter, B. *Quantum Semiconductor Structures: Fundamentals and Applications*. Academic , Boston, (1991).
- [4] Singh, J. *Semiconductor devices: basic principles*. John-Wiley, (2001).
- [5] Sze, S. M. *Semiconductor devices: physics and technology*. John Wiley & Sons, (20012).
- [6] Zory, P. S., editor. *Quantum well lasers*. Academic Press, (1993).
- [7] Shik., A. *Quantum wells: physics and electronics of two-dimensional systems*. World Scientific, (1997).
- [8] Engel, Y., Elnathan, R., Pevzner, A., Davidi, G., Flaxer, E., and Patolsky, F. *Angewandte Chemie International Edition* **49**(38), 6830–6835 (2010).

- [9] Appenzeller, J., Knoch, J., Bjork, M. T., Riel, H., Schmid, H., and Riess, W. *IEEE Transactions on Electron Devices* **55**(11), 2827–2845 Nov (2008).
- [10] Stevenson, R. M., Thompson, R. M., Shields, A. J., Farrer, I., Kardynal, B. E., Ritchie, D. A., and Pepper, M. *Phys. Rev. B* **66**, 081302 Aug (2002).
- [11] Gisin, N., Ribordy, G., Tittel, W., and Zbinden, H. *Rev. Mod. Phys.* **74**, 145–195 Mar (2002).
- [12] Skogen, E. J., Vawter, G. A., Tauke-Pedretti, A., Alford, C. R., Overberg, M. E., and Sullivan, C. T. *IEEE Photonics Technology Letters* **25**(17), 1684–1686 Sept (2013).
- [13] Zilkie, A. J., Meier, J., Mojahedi, M., Poole, P. J., Barrios, P., Poitras, D., Rotter, T. J., Yang, C., Stintz, A., Malloy, K. J., Smith, P. W. E., and Aitchison, J. S. *IEEE Journal of Quantum Electronics* **43**(11), 982–991 Nov (2007).
- [14] Zilkie, A. J., Meier, J., Smith, P. W. E., Mojahedi, M., Aitchison, J. S., Poole, P. J., Allen, C. N., Barrios, P., and Poitras, D. *Opt. Express* **14**(23), 11453–11459 Nov (2006).
- [15] Takahashi, R., Kawamura, Y., Kagawa, T., and Iwamura, H. *Appl. Phys. Lett.* **65**, 1790 (1994).
- [16] Cohen, R. M., Kitamura, M., and Fang, Z. M. *Appl. Phys. Lett.* **50**, 1675 (1987).
- [17] Akahane, Y., Asano, T., Song, B. S., and Noda, S. *Nature* **425**, 944 (2003).
- [18] Wolf, S. A., Awschalom, D. D., Buhrman, R. A., Daughton, J. M., von Molnár, S., Roukes, M. L., Chtchelkanova, A. Y., and Treger, D. M. *Science* **294**(5546), 1488–1495 (2001).

- [19] Schmidt, G. *Journal of Physics D: Applied Physics* **38**(7), R107 (2005).
- [20] Wolpert, C., Dicken, C., Atkinson, P., Wang, L., Rastelli, A., Schmidt, O. G., Giessen, H., , and Lippitz, M. *Nano Lett.*, 2012, 12 (1), pp 453–457 **12**(1), 453–457 (2012).
- [21] Callan, J. P. *Ultrafast Dynamics And Phase Changes In Solids Excited By Femtosecond Laser Pulses*. PhD thesis, Harvard Univ., Cambridge, (2000).
- [22] Shah, J. *Ultrafast Spectroscopy of Semiconductors and Semiconductor Nanostructures*. Springer Series in Solid StateSpringer, (1999).
- [23] Petroff, P. and DenBaars, S. *Superlattices and Microstructures* **15**(1), 15 – (1994).
- [24] Notzel, R., Temmyo, J., and Tamamura, T. *Jpn. J. Appl. Phys.* **33**, L275 (1994).
- [25] Cheng, K. Y. *Proceedings of the IEEE* **85**(11), 1694–1714 Nov (1997).
- [26] Kalt, H. *Optical Properties of III-V Semiconductors*. Springer, (1996).
- [27] Bergman, J. P., Zhao, Q. X., Holtz, P. O., Monemar, B., Sundaram, M., Merz, J. L., and Gossard, A. C. *Phys. Rev. B* **43**, 4771–4776 Feb (1991).
- [28] Gao, G., Fan, Z., Blackburn, D. L., ĀIjnlĀij, M. S., Chen, J., Adomi, K., and MorkoĀğ, H. *Applied Physics Letters* **58**(10), 1068–1070 (1991).
- [29] Hall, R. N., Fenner, G. E., Kingsley, J. D., Soltys, T. J., and Carlson, R. O. *Phys. Rev. Lett.* **9**, 366–368 Nov (1962).
- [30] Malaeg, A., Daebrowska, E., and Grodecki, K. *J. Appl. Phys.* **103**, 113109 (2008).

-
- [31] G.Erbert, Bugge, F., knauer, A., Sebastian, J., Thies, A., Wenzel, H., m. Weyers, and trankle, G. *IEEE J. S. T. Q. E.* **5(3)**, 780 (1999).
- [32] Sundaram, S. K. and Mazur, E. *Nature Materials* **1**, 217 (2002).
- [33] Shah, J. *Hot Carrier in Semiconductor Nanostructure Nanostructures: Physics and Applications*. Academic , Boston, (1992).
- [34] Moison, J. M., Elcess, K., Houzay, F., Marzin, J. Y., Gerard, J. M., Barthe, F., and Bensoussan, M. *Phys. Rev. B* **41**, 12945 (1990).
- [35] Symonds, C., mangeney, J., Saint-Girons, G., and Sagnes, I. *Appl. Phys. Lett.* **87**, 012107 (2005).
- [36] Emiliani, V., Bonanni, B., Presilla, C., Capizzi, C., Frova, A., Chang, Y.-L., Tan, I.-H., Merz, J. L., Colocci, M., and Gurioli, M. *J. Appl. Phys.* **75**, 5114 (1994).
- [37] Bazin, A., Lengli, K., Gay, M., Monnier, P., Bramerie, L., Braive, R., Beaudoin, G., Sagnes, I., Raj, R., and Raineri, F. *Appl. Phys. Lett.* **104**, 011102 (2014).
- [38] Kojima, O., Mizoguchi, K., and Nakayama, M. *J. Appl. Phys.* **112**, 043522 (2012).
- [39] Priyadarshi, S., Pierz, K., Siegner, U., Dawson, P., and Bieler, M. *Phys. Rev. B* **83**, 121307 (2011).
- [40] van der Poel, W., Severens, A., and Foxon, C. *Optics Communications* **76(2)**, 116 – 120 (1990).
- [41] Dong, Q., Liang, Y. X., Ferry, D., Cavanna, A., Gennser, U., Couraud, L., and Jina, Y. *Appl. Phys. Lett.* **105**, 013504 (2014).

- [42] Liou, J. and Huang, C. *Microelectronics Journal* **32**, 419 (2001).
- [43] Chuang, S. L. *Physics of optoelectronic Devices*. Wiley-Interscience, (1995).
- [44] Stern, F. and Sarma, S. D. *Phys. Rev. B* **142**, 284 (1984).
- [45] Gilliland, G. D., Wolford, D. J., Northrop, G. A., Petrovic, M. S., Kuech, T. F., and Bradley, J. A. *Journal of Vacuum Science & Technology B* **10**(4), 1959–1964 (1992).
- [46] Rizo, P. J., Pugzlys, A., Slachter, A., Denega, S. Z., Reuter, D., Wieck, A. D., van Loosdrecht, P. H. M., and van der Wal, C. H. *New Journal of Physics* **12**, 113040 (2010).
- [47] MARTÍNEZ-CRIADO, G., MISKYS, C., KARRER, U., AMBACHER, O., and STUTZMANN, M. *Japanese Journal of Applied Physics* **43**, 3360 (2004).
- [48] Pugzlys, A., Rizo, P. J., Ivanin, K., Slachter, A., Reuter, D., Wieck, A. D., van der Wal, C. H., and van Loosdrecht, P. H. M. *J. Phys.: Condens. Matter* **19**, 295206 (2007).
- [49] Kittel, C. *Introduction to solid state physics*. John Wiley & Sons (Asia) Pte. Ltd., (2004).
- [50] Bovensiepen, U., Petek, H., and Wolf, M., editors. *Dynamics at Solid State Surfaces and Interfaces: Volume 2: Fundamentals*. WILEY-VCH, (2012).
- [51] Bhattacharya, P. *Semiconductor Optoelectronic Devices*. Prentice-Hall India, (2000).
- [52] Ilaiwi, K., El-Kawni, M., and Tomak, M. *Superlattices and Microstructures* **24**(1), 61 – 67 (1998).

- [53] Yuan, Y. R., Pudensi, M. A. A., Vawter, G. A., and Merz, J. L. *J. Appl. Phys.* **58**, 397 (1985).
- [54] Pfeiffer, L., West, K. W., Stormer, H. L., and Baldwin, K. W. *Applied Physics Letters* **55**(18), 1888–1890 (1989).
- [55] Shockley, W. *Phys. Rev.* **56**, 317–323 Aug (1939).
- [56] Tamm, I. E. *Z. Phys* **76**, 849 (1932).
- [57] Prutton, M. *Introduction to Surface Physics*. Oxford Science Publications, (1994).
- [58] Bovensiepen, U., Petek, H., and Wolf, M., editors. *Dynamics at Solid State Surfaces and Interfaces: Volume 1 - Current Developments*. WILEY-VCH, (2011).
- [59] Emiliani, V., Bonanni, B., Frova, A., Capizzi, M., Martelli, F., and Stone, S. S. *J. Appl. Phys.* **77**(11), 5712 (1995).
- [60] Haring, R., Paschotta, R., Aschwanden, A., Gini, E., Morier-Genoud, F., and Keller, U. *IEEE J. Quantum Electron* **38**, 1268 (2002).
- [61] Garnache, A., Hoogland, S., Tropper, A. C., Sagnes, I., Saint-Girons, G., and Roberts, J. S. *Appl. Phys. Lett.* **80**, 3892 (2002).
- [62] Huang, L. *Semiconductor under Ultrafast Laser Excitation: Optical Studies of the Dynamics*. PhD thesis, Harvard University, (1997).
- [63] Kim, A. M.-T., Callan, J. P., Roeser, C. A. D., and Mazur, E. *Phys. Rev. B* **66**, 245203 Dec (2002).
- [64] Saeta, P. *Optical studies of ultrafast carrier dynamics in semiconducting materials*. PhD thesis, Harvard University, (1991).

- [65] Schmid, M., Benchabane, S., T.-Goudarzi, F., Abram, R., Ferguson, A. I., and Riis, E. *Appl. Phys. Lett.* **84**, 4860 (2004).
- [66] Beister, G., Bugge, F., Buhandt, E., Erbert, G., Hansel, H. G., Hulsewede, R., Knauer, A., Pittroff, W. K., Staske, R., Schroder, M., Wenzel, H., Weyers, M., and Trankle, G. *IEEE J. S. T. Q. E.* **7**, 334 (2001).
- [67] Wenzel, H., Klehr, A., Braun, M., Bugge, F., Erbert, G., Fricke, J., Knauer, A., Weyers, M., and Trankle, G. *Electron Lett.* **40**, 123 (2004).
- [68] Yang, C. H. and Lyon, S. A. *Appl. Phys. Lett.* **53**, 285 (1988).
- [69] Norris, P. M., Caffrey, A. P., Stevens, R. J., Klop, M. J., McLeskey, J. T., and Smith, A. N. *Rev. Sci. Instrum.* **74**, 400 (2003).
- [70] Poel, C. J. V. D., Ambrosius, H. P. M. M., Linders, R. W. M., Peeters, R. M. L., Acket, G. A., and Krijn, M. P. C. M. *Appl. Phys. Lett.* **63**, 2312–2314 (1993).
- [71] Pankove, J. I. *Optical processes in semiconductors*. Dover Publications, (1971).
- [72] Tignon, J., Heller, O., Roussignol, P., Martinez-Pastor, J., Lelong, P., Bastard, G., Iotti, R. C., Andreani, L. C., Thierry-Mieg, V., and Planel, R. *Phys. Rev. B* **58**, 7076–7085 Sep (1998).
- [73] Fouquet, J. E. and Siegman, A. E. *Applied Physics Letters* **46**(3), 280–282 (1985).
- [74] Glembocki, O. J., Shanabrook, B. V., Bottka, N., Beard, W. T., and Comas, J. *Applied Physics Letters* **46**(10), 970–972 (1985).
- [75] Ghosh, S. and Arora, B. M. *Review of Scientific Instruments* **69**(3), 1261–1266 (1998).

- [76] Kouyama, K., Kubo, Y., Ema, K., and Kuwahara, H. *J. Phys. Soc. Jpn.* **76**, 123702(1–3) (2007).
- [77] Ning, J. Q., Xu, S. J., Shi, S. L., and Xie, M. H. *Appl. Phys. Lett.* **90**, 061109(1–3) (2007).
- [78] Heavens, O. S. *Optical properties of thin solid films*. Dover Publications, (1991).
- [79] Born, M. and Wolf, E. *Principles of Optics*. Cambridge, (1999).
- [80] Palik, E. D. *Handbook of Optical Constants of Solids*. Academic Press, (1998).
- [81] Madelung, O., editor. *Semiconductors: Data Handbook*. Springer, (2004).
- [82] Atapina, N. V., Garipogly, D. N., Drobyshev, A. S., and Maksimov, S. L. *J. Eng. Phys. Thermophys.* **63(4)**, 1023–1–26 (1992).
- [83] Drobyshev, A., Aldiyarov, A., Zhumagaliuly, D., Kurnosov, V., and Tokmoldin, N. *Low Temp. Phys.* **33(4)**, 355–361 (2007).
- [84] Prabhu, S. S. and Vengurlekar, A. S. *J. Appl. Phys.* **95**, 7803 (2004).
- [85] Burstein, E. *Phys. Rev.* **93**, 632–633 Feb (1954).
- [86] Wolff, P. A. *Phys. Rev.* **126**, 405–412 Apr (1962).
- [87] Abram, R. A., Childs, G. N., and Saunderson, P. A. *Journal of Physics C: Solid State Physics* **17(34)**, 6105 (1984).
- [88] Bennett, H. S. and Lowney, J. R. *Journal of Applied Physics* **62(2)**, 521–527 (1987).
- [89] Rossi, J. A., Keune, D. L., Holonyak, N., Dapkus, P. D., and Burnham, R. D. *Journal of Applied Physics* **41(1)**, 312–320 (1970).

- [90] Camassel, J., Auvergne, D., and Mathieu, H. *Journal of Applied Physics* **46**(6), 2683–2689 (1975).
- [91] Casey, H. C. and Stern, F. *Journal of Applied Physics* **47**(2), 631–643 (1976).
- [92] Tarucha, S., Kobayashi, H., Horikoshi, Y., and Okamoto, H. *Japanese Journal of Applied Physics* **23**(7R), 874 (1984).
- [93] Bugajski, M. and Lewandowski, W. *Journal of Applied Physics* **57**(2), 521–530 (1985).
- [94] Henry, C. H., Logan, R. A., and Bertness, K. A. *Journal of Applied Physics* **52**(7), 4457–4461 (1981).
- [95] Bennett, B. R., Soref, R. A., and Alamo, J. A. D. *IEEE Journal of Quantum Electronics* **26**, 113 (1990).
- [96] Klingshirn, C. *Semiconductor optics*. Springer, (2005).
- [97] Berggren, K. F. and Sernelius, B. E. *Phys. Rev. B* **24**, 1971–1986 Aug (1981).
- [98] Chang, Y., Tan, I., Zhang, Y., Merz, J., Hu, E., Frova, A., and Emiliani, V. *Applied Physics Letters* **62**(21), 2697–2699 (1993).
- [99] Gobel, E. O., Leo, K., Damen, T. C., Shah, J., Schmitt-Rink, S., Schafer, W., Muller, J. F., and Kohler, K. *Phys. Rev. Lett.* **64**, 1801 (1990).
- [100] Ohta, S., Kojima, O., Kita, T., and Isu, T. *J. Appl. Phys.* **111**, 023505 (2012).
- [101] Kojima, O., Isu, T., Ishi-Hayase, J., Kanno, A., Katouf, R., Sasaki, M., and Tsuchiya, M. *J. Phys. Soc. Jpn.* **77**, 044701 (2008).
- [102] Hasegawa, T., Mizoguchi, K., and Nakayama, M. *J. Lumin.* **128**, 1056 (2008).

- [103] Othonos, A., Itskos, G., Bradley, D., Dawson, M., and Watson, I. M. *Appl. Phys. Lett.* **94**, 203102 (2009).
- [104] Dreybrodt, J., Daiminger, F., Reithmaier, J. P., and Forchel, A. *Phys. Rev. B* **51**, 4657–4660 Feb (1995).
- [105] B. Bonanni, M. Capizzi, R. D. V. E. A. F. C. P. M. C. M. G. A. V. F. M. Y.-L. C. J. M. S.-S. S. In *The Physics of Semiconductors Proceedings of the 22nd International Conference*, Lockwood, D., editor, 1043–1046. World Scientific, Singapore, (1995).
- [106] MalÄg, A., DÄbrowska, E., and Grodecki, K. *Journal of Applied Physics* **103**(11) (2008).
- [107] Schmid, M., Benchabane, S., Torabi-Goudarzi, F., Abram, R., Ferguson, A. I., and Riis, E. *Applied Physics Letters* **84**(24), 4860–4862 (2004).
- [108] Hasegawa, T., Mizoguchi, K., and Nakayama, M. *J. Lumin.* **128**, 1056 (2008).
- [109] Pal, S., Singh, S. D., Porwal, S., Dsouza, S. W., Barman, S. R., and Oak, S. M. *J. Vac. Sci. Technol. A* **28**, 1319 (2010).
- [110] Wei-liang, L., Zhi-ren, Q., Wen-ji, P., huang Xu-guang, Jian-ying, Z., and Zhen-xin, Y. *Chin. Phys. Lett.* **13**, 237 (1996).
- [111] Pal, S., Singh, S. D., Porwal, S., Sharma, T. K., Khan, S., Jayabalan, J., Chari, R., and Oak, S. M. *Semicond. Sci. Technol.* **28**, 035016 (2013).
- [112] Rossi, F. and Kuhn, T. *Rev. Mod. Phys.* **74**, 895 (2002).
- [113] Bonilla, L. L., Älvaro, M., and Carretero, M. *Europhys. Lett.* **95**, 47001 (2011). And the references there in.

- [114] HÄijgel, W., Heinrich, M., and Wegener, M. *physica status solidi (b)* **221**, 473 (2000).
- [115] Xiu-Xun, H., Jie-Jun, W., Jie-Min, L., Guang-Wei, C., Xiang-Lin, L., Qin-Sheng, Z., and Zhan-Guo, W. *Chinese Physics Letters* **22**(8), 2096 (2005).
- [116] Shen, J. X., Oka, Y., Hu, C. Y., Ossau, W., Landwehr, G., Friedland, K.-J., Hey, R., Ploog, K., and Weimann, G. *Phys. Rev. B* **59**, 8093–8104 Mar (1999).
- [117] LundstrÄom, T., Holtz, P., Bergman, J., Buyanov, A., Monemar, B., Campman, K., Merz, J., and Gossard, A. *Physica B: Physics of Condensed Matter* **249-251**, 767–770 (1998).
- [118] Slachter, A. Master’s thesis, (2006).
- [119] SchlÄpfer, F., Dietsche, W., Reichl, C., Faelt, S., and Wegscheider, W. *Journal of Crystal Growth* **442**, 114 – 120 (2016).
- [120] Yang, Y., Gu, J., Young, J. L., Miller, E. M., Turner, J. A., Neale, N. R., and Beard, M. C. *Science* **350**(6264), 1061–1065 (2015).